12-15-2014

Cationic Metallocene-Containing Polymers: From Synthesis to Applications

Jiuyang Zhang
University of South Carolina - Columbia

CATIONIC METALLOCENE-CONTAINING POLYMERS: FROM SYNTHESIS TO APPLICATIONS

by

Jiuyang Zhang

Bachelor of Science
Nanjing University, 2010

Submitted in Partial Fulfillment of the Requirements

For the Degree of Doctor of Philosophy in

Chemistry

College of Arts and Sciences

University of South Carolina

2014

Accepted by:

Chuanbing Tang, Major Professor

John J. Lavigne, Committee Member

Andrew B. Greytak, Committee Member

Peisheng Xu, Committee Member

Lacy Ford, Vice Provost and Dean of Graduate Studies

ACKNOWLEDGEMENTS

I would like to express my deepest appreciation to my advisor, Prof. Chuanbing Tang, who carefully introduced me into polymer sciences in the past five years. I also want to thank my committee members, Prof. John J. Lavigne, Prof. Andrew B. Greytak, and Prof. Peisheng Xu, for their kind suggestion and efforts during my Ph.D. studies. In addition, a thank you to my group members and collaborators, Prof. Alan Decho, Prof. Zheng Gai, Prof. Jihua Chen, Prof. Ken Shimizu, Prof. Mitzi Nagarkatti, Prof. Lixia Ren, Dr. Yan Yi, Dr. Yali Qiao, Dr. Yun-ping Chen, Jeff, Perry, Dr. Kejian, Jihua Chen and Dr. Chris, who shared with their research experience and also their happiness during my Ph.D. study. I also want to thank my friends, Haorui Wu, Yi Shen, Weiwei Xu and Ping Li, who helped me a lot during my studies and life. Finally, I would like to thank my family for their great support during my academic career to allow me to achieve this stage.

ABSTRACT

Metallopolymers, with the combination of metals and polymeric framworks, have attracted a lot of attention during the past decades. The development of metallopolymers has been largely driven by the desire to combine the synthetic efficiency and versatility of an organic polymer framework with the unique redox, responsive and catalytic properties of inorganic metals. Among different kinds of metallopolymers, metallocene-containing polymers， have been widely utilized for applications ranging from electrochemical sensors to templates for advanced inorganic catalysts to battery materials, due to their unique physicochemical properties. In the first part of my thesis, we showed controlled/living polymerization strategies to prepare well-defined metallocene-containing polymers. We majorly focused on charged metallocenium-containing polymers. In Chapters 3-6, unique properties of these cobaltocenium-containing polymers were discussed, including self-assembly studies, anion-exchange ability and bioactivities. Specifically, these cobaltocenium-containing polymeric materials were used as novel precursors to prepare various inorganic metal/carbon magnetic nanomaterials (cobalt-containing) and also utilized as novel antimicrobial materials to revitalize conventional antibiotics or directly act against multi-drug resistant bacteria.

TABLE OF CONTENTS

LIST OF TABLES

LIST OF FIGURES

Figure 6.16. *Splenocytes are resistant to induction of apoptosis following in vitro treatment with the polymers.* Splenocytes from mice were cultured for 24 h with vehicle or the polymers, at 10 and 50µg/mL and apoptosis was detected following TUNEL staining using flow cytometry. **Figure 6.16a** and **6.16c**: Representative figures after flow cytometry analysis of apoptotic cells detected following treatment with vehicle, I^-, Br^-, Cl^- and PF_6^--paired metallopolymers following TUNEL staining. Upper left panel represents negative control of unstained cells. **Figure 6.16b** and **6.16d** represent mean ± S.E. of the apoptotic cell percentages of triplicates. In order to determine the toxicity of the polymers, we first examined their ability to mediate programmed cell death known as apoptosis. For this purpose, we cultured the cells with vehicle, 10 or 50µg/mL of I^- or Br^- metallopolymers (**Figure 6.16a** and **6.16c**), Cl^- or PF_6^- metallopolymers (**Figure 6.16b** and **6.16d**) for 24 h and then performed the TUNEL assay to determine apoptotic cells. There was no significant change in the percentages of the apoptotic cells when the cells were treated with 10µg/mL of the polymers. The percentages of apoptotic cells after treatment with 50µg/mL of polymers were very similar to that of the vehicle-treated groups except for PF_6^- wherein we observed a slight increase in the percentage of apoptotic cells at only the higher concentration of 50µg/mL 129

Figure 6.17. *In vivo treatment of mice with polymers does not affect the induction of apoptosis in splenocytes when compared to vehicle-treated group.* Splenocytes from mice injected with the polymers at 10mg/kg body weight were harvested 48 h following treatment. The cells were cultured for 24 h and subjected to TUNEL followed by detection of apoptosis by flow cytometry. The percentages of apoptotic cells in each of the panels are depicted (**Figure 6.17**). No mice died and and no evidence of adverse effects on mice was observed after treatment with metallopolymers at 10mg/kg body weight. There was no significant change in the percentages of apoptotic cells between the vehicle and polymer treated groups. **Figure 6.17b** is a graphical representation of the mean±S.E. values of the groups. To study the in vivo effect of the polymers on the immune cells, we administered mice with the polymers through intravenous injection of a single dose of 10mg/kg body weight and 48hr later harvested the spleens. Freshly isolated splenocytes from the vehicle or polymer-injected mice were cultured for an additional 24 h and analyzed for apoptosis by TUNEL assay followed by flow cytometry. As seen from the results (**Figure 6.17a** and **6.17b**), there was no significant difference in the percentages of apoptotic splenocytes in I^-, Br^- and Cl^--paired metallopolymers-treated mice when compared with the PBS vehicle-treated group. Similarly, there was no difference between apoptotic cells in the PF_6^--paired metallopolymers-treated group when compared with the
DMSO-treated vehicle controls 130

Figure 6.18. *In vivo treatment with polymers did not alter the ratios of T and B cells in the spleen.* Mice were injected with vehicle or the polymers at 10mg/kg body weight and 48 h later, the spleen cell CD3+CD4+ and CD3+CD8+ T cell subpopulations as well as B cells (CD19+) were determined by flow cytometry. **Figure 6.18**: Top panels represent dot plots of CD3+CD4+T helper/regulatory cells in the upper right quadrant. Lower panel represents CD3+CD8+ cytotoxic T cells in the upper right quadrant. **Figure 6.18b** represents histograms of B cells stained with FITC-anti-CD19 Abs. We enumerated the T

CHAPTER 1

INTRODUCTION

[†]C. G. Hardy,[*] J. Zhang,[*] Y. Yan, L. Ren and C. Tang, *Prog. Polym. Sci.* **2014**, *39*, 1742-1796. ([*]Co-first Author)

1.1 BACKGROUND

Incorporation of metal centers into macromolecules has led to materials that combine the catalytic, magnetic, and electronic properties of metals with desirable mechanical and processing properties of polymeric frameworks. Research in this area has flourished over the past thirty years, as metallopolymers (or organometallic polymers) have been used as materials for a variety of applications such as sensing, catalysis and media storage.[1-13] Recent advances in polymerization techniques have provided ample opportunities to prepare polymers with tunable chemistry and compositions with predetermined molecular weight and low polydispersity index values (PDI). Furthermore, living and controlled polymerization techniques allow for the preparation of well-defined polymers with diverse topologies including gradient, grafted, and block copolymers. [14-15]

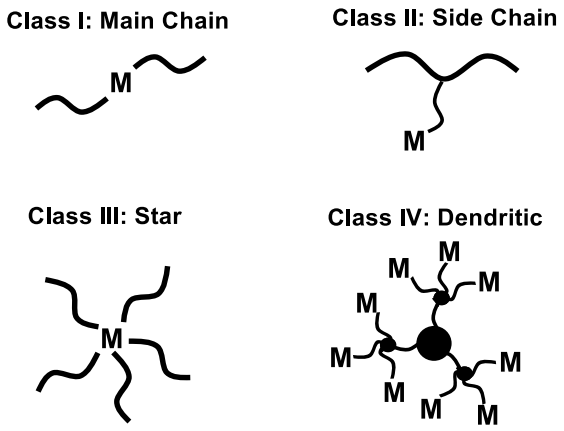

Figure 1.1. Classes of metallopolymers.

Metallopolymers can be classified by the position where the metal center is incorporated into the macromolecule. The most extensively studied metallopolymers are those when the metal center is included in a linear polymer. Generally, there are two major classes of metal-containing linear polymers: main-chain metallopolymers (Class I)

in which the metal center is incorporated as an integral part of polymer backbone, and side-chain metallopolymers (Class II) in which the metal center is a pendant group away from the polymer backbone (**Figure 1.1**). Other types of metallopolymers include star-shaped (Class III) and dendritic (Class IV) macromolecules.[16-21] In recent years, cobaltocene/cobaltocenium moieties have attracted a lot of attention due to their unique properties such as extraordinary stability toward oxidation and potential biological applications.[22-24] However, compared with ferrocene units, it is challenging to prepare derivatives from cobaltocene or cobaltocenium by electrophilic substitution due to the ease in oxidation of cobaltocene and the inertness of cobaltocenium salts.[25] As a result, the incorporation of cobaltocene/cobaltocenium units into polymers has been far less explored than ferrocene. Sheats *et al.* pioneered early work on cobaltocenium-containing polymers that consisted of main-chain cobaltocenium-containing oligomers with poor solubility.[26-28]

Manners *et al.* overcame this problem by using ring-opening polymerization (ROP) techniques to polymerize a ring-tilted dicarba[2]cobaltococenophane.[29] Whereas anion ROP has been utilized to prepare high molecular weight polymers from ferrocenophane monomers with low PDIs, low molecular weight oligomers.[30] Tang et al. developed synthetic Nearly at the same time, Tang and coworkers established a synthetic platform to prepare side-chain cobaltocenium-containing polymers.[31-32] Instead of using electrophilic substitution reactions with cobaltocene to prepare monomers, Tang *et al*. used a direct synthesis route to obtain monosubstituted cobaltocenium-containing compounds. The obtained mono-functionalized

cobaltocenium carboxylic acid can be modified to react with side-chain hydroxyl groups of a diblock copolymer.

1.2 Dissertation Outline

The goal of this thesis is to investigate novel cobaltocenium-containing polymers for advanced applications in nanostructured inorganic materials, magnetic materials, and biomaterials. Different controlled living polymerization techniques have been applied for cationic cobaltocenium-containing monomers to prepare metallopolymers with diverse architectures for different utilizations.

Chapter 2 describes the synthesis of cobaltocenium-containing methacrylate monomers and their polymerization via reversible additional fragmentation chain-transfer polymerization (RAFT). The properties of cobaltocenium-containing diblock copolymers are carefully investigated.

Chapter 3 focuses on the ionic nature of cationic cobaltocenium-containing polyelectrolytes. A quantitative and qualitative counterion exchange in cationic metallocene-containing polyelectrolytes was investigated via 2D-Diffusion NMR. Cationic cobaltocenium-containing polymer brushes were prepared and the ion-exchange effects on the polymer brushes were studied.

Chapters 4-5 discuss the utilization of cobaltocenium-containing polymers as novel precursors to prepare inorganic nanostructured magnetic materials. With different block compositions, metallopolymers offered different inorganic materials with controlled magnetic materials. Metal/carbon nanotube hybrid materials were obtained due to the unique catalytic property of ferrocene. A facile phase transfer technique was

applied for metallocenium-containing polymers for their advanced use as novel precursors. The synthesis, self-assembly and ion-exchange for cationic cobaltocenium-containing polymers were also discussed.

In Chapters 6, commercially available β-lactam antibiotics were utilized as novel anions to form bioconjugates with cationic cobaltocenium-containing polymers. Such bioconjugates could protect antibiotics from the hydrolysis by β-lactamase in drug resistant bacteria, which led antibiotics to regain the ability to fight against drug resistant bacteria. Futhermore, cationic metallopolymers themselves had very high efficiency to kill drug resistant bacteria, while showed extremely low toxicity in *in vitro* and *in vivo* studies. This chapter demonstrated cobaltocenium-containing polymers as a novel type of antimicrobial materials.

1.3 REFERENCES

1. F. Jäkle, *Chem. Rev.* **2010**, *110*, 3985-4022.
2. A. S. Abd-El-Aziz and I. Manners, *Frontiers in Transition-Metal-Containing Polymers*, Wiley, Hoboken, NJ, **2007**, p.
3. I. Manners, *Synthetic Metal-Containing Polymers*, Wiley-VCH, Weinheim, **2004**, p.
4. U. S. Schubert, G. R. Newkome and I. Manners, *Metal-Containing and Metallosupramolecular Polymers and Materials*, **2006**, p. null.
5. J. E. Sheats, J. C. E. Carraher, J. C. P. Pittman, M. Zeldin and B. Currell, *Inorganic and Metal-Containing Polymeric Materials*, **1985**, p. null.
6. A. S. Abd-El-Aziz, *Macromol. Rapid Comm.* **2002**, *23*, 995-1031.
7. J. B. Beck, J. M. Ineman and S. J. Rowan, *Macromolecules* **2005**, *38*, 5060-5068.
8. K. J. Calzia and G. N. Tew, *Macromolecules* **2002**, *35*, 6090-6093.
9. P. Y. Keng, B. Y. Kim, I.-B. Shim, R. Sahoo, P. E. Veneman, N. R. Armstrong, H. Yoo, J. E. Pemberton, M. M. Bull, J. J. Griebel, E. L. Ratcliff, K. G. Nebesny and J. Pyun, *Acs. Nano* **2009**, *3*, 3143-3157.
10. B. D. Korth, P. Keng, I. Shim, S. E. Bowles, C. Tang, T. Kowalewski, K. W. Nebesny and J. Pyun, *J. Am. Chem. Soc.* **2006**, *128*, 6562-6563.
11. S. K. Yang, A. V. Ambade and M. Weck, *Chem. Soc. Rev.* **2011**, *40*, 129-137.
12. X. Wang and R. McHale, *Macromol. Rapid Comm.* **2010**, *31*, 331-350.
13. X. Wang, K. Cao, Y. Liu, B. Tsang and S. Liew, *J. Am. Chem. Soc.* **2013**, *135*, 3399-3402.

14. M. Szwarc, *Nature* **1956**, *178*, 1168-1169.
15. N. Hadjichristidis, M. Pitsikalis, S. Pispas and H. Iatrou, *Chem. Rev.* **2001**, *101*, 3747-3792.
16. I. Manners, *Science* **2001**, *294*, 1664-1666.
17. R. D. A. Hudson, *J. Organomet. Chem.* **2001**, *637–639*, 47-69.
18. A. S. Abd-El-Aziz and E. A. Strohm, *Polymer* **2012**, *53*, 4879-4921.
19. A. Abd-El-Aziz and I. Manners, *J. Inorg. Organomet. P.* **2005**, *15*, 157-195.
20. A. S. Abd-El-Aziz, P. O. Shipman, B. N. Boden and W. S. McNeil, *Prog. Polym. Sci.* **2010**, *35*, 714-836.
21. P. Nguyen, P. Gómez-Elipe and I. Manners, *Chem. Rev.* **1999**, *99*, 1515-1548.
22. N. G. Connelly and W. E. Geiger, *Chem. Rev.* **1996**, *96*, 877-910.
23. C. M. Casado, B. González, I. Cuadrado, B. Alonso, M. Morán and J. Losada, *Angew. Chem. Int. Ed.* **2000**, *39*, 2135-2138.
24. G. R. Whittell and I. Manners, *Adv. Mater.* **2007**, *19*, 3439-3468.
25. J. E. Sheats and M. D. Rausch, *J. Org. Chem.* **1970**, *35*, 3245-3249.
26. C. E. Carraher, G. F. Peterson, J. E. Sheats and T. Kirsch, *Die Makromol. Chem.* **1974**, *175*, 3089-3096.
27. C. U. Pittman, O. E. Ayers, S. P. McManus, J. E. Sheats and C. E. Whitten, *Macromolecules* **1971**, *4*, 360-362.
28. C. U. Pittman, O. E. Ayers, B. Suryanarayanan, S. P. McManus and J. E. Sheats, *Die Makromol. Chem.* **1974**, *175*, 1427-1437.
29. U. F. J. Mayer, J. B. Gilroy, D. O'Hare and I. Manners, *J. Am. Chem. Soc.* **2009**, *131*, 10382-10383.
30. J. B. Gilroy, S. K. Patra, J. M. Mitchels, M. A. Winnik and I. Manners, *Angew. Chem. Int. Ed.* **2011**, *50*, 5851-5855.
31. L. Ren, C. G. Hardy and C. Tang, *J. Am. Chem. Soc.* **2010**, *132*, 8874-8875.
32. L. Ren, C. G. Hardy, S. Tang, D. B. Doxie, N. Hamidi and C. Tang, *Macromolecules* **2010**, *43*, 9304-9318.

CHAPTER 2

COBALTOCENIUM-CONTAINING METHACRYLATE HOMOPOLYMERS, BLOCK COPOLYMERS AND HETEROBIMETALLIC POLYMERS VIA RAFT POLYMERIZATION[†]

[†]J. Zhang, L. Ren, C. Hardy and C. Tang, *Macromolecules* **2012**, *45*, 6857-6863. Reprinted here with permission of publisher.

2.1 ABSTRACT

Cobaltocenium-containing methacrylate homopolymer, poly(2-(methacrylolyoxy) ethyl cobaltoceniumcarboxylate hexafluorophosphate) ($PMAECoPF_6$), was prepared by reversible addition-fragmentation chain transfer polymerization (RAFT). Using the homopolymer as a macroinitiator, three different diblock copolymers, including a novel heterobimetallic diblock copolymer with ferrocene units as the second block, were synthesized via chain extensions. Kinetic studies show that all chain extensions followed a controlled/living process under relatively lower conversion. The heterobimetallic diblock copolymer self-assembled into spherical micelles in selective solvents and showed different stability depending on the location of the ferrocene block in the micelles.

2.2 INTRODUCTION

In recent years, various metallocene-containing functional materials have been prepared and utilized for applications such as biosensors, catalysts, lithography and battery materials.[1-12]. Metallocene-containing polymers combining inorganic metal centers and organic framework show unique properties in many aspects.[13-16] For example, metallocene-containing block copolymers can self-assemble into a variety of nanostructures, which can be used as thin film resists for lithography or micelles templates for magnetic nanoparticles.[17-19] For ferrocene-containing polymers, tremendous progress has been made in last two decades.[20-22] Other kinds of metallocene-containing polymers are much less explored. Recently, cobaltocenium-containing polymers have attracted much attention.[23-27] Different from 18-electron ferrocene (18-e), cobaltocene is 19-electron metallocene (19-e), which can be easily oxidized into 18-e cobaltocenium.[28-29] Compared with ferrocene-containing polymers, cobaltocenium-

containing polymers are a class of polyelectrolytes that show higher stability toward further oxidation, unique counter-ion dependent solubility and fully reversible redox chemistry.[17, 30-31] Cobaltocenium-containing polymers have already been utilized in electrochemistry, biosensing, cell nuclear delivery and magnetic materials.[28, 31-37]

However, due to the high chemical stability of cobaltocenium,[38] monosubstituted cobaltocenium is difficult which means it is challenging to synthesize well-defined cobaltocenium-containing polymers by controlled polymerization is.[17] Most cobaltocenium-containing polymers in early work were main-chain cobaltocenium-containing oligomers with poor solubility.[1, 39-40] Recently, Manners et al. overcame the challenge and synthesized high molecular weight main-chain cobaltocenium-containing polymers with anionic ring-opening polymerization of a cyclic ring-strained monomer.[41] However, some of their main-chain cobaltocenium-containing polymers with hexafluorophosphate and chloride ion as counter ions still had poor solubility and were actually low molecular weight oligomers.[41-42] Recently, we synthesized side-chain cobaltocenium-containing polymers by both post polymerization-modification and free radical polymerization.[17, 30] But post-polymerization modification only resulted in side-chains randomly decorated with cobaltocenium. For free radical polymerization, only low molecular weight acrylic polymers were obtained without control on the polymerization process.[30, 43] More recently, we utilized ring-opening metathesis polymerization (ROMP) to produce high molecular weight side-chain cobaltocenium-containing homopolymers and block copolymers.[43-44]

Scheme 2.1. Synthesis of side-chain cobaltocenium-containing homopolymer and diblock copolymers by RAFT.

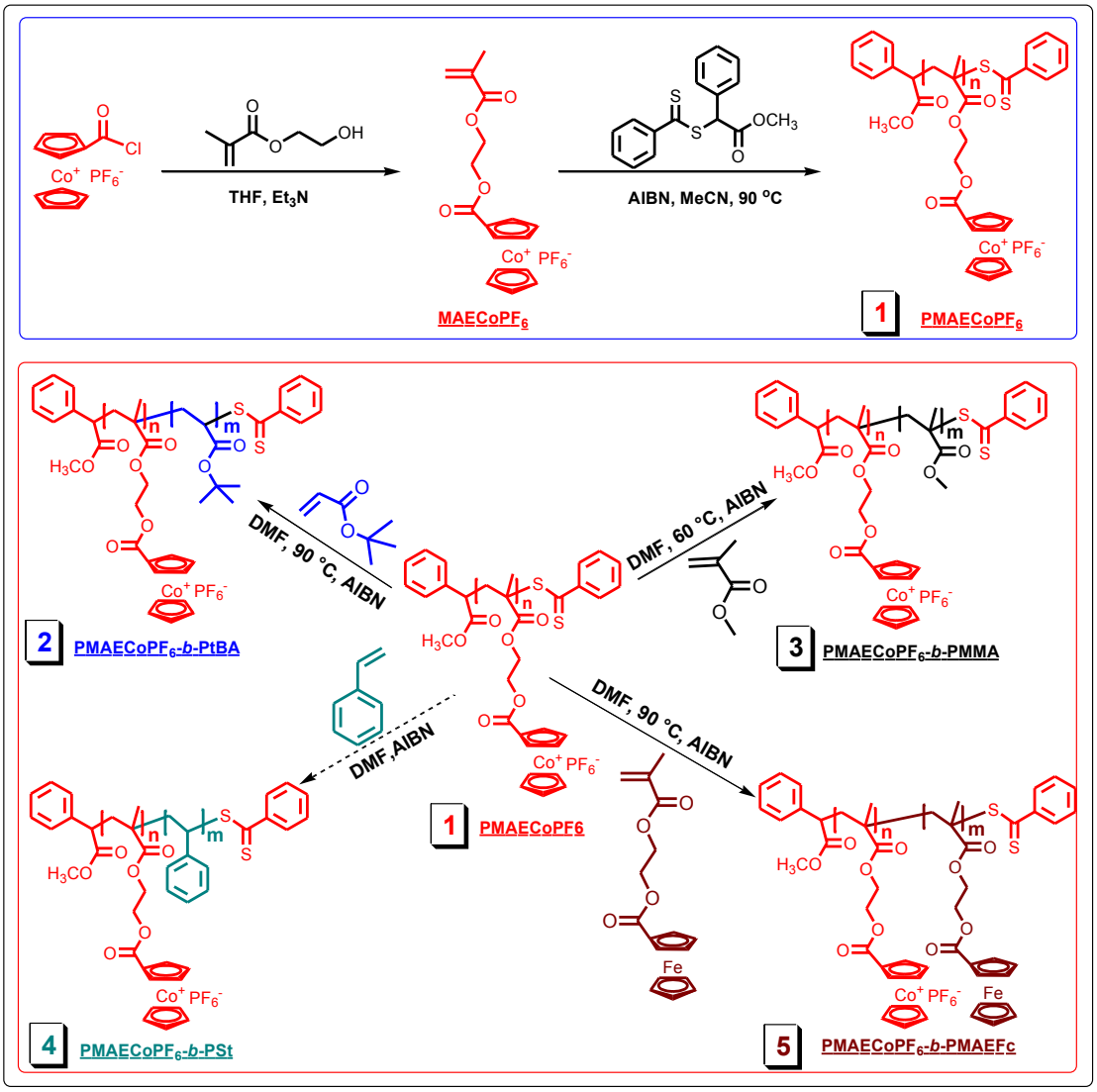

Controlled/living radical polymerization (CRP) has achieved great success in developing a variety of polymeric systems using ionic, nonionic, hydrophobic or hydrophilic monomers. CRP allows the preparation of well-defined polymers with controlled molecular weight, low polydispersity and various architectures.[45-46] Atom transfer radical polymerization (ATRP), reversible addition-fragmentation chain transfer polymerization (RAFT) and nitroxide mediated polymerization (NMP) are three of the

most widely used CRP techniques. Our early free radical polymerization showed low reactivity of acrylate-based cobaltocenium-containing monomers.[30] Our initial studies using ATRP for cobaltocenium-containing monomers under various conditions showed no polymerization. This may be due to the catastrophic ion-exchange between ATRP catalysts and counter ions of cobaltocenium monomers.[47] RAFT is probably the best technique among CRP for polymerization of a variety of functional monomers, including ionic monomers.

Herein, we report the use of RAFT technique to synthesize well-defined cobaltocenium-containing methacrylate homopolymers (**Scheme 2.1**). In addition, three different diblock copolymers were prepared by using the methacrylate homopolymer as a macroinitiator. A novel cobaltocenium and ferrocene-containing heterobimetallic diblock copolymer was further prepared via RAFT.

2.3 EXPERIMENTAL

Materials. 2-Hydroxyethyl methacrylate (HEMA, 95%, VWR), *tert*-butyl acrylate (*t*BA, 97%, Aldrich), methyl methacrylate (MMA, 99%, Aldrich), and styrene (St, 99%, Aldrich) were passed through a basic alumina column before use. Monocarboxycobaltocenium and 2-(methacryloyloxy)ethyl ferrocenecarboxylate (MAEFc) were synthesized according to previous reports.[17, 29, 48] RAFT chain transfer agent (CTA), *s*-methoxycarbonylphenylmethyl dithiobenzoate (MCPDB), was synthesized according to a previous report.[49] Triethylamine (99%, Aldrich) was dried over molecular sieves. 2,2-Azobisisobutyronitrile (AIBN) was recrystallized from

methanol. All other reagents were from commercial resources and used as received unless otherwise noted.

Characterization: ^{1}H (300 MHz) and ^{13}C (75 MHz) NMR spectra were recorded on a Varian Mercury 400 NMR spectrometer with tetramethylsilane (TMS) as an internal reference. Mass spectrometry was conducted on a Waters Micromass Q-Tof mass spectrometer with an ionization source from positive ion electrospray. TGA was conducted on a TA Instruments Q5000 with a heating rate of 10 ^{o}C /min from 40 to 1000 ^{o}C under constant nitrogen flow. Hitachi 8000 transmission electron microscope was applied to take TEM images at an operating voltage of 150 kV. TEM samples were prepared by dropping solution on carbon-supported copper grids and then dried before observation. Dynamic light scattering was performed on a submicron particle sizer (Autodiluter Model 370, Particle Sizing Systems, Inc., Santa Barbara, California, USA) at a scattering angle of 90 °. BAS CV-50W Voltametric Analyzer was used to perform cyclic voltametry (CV) characterization. Samples were dissolved in 0.1 M tetra-n-butylammonium hexafluorophosphate solution in *N,N*-dimethylformamide (DMF) at a concentration of 0.5 mM. The samples were scanned at a rate of 50 mV/s with different potential ranges vs Ag/AgCl.

Synthesis of monomer 2-(methacrylolyoxy)ethyl cobaltoceniumcarboxylate hexafluorophosphate. ($MAECoPF_6$) The synthesis of $MAECoPF_6$ was carried out as previously reported.[30] HEMA (493 mg, 3.8 mmol) and triethylamine (1.0 mL, 0.70 mmol) were dissolved in dry THF (30 mL) at room temperature. Monosubstitued cobaltocenium acyl chloride (736 mg, 1.9 mmol) was then slowly added into the mixture. The solution was stirred under room temperature for four days. The reaction mixture was

then concentrated, dissolved in 50 mL dichloromethane and extracted with water three times. The organic phase was collected, and the solvent was evaporated to obtain a yellow solid. Yield: 657 mg, 72%. ^{1}H NMR (CD_3COCD_3, δ, ppm): 6.39 (t, 2H, Cp, *J*=2.20 Hz), 6.24 (m, 1H, C*H*$_2$=C), 6.20 (t, 2H, Cp, *J*=2.10 Hz), 6.12 (s, 5H, Cp), 5.70 (m, 1H, C*H*$_2$=C), 4.61 (m, 2H, OC*H*$_2$CH$_2$O), 4.49 (m, 2H, OCH$_2$C*H*$_2$O), 1.91 (m, 3H, C*H*$_3$). ^{13}C NMR (CD_3COCD_3, δ, ppm): 166 (CH$_2$CH*C*OO); 164 (Cp*C*OO); 137 (CH$_2$*C*H); 126 (*C*H$_2$CH); 85-90 (Cp ring); 61, 64 (*C*H$_2$*C*H$_2$); 19 (*C*H$_3$)

Synthesis of homopolymer poly(2-(methacrylolyoxy)ethyl cobaltoceniumcarboxylate hexafluorophosphate) (PMAECoPF$_6$, 1) via RAFT polymerization. MAECoPF$_6$ (572.6 mg, 1.17 mmol), s-methoxycarbonylphenylmethyl dithiobenzoate (MCPDB) (4.43 mg, 0.015 mmol) and AIBN (0.96 mg, 5.8×10^{-3} mmol) were dissolved in 1.2 mL acetonitrile in a 10 mL Schlenk flask and then degassed with three cycles of freeze-pump-thaw. The reaction was heated under 90 ºC for 6.5 h. The reaction mixture was precipitated in dichloromethane three times and vacuum dried. Yield: 238 mg, 41.6%. M_n (from ^{1}H NMR end group analysis): 31,700 g/mol. ^{1}H NMR (DMSO-d$_6$, δ): 6.31 (broad, 2H, Cp), 6.22 (broad, 2H, Cp), 6.02 (broad, 5H, Cp), 4.49 (broad, 2H, OC*H*$_2$CH$_2$O), 4.32 (broad, 2H, OCH$_2$C*H*$_2$O), 2.08 (broad, 2H, C*H*$_2$C), 0.60-1.00 (broad, 3H, C*H*$_3$).

Chain extension to prepare diblock copolymers. Three diblock copolymers were synthesized by using PMAECoPF$_6$ as a macroinitiator (Scheme 1). A typical procedure was as follows: homopolymer PMAECoPF$_6$ (1 eq) and AIBN (0.2 eq) were dissolved in 1.0 mL DMF in a 10mL Schlenk flask and purged with nitrogen gas for 30 minutes. Degassed monomer (200 eq) was then charged into the flask under the

protection of nitrogen. *Tert*-butyl acrylate and methyl methacrylate were polymerized at 90 ^{o}C and 60 ^{o}C. For styrene, polymerizations were carried out at 90 ^{o}C , 100 ^{o}C or 105 ^{o}C. Samples were taken out during the polymerization to monitor the conversion of monomers. The final diblock copolymers were obtained by precitation in diethyl ether three times.

Synthesis of heterobimetallic diblock copolymer poly(2-(methacrylolyoxy)ethyl cobaltoceniumcarboxylate hexafluorophosphate)–*b*-poly-(2-(methacrylolyoxy) ethyl ferrocenecarboxylate)) (PMAECoPF$_6$-*b*-PMAEFc) The synthesis of diblock copolymer PMAECoPF$_6$-*b*-PMAEFc with different block ratios were synthesized by using PMAECoPF$_6$ as a macroinitiator through chain extension with MAEFc (**Scheme 2.1**). PMAECoPF$_6$ (505 mg, 0.016 mmol), AIBN (0.52 mg, 0.0032 mmol) and 2-(methacrylolyoxy) ethyl ferrocenecarboxylate (MAEFc) (1.08 g, 3.16 mmol) were dissolved in 1.2 mL dimethylformamide (DMF) in a 10 mL Schlenk flask and degassed by three cycles of freeze-pump-thaw. The reaction was stirred for 5 h under 90 ^{o}C and stopped at a conversion of 63%. The reaction mixture was precipitated in diethyl ether three times and vacuum dried to yield a yellow solid. Yield: 0.86 g, 54.2%. Mn (Determined by conversion of monomer from ^{1}H NMR): 71,900 g/mol. ^{1}H NMR (DMSO-d$_6$, δ): 6.31 (broad, Cp from Cp_2Co), 6.00-5.90 (broad, Cp from Cp_2Co), 4.81 (broad, Cp from Cp_2Fe), 4.20-4.59 (broad, OCH_2CH_2O Cp_2Fe), 2.09 (broad, CH_2C), 0.60-1.00 (s, CH_3).

Kinetic studies of polymerization for PMAECoPF$_6$ and diblock copolymers. All kinetic studies followed a similar procedure. For example, macroinitiator PMAECoPF$_6$ (235.7 mg, 0.0093 mmol) was dissolved in 1.0 mL dimethylformamide and

then charged into a 10 mL Schlenk flask, purged with nitrogen for 30 min. Degassed *tert*-butyl acrylate (218.6 mg, 1.70 mmol) and AIBN (0.28 mg, 0.00170 mmol) was transferred into the reaction flask. The polymerization was performed at 90 ^{o}C. Samples were taken out at different intervals under the protection of nitrogen. ^{1}H NMR was used to determine the conversion of monomers.

2.4 Results and Discussion

Synthesis and RAFT polymerization of $MAECoPF_6$. The synthesis of monomer $MAECoPF_6$ followed a similar method as reported in an earlier work.[30] $MAECoPF_6$ was synthesized by an esterification reaction between 2-hydroxyethyl methacrylate and monosubstituted cobaltocenium acyl chloride in the presence of triethylamine. **Figure 2.1a** shows the ^{1}H NMR spectrum of $MAECoPF_6$ monomer. Signals at ~6.21 ppm and ~5.70 ppm corresponded to vinyl protons from methacrylate double bonds. The peaks at ~6.39, ~6.20 and ~6.12 ppm corresponded to the cyclopentadiene (Cp) rings of the cobaltocenium unit. Chemical shifts of two multipeaks at ~4.61 and ~4.49 ppm were assigned to the ethylene protons of $MAECoPF_6$. ^{13}C NMR (**Figure 2.1b**) further confirmed the structure of the monomer $MAECoPF_6$. As shown in **Figure 2.1b**, all carbons were clearly assigned, consistent with the monomer structure. High resolution MS spectrum was used to verify the monomer structure. From MS spectrum (not shown), the peak at 345.10 showed a good agreement with the theoretical value (345.26), further demonstrating the successful synthesis of $MAECoPF_6$ monomer.

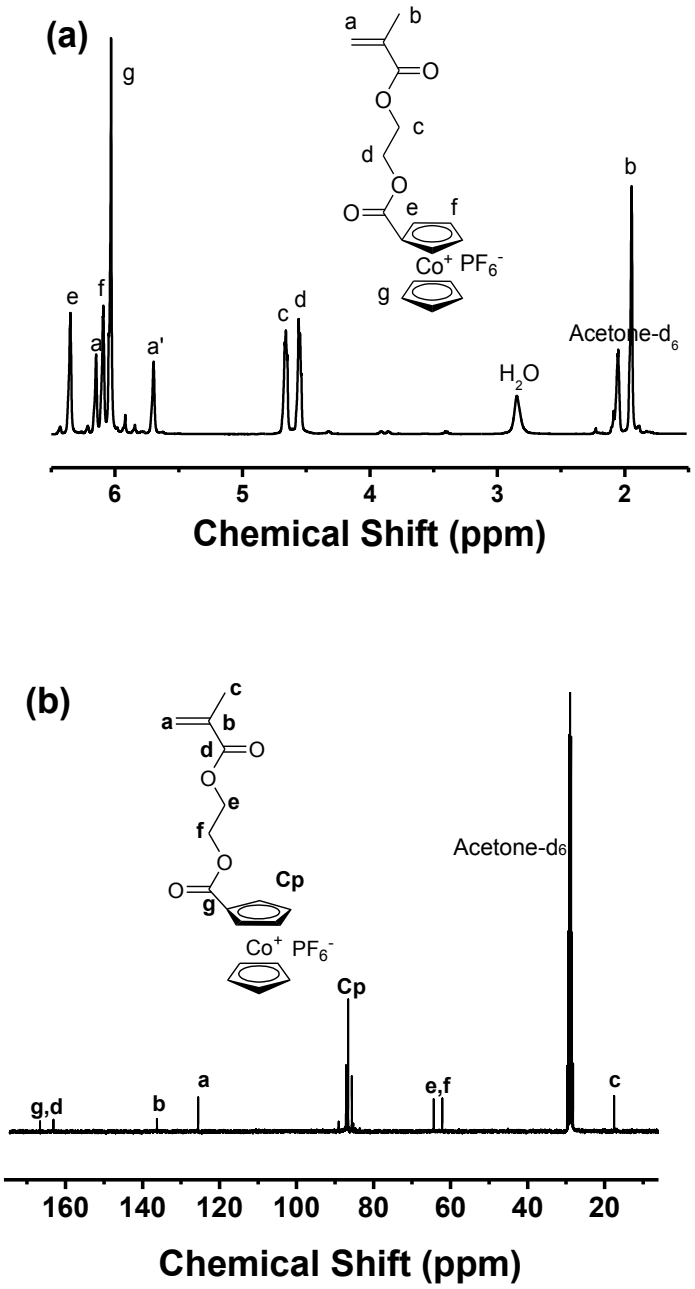

Figure 2.1. (a) ^{1}H NMR spectrum and (b) ^{13}C NMR spectrum of monomer MAECoPF$_6$.

RAFT polymerization was utilized to synthesize side-chain cobaltocenium-containing homopolymers from monomer MAECoPF$_6$. The polymerization was carried out at 90 ^{o}C with MCPDB as a chain transfer agent. **Figure 2.2** shows ^{1}H NMR spectrum

of the synthesized homopolymer PMAECoPF$_6$. The disappearance of the vinyl protons from the methacrylate and appearance of new broad peaks at 0.80-1.00 ppm and 1.80-2.20 ppm indicated the successful polymerization.

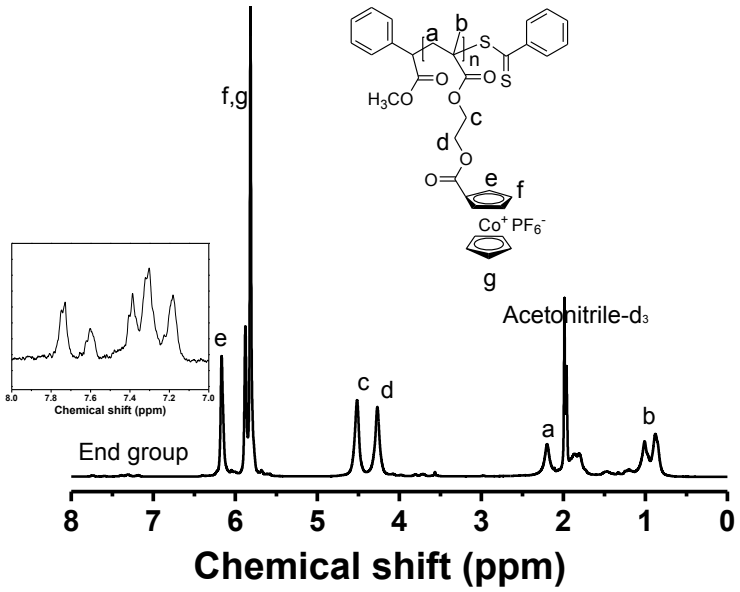

Figure 2.2. ^{1}H NMR spectrum of homopolymer PMAECoPF6. Insert: phenyl protons from end group.

A kinetic study was carried out to monitor RAFT polymerization of cobaltocenium-containing monomer MAECoPF$_6$. The conversion was determined by comparing the peaks from vinyl proton at ~5.70 ppm with peaks from Cp rings at 6.00-6.40 ppm. As shown in **Figure 2.3**, the semilogarithmic plot showed a linear relationship between reaction time and ln([M]$_0$/[M]), demonstrating that the RAFT polymerization followed a controlled/living character. The conversion achieved ~45% after about 6h. Due to strong electrostatic interaction between the cationic cobaltocenium moieties and stationary phase of microstyragel columns,[30] it was not possible to observe GPC signal

from the cobaltocenium-containing polymer. We first hydrolyzed the homopolymer to cleave the cobaltocenium moiety. The unimodal distribution of the hydrolyzed polymer (PDI=1.32) further demonstrated the control of polymerization.

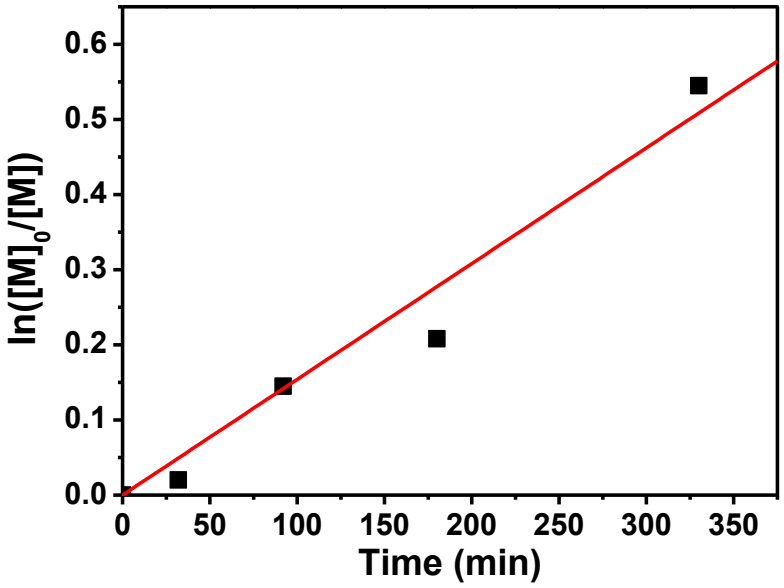

Figure 2.3. A semilogarithmic plot of polymerization of $MAECoPF_6$ by RAFT.

Chain extension to prepare diblock copolymers and kinetic studies. Side-chain cobaltocenium-containing diblock copolymers were prepared by using $PMAECoPF_6$ as a macroinitiator (**Scheme 2.1**). Three different classes of monomers, tBA, MMA and St, were used to prepare diblock copolymers. All polymerizations were carried out in DMF with a molar ratio of [Macroinitiator] : [AIBN] : [Monomer] = 1 : 0.2 : 200. Block copolymer $PMAECoPF_6$-*b*-PMMA and $PMAECoPF_6$-*b*-PtBA were successfully obtained. However, the polymerization of styrene was not successful. The polymerization was carried out at 90, 100 and 105 ^{0}C for 70 hours and did not yield any block copolymers containing styrene.

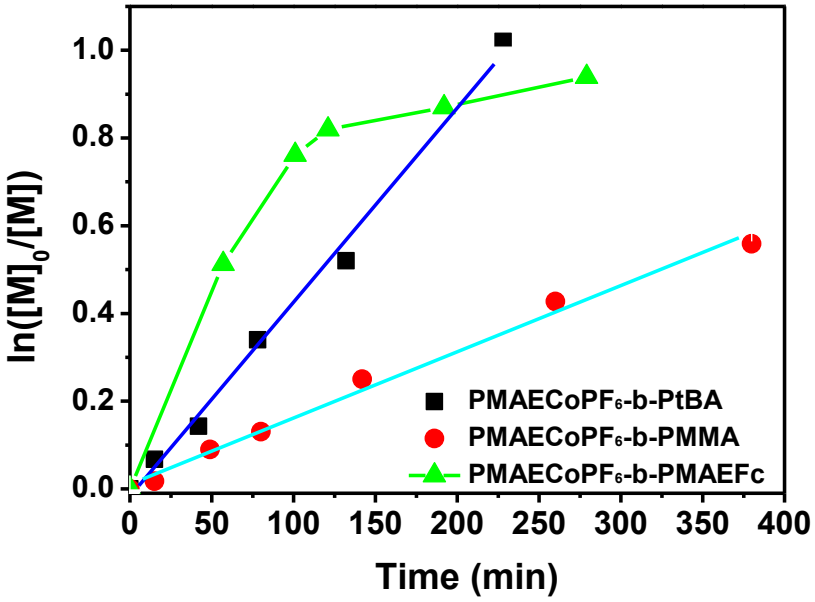

Figure 2.4. Semilogarithmic plots of chain extension to prepare diblock copolymers using PMAECoPF$_6$ as a macroinitiator.

Kinetic studies were taken to determine the control of the polymerization. For tBA and MMA, both semilogarithmic plots (**Figure 2.4**) showed a linear relationship between reaction time and ln([M]$_0$/[M]) indicating the well-controlled/living chain extension reaction.

Synthesis of side-chain heterobimetallic diblock copolymer. As shown in **Scheme 2.1**, by introducing ferrocene units in the second block, a novel side-chain heterobimetallic diblock copolymer, PMAECoPF$_6$-*b*-PMAEFc, was synthesized through chain extension of cobaltocenium-containing block with MAEFc. **Figure 2.5** showed ^{1}HNMR spectrum of PMAEPF$_6$-*b*-PMAEFc. Peaks at 5.70-6.30 ppm corresponded to Cp protons from cobaltocenium. While chemical shifts of Cp protons from ferrocene located at 3.80-5.10 ppm, which overlapped with protons from ester groups in the side-chain of the polymer. Block copolymer composition was determined by integration of these

proton signals. The kinetic plot (**Figure 2.4**) showed a linear relationship between $\ln([M]_0/[M])$ and time when the conversion was below 50%, indicating the controlled/living character. However, when the conversion was higher than 50%, the polymerization rate showed significant decrease, indicating that there were significant termination reactions in polymerization. Similar behaviors were also observed in other polymerization of ferrocene-containing monomers.[50-51]

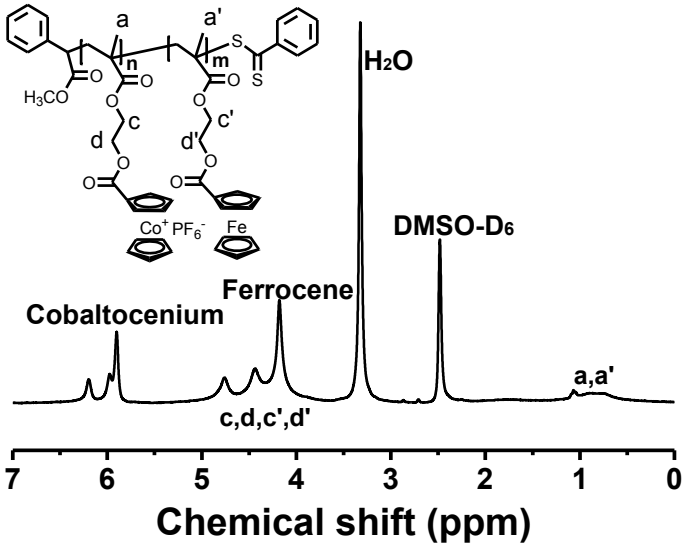

Figure 2.5. ^{1}H NMR spectrum of heterobimetallic diblock copolymer PMAECoPF$_6$-*b*-PMAEFc.

Electrochemical properties of side-chain cobaltocenium-containing polymers. The electrochemical properties of these side-chain cobaltocenium-containing methacrylate homopolymer and diblock copolymers were studied in DMF solution using *tetra*-n-butylammonium hexafluorophosphate as electrolytes. The homopolymer showed a fully reversible redox process with reduction and oxidation potential at about -0.90V and -0.60V due to the reversible electrochemistry of the cobaltocenium moiety.[30] For

the heterobimetallic diblock copolymer PMAECoPF$_6$-*b*-PMAEFc, a fully redox process from cobaltocenium was observed, but an irreversible redox chemistry from ferrocene. Only in the first cycle (**Figure 2.6**) a small reduction peak of ferrocene was observed and no oxidation peak of ferrocene was shown. After two days, the polymer completely precipitated from the solution (**Figure 2.7C**). The solubility change could be due to the formation of ferrocenium, which could induce the crosslinking for the polymer. The generated ferrocenium would be further oxidized to $[Fc\text{-}O\text{-}O\text{-}Fc]^+$, which could decompose into cyclopentdiene or 4-cyclopenten-1,3-dione (with the formation of Fe_2O_3). Earlier work showed that with oxygen, both cyclopentdiene and 4-cyclopenten-1,3-dione can react with themselves via Diels-Alder dimerization or radical polymerization, which could crosslink the micelles.[52-53] As shown in **Figure 2.7A**, fresh-prepared samples in DMF were clear and yellow. After two days, the solution turned turbid and brown, probably due to the oxidation of ferrocene (**Figure 2.7B**). This phenomenon was more prominent after running CV experiments. After running CV and then keeping for two days, all polymers precipitated out from solution and the solution was clear and almost colorless (**Figure 2.7C**). These results indicated that the CV run facilitated the oxidation and subsequent catastrophic decomposition of ferrocene.

Solution self-assembly of heterobimetallic diblock copolymers PMAECoPF$_6$-*b*-PMAEFc. Due to significantly different solubility of PMAECoPF$_6$ and PMAEFc blocks, solution self-assembly of this side-chain heterobimetallic diblock copolymer was studied. The block ratio for a chosen diblock copolymer was 62:122. The self-assembly was performed in the mixture of DMF/THF (v/v: 1:2) or DMF/MeCN (v/v: 1:2). DMF is a good solvent for both blocks, while acetonitrile is a selective solvent for cobaltocenium-

containing block PMAECoPF$_6$, and THF can only dissolve ferrocene-containing block PMAEFc. As shown in **Figure 2.8**, TEM images of PMAECoPF$_6$-*b*-PMAEFc micelles showed spherical micelles in both solvent mixtures with the diameter in the range of 45-65nm. In DMF/THF, the micelles tended to aggregate. However, in DMF/MeCN, the micelles were much better separated (a few of them aggregated into larger spherical micelles). From DLS results, **Figure 2.8C** showed an average of size about ~60 nm for the micelles, consistent with TEM results (**Figure 2.8A**). However, **Figure 2.8D** showed an increase of the size (~110nm), compared with the TEM observation (**Figure 2.8B**). This could be caused by the significant aggregation. In DMF/THF, the structure contained ferrocene-containing block in the shell and cobaltocenium-containing block in the core, which could induce the aggregation of micelles. The aggregation may be also due to the oxidation of ferrocene to ferrocenium as we discussed above.[52-53] However, in DMF/MeCN, the micellar structure was completely different, in which cobaltocenium-containing block located in the shell part and ferrocene-containing block stayed in the core, thus potentially avoided the crosslinking effect.

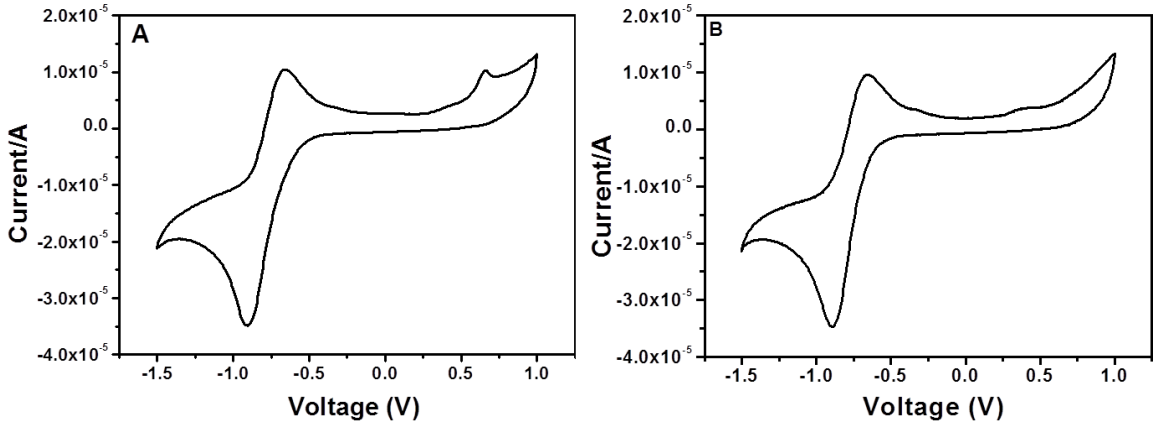

Figure 2.6. Cyclic voltammetry plots for heterobimetallic diblock copolymer PMAECoPF$_6$-*b*-PMAEFc: (A) The first cycle and (B) the second cycle.

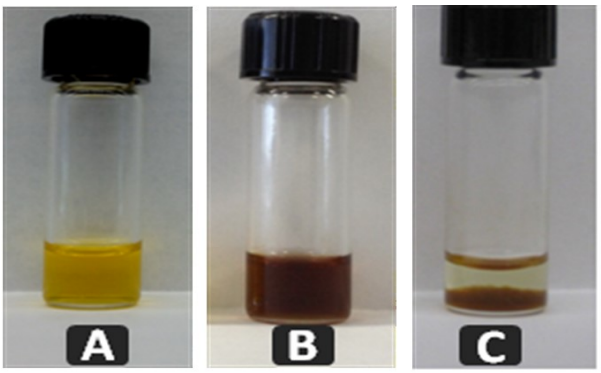

Figure 2.7. Solubility of heterobimetallic diblock copolymer PMAECoPF$_6$-*b*-PMAEFc in different conditions: (A) Sample in DMF, fresh prepared. (B) Sample in DMF for two days. (c) Sample in DMF for two days after running cyclic voltammetry.

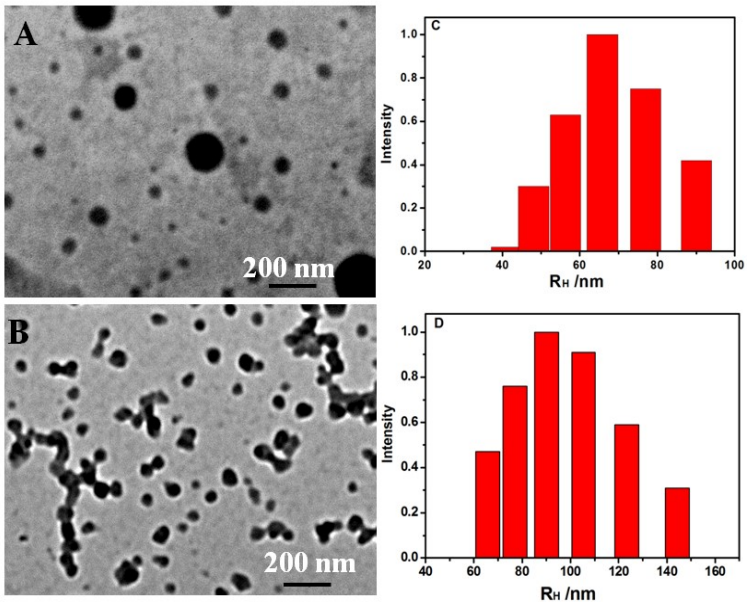

Figure 2.8. TEM images of (PMAECoPF$_6$)$_{62}$ -*b*-(PMAEFc)$_{122}$ micelles in (A) DMF/MeCN (v/v: 1:2) and (B) DMF/THF (v/v: 1:2). Particle size distribution (DLS) results for the self-assembly in (C) DMF/THF (v/v: 1:2), and (D) DMF/MeCN (v/v: 1:2).

2.5 CONCLUSION

In conclusion, a side-chain cobaltocenium-containing methacrylate homopolymer was prepared via a controlled/living RAFT polymerization. After chain extension, three diblock copolymers were synthesized, including a heterobimetallic block copolymer containing cobaltocenium and ferrocene. Kinetic studies verified the controlled/living character of RAFT polymerization and effective chain-extension for methacrylic and

acrylic monomers, while the chain extension for styrene was unsuccessful. These polymers showed a fully reversible redox process for the cobaltocenium units. However, the heterobimetallic polymer showed an irreversible reduction/oxidization process for ferrocene, probably due to the instability of the higher oxidation state ferrocenium. Solution self-assembly of the heterobimetallic diblock copolymer was studied in two different co-solvents (DMF/MeCN and DMF/THF). In both solvent systems, self-assembly of block copolymers resulted in spherical micelles. In different solvents, separated or aggregated micelles were obtained in different solvent systems. In DMF/MeCN, micelles tended to separated, while in DMF/THF, aggregated micelles were observed.

2.6 ACKNOWLEDGMENT

We would like to acknowledge the University of South Carolina for providing start-up fund.

2.7 REFERENCES

1. C. E. Carraher, G. F. Peterson, J. E. Sheats and T. Kirsch, *Makromol. Chem.* **1974**, *175*, 3089-3096.
2. J. M. Calvert, J. V. Caspar, R. A. Binstead, T. D. Westmoreland and T. J. Meyer, *J. Am. Chem. Soc.* **1982**, *104*, 6620-6627.
3. P. Nguyen, P. Gomez-Elipe and M. I, *Chem. Rev.* **1999**, *99*, 1515-1548.
4. P. G. Pickup, *J. Mater. Chem.* **1999**, *9*, 1641-1653.
5. A. S. Abd-El-Aziz, *Macromol. Rapid Comm.* **2002**, *23*, 995-1031.
6. W. Kaminsky, *J. Polym. Sci. Pol. Chem.* **2004**, *42*, 3911-3921.
7. L. A. Miinea, L. B. Sessions, K. D. Ericson, D. S. Glueck and R. B. Grubbs, *Macromolecules* **2004**, *37*, 8967-8972.
8. R. B. Grubbs, *J. Polym. Sci. Pol. Chem.* **2005**, *43*, 4323-4336.
9. C. Ornelas, J. Ruiz, C. Belin and D. Astruc, *J. Am. Chem. Soc.* **2009**, *131*, 590-601.
10. B. Hu, M. Meng, Z. Wang, W. T. Du, J. S. Fossey, X. Q. Hu and W. P. Deng, *J. Am. Chem. Soc.* **2010**, *132*, 17041-17044.
11. M. Burnworth, L. M. Tang, J. R. Kumpfer, A. J. Duncan, F. L. Beyer, G. L. Fiore, S. J. Rowan and C. Weder, *Nature* **2011**, *472*, 334-U230.
12. G. Erker, *Organometallics* **2011**, *30*, 358-368.

13. I. Manners, *J. Polym. Sci. Pol. Chem.* **2002**, *40*, 179-191.
14. I. Manners, *Angew. Chem. Int. Ed.* **1996**, *35*, 1603-1621.
15. Z. M. Al-Badri, R. R. Maddikeri, Y. P. Zha, H. D. Thaker, P. Dobriyal, R. Shunmugam, T. P. Russell and G. N. Tew, *Nat. Commun.* **2011**, 2.
16. Z. M. Al-Badri and G. N. Tew, *Macromolecules* **2008**, *41*, 4173-4179.
17. L. X. Ren, C. G. Hardy and C. B. Tang, *J. Am. Chem. Soc.* **2010**, *132*, 8874-8875.
18. J. Massey, K. N. Power, I. Manners and M. A. Winnik, *J. Am. Chem. Soc.* **1998**, *120*, 9533-9540.
19. S. E. Bowles, W. Wu, T. Kowalewski, M. C. Schalnat, R. J. Davis, J. E. Pemberton, I. Shim, B. D. Korth and J. Pyun, *J. Am. Chem. Soc.* **2007**, *129*, 8694-8670.
20. G. R. Whittell and I. Manners, *Adv. Mater.* **2007**, *19*, 3439-3468.
21. T. Gadt, N. S. Ieong, G. Cambridge, M. A. Winnik and I. Manners, *Nat. Mater.* **2009**, *8*, 144-150.
22. X. S. Wang, G. Guerin, H. Wang, Y. S. Wang, I. Manners and M. A. Winnik, *Science* **2007**, *317*, 644-647.
23. L. Lu, H. Fan, B. G. Li and S. P. Zhu, *Indust. Chem. Res.* **2009**, *48*, 8349-8355.
24. C. S. Kim, S. Lee, L. L. Tinker, S. Bernhard and Y. L. Loo, *Chem. Mater.* **2009**, *21*, 4583-4588.
25. A. Jaworskaaugustyniak and J. Wojtczak, *Transit. Metal. Chem.* **1987**, *12*, 167-171.
26. D. A. Foucher, B. Z. Tang and I. Manners, *J. Am. Chem. Soc.* **1992**, *114*, 6246-6248.
27. F. S. Arimoto and A. C. Haven, *J. Am. Chem. Soc.* **1955**, *77*, 6295-6297.
28. Herberic.Ge, E. Bauer and Schwarze.J, *J. Organomet. Chem.* **1969**, *17*, 445-452.
29. J. E. Sheats and M. D. Rausch, *J. Org. Chem* **1970**, *35*, 3245-&.
30. L. X. Ren, C. G. Hardy, S. F. Tang, D. B. Doxie, N. Hamidi and C. B. Tang, *Macromolecules* **2010**, *43*, 9304-9310.
31. W. Ong and A. E. Kaifer, *Organometallics* **2003**, *22*, 4181-4183.
32. B. Alonso, P. G. Armada, J. Losada, I. Cuadrado, B. Gonzalez and C. M. Casado, *Biosensors & Bioelectronics* **2004**, *19*, 1617-1625.
33. P. D. Beer, D. Hesek, J. E. Kingston, D. K. Smith, S. E. Stokes and M. G. B. Drew, *Organometallics* **1995**, *14*, 3288-3295.
34. N. G. Connelly and W. E. Geiger, *Chem. Rev.* **1996**, *96*, 877-910.
35. F. Noor, A. Wustholz, R. Kinscherf and N. Metzler-Nolte, *Angew. Chem. Int. Ed.* **2005**, *44*, 2429-2432.
36. C. M. Casado, B. Gonzalez, I. Cuadrado, B. Alonso, M. Moran and J. Losada, *Angew. Chem. Int. Ed.* **2000**, *39*, 2135-2138.
37. G. A. Yu, Y. Ren, J. T. Guan, Y. Lin and S. H. Liu, *J. Organomet. Chem.* **2007**, *692*, 3914-3921.
38. G. Laus, H. Schottenberger, K. Wurst, R. H. Herber and U. Griesser, *J. Phys. Chem. B* **2004**, *108*, 5082-5087.
39. C. U. Pittman, O. E. Ayers, S. P. Mcmanus, J. E. Sheats and C. E. Whitten, *Macromolecules* **1971**, *4*, 360-362.
40. C. U. Pittman, O. E. Ayers, Suryanar.B, S. P. Mcmanus and J. E. Sheats, *Makromol. Chem.* **1974**, *175*, 1427-1437.

41. U. F. J. Mayer, J. B. Gilroy, D. O'Hare and I. Manners, *J. Am. Chem. Soc.* **2009**, *131*, 10382-10383.
42. J. B. Gilroy, S. K. Patra, J. M. Mitchels, M. A. Winnik and I. Manners, *Angew. Chem. Int. Ed.* **2011**, *50*, 5851-5855.
43. L. X. Ren, J. Y. Zhang, X. L. Bai, C. G. Hardy, K. D. Shimizu and C. B. Tang, *Chem. Sci.* **2012**, *3*, 580-583.
44. L. X. Ren, J. Y. Zhang, C. G. Hardy, S. G. Ma and C. B. Tang, *Macromol. Rapid Comm.* **2012**, *33*, 510-516.
45. H. F. Gao and K. Matyjaszewski, *Prog. Polym. Sci.* **2009**, *34*, 317-350.
46. W. A. Braunecker and K. Matyjaszewski, *Prog. Polym. Sci.* **2008**, *33*, 165-165.
47. L. X. Ren, J. Y. Zhang, C. G. Hardy, D. Doxie, B. Fleming and C. B. Tang, *Macromolecules* **2012**, *45*, 2267-2275.
48. C. G. Hardy, L. X. Ren, T. C. Tamboue and C. B. Tang, *J. Polym. Sci. Pol. Chem.* **2011**, *49*, 1409-1420.
49. C. B. Tang, E. M. Lennon, G. H. Fredrickson, E. J. Kramer and C. J. Hawker, *Science* **2008**, *322*, 429-432.
50. M. Gallei, R. Klein and M. Rehahn, *Macromolecules* **2010**, *43*, 1844-1854.
51. M. Shi, A. L. Li, H. Liang and J. Lu, *Macromolecules* **2007**, *40*, 1891-1896.
52. G. Zotti, G. Schiavon, S. Zecchin and D. Favretto, *J. Electroanal. Chem.* **1998**, *456*, 217-221.
53. J. Lorans, F. Pierre, L. Toupet and C. Moinet, *Chem. Commun.* **1997**, *28*, 1279-1280.

CHAPTER 3

QUANTITATIVE AND QUALITATIVE COUNTERION EXCHANGE IN CATIONIC METALLOCENE POLYELECTROLYTES [†]

[†] J. Zhang, P. Pellechia, J. Hayat, C. Hardy and C. Tang, *Macromolecules* **2013**, *46*, 1618-1624. Reprinted here with permission of publisher.

3.1 ABSTRACT

Quantitative analysis of counterion exchange was carried out in cationic cobaltocenium-containing polyelectrolytes by diffusion NMR, which determined molar fractions of free and complexed ions as well as ion-exchange constant. Qualitative impact of counterion-exchange on macromolecular conformation was directly observed from cobaltocenium-containing molecular brushes.

3.2 INTRODUCTION

Charged polymers, or polyelectrolytes have been widely used in many industrial applications, such as polyelectrolyte multilayers,[1-2] water treatment[3-4] and high charge density batteries[5]. Among these applications, the utilization of counterions plays crucial roles on many aspects of their polyelectrolytes, including chemical, electrical and mechanical properties.[6-9] Metallocene-containing polyelectrolytes, mostly based on ferrocene, show many unique properties in redox chemistry, therapeutics encapsulation and release, molecular electronics, sensing and medicinal chemistry (e.g. use as prodrugs). Mostly often this class of polyelectrolytes combines neutral metallocene as functional building block with external ionic groups, thus limiting the direct impact on tuning metallocene properties. Cationic metallocene such as cobaltocenium and rhodocenium possesses intrinsic cationic metal centers coupled with counterions. The control of counterions is expected to directly tune the properties such as the strength of association/dissociation, electrostatic Coulomb interaction and hydrophobicity/hydrophilicity. However, in either scenario, a quantitative analysis of counterion exchange has been rarely explored.

After almost half-century hibernation, cationic cobaltocenium-containing polyelectrolytes have recently attracted attention, as they show extraordinary stability to maintain the vital sandwiched structures, unique counterion-dependent solubility,[10-14] and are used as versatile candidates in electrocatalytic films, gene delivery and templates for functional inorganic materials.[15] Among these applications, the utilization of counterion exchange for cobaltocenium-containing polymers receives special attention and allows for the preparation of amphiphilic diblock copolymers,[16] ion shuttles,[17] molecular capsules[18] and DNA cooperation[19].

To afford a rational foundation for these applications, herein we report the first quantitative analysis on counterion exchange of cationic metallocene polyelectrolytes (**Scheme 3.1**). Specifically, we target on cobaltocenium-containing polyelectrolytes using diffusion nuclear magnetic resonance (NMR) technique as a main tool to precisely determine the level of counterion association and dissociation with the metal center and their association constant. To directly observe the counterion exchange effect on these polyelectrolytes, we prepared the first cobaltocenium-containing molecular brushes, whose counterion-dependent morphologies were directly imaged by atomic force microscopy (AFM).

Scheme 3.1. Counterion exchange of cobaltocenium-containing polyelectrolytes.

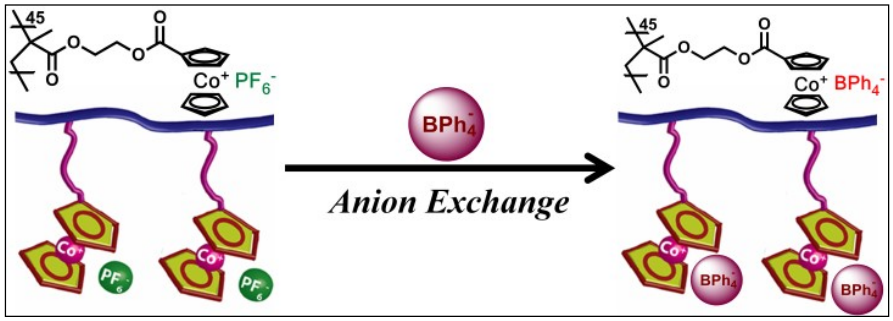

3.3 RESULTS AND DISCUSSION

To perform a quantitative study, diffusion NMR based on the bipolar pulse longitudinal eddy current delay pulse sequence (BBP-LED)[20-21] was used to investigate the association/dissociation behaviors between cobaltocenium-containing polymers and their counterions by measuring their diffusion coefficients. Qualitative counterion exchange on cobaltocenium-containing monomers and polymers have been reported.[10, 22] Due to the obvious difference in the hydrodynamic radii of polymers and free counterions, a significant increase of diffusion coefficient for counterions would be observed if the counterions dissociate from cobaltocenium cations on polymers. Thus, an experiment was designed by gradually increasing the amount of sodium tetraphenylborate ($NaBPh_4$) in cobaltocenium-containing polymer solution (with hexafluorophosphate (PF_6) as counterions) (**Scheme 3.1**). We chose poly(2-(methacrylolyoxy)ethyl cobaltoceniumcarboxylate hexafluorophosphate) ($PMAECoPF_6$), which was prepared by reversible addition−fragmentation chain transfer polymerization (RAFT) according to our early work. The diffusion coefficients of cobaltocenium polymers, BPh_4 and PF_6 anions were measured by ^1H (cyclopentadienyl protons), ^1H (phenyl protons) and ^{19}F diffusion NMR in acetonitrile respectively, as shown in **Figure 3.1**, **Figure 3.4** and **Table 3.1**. When the amount of BPh_4 anions was gradually increased in polymer solution, an uptrend of diffusion coefficient for PF_6 was observed (**Figure 3.1**). Considering the increase of BPh_4 anions in solution, PF_6 anions were continuously exchanged with BPh_4, resulting in more PF_6 to be released from polymer and therefore an increase of diffusion coefficient. Besides, a slight upfield shift of fluorine signal was also observed. It was

probably led by the environmental change of PF_6 anions due to their dissociation from cobaltocenium cations, further indicating the occurrence of ion exchange.

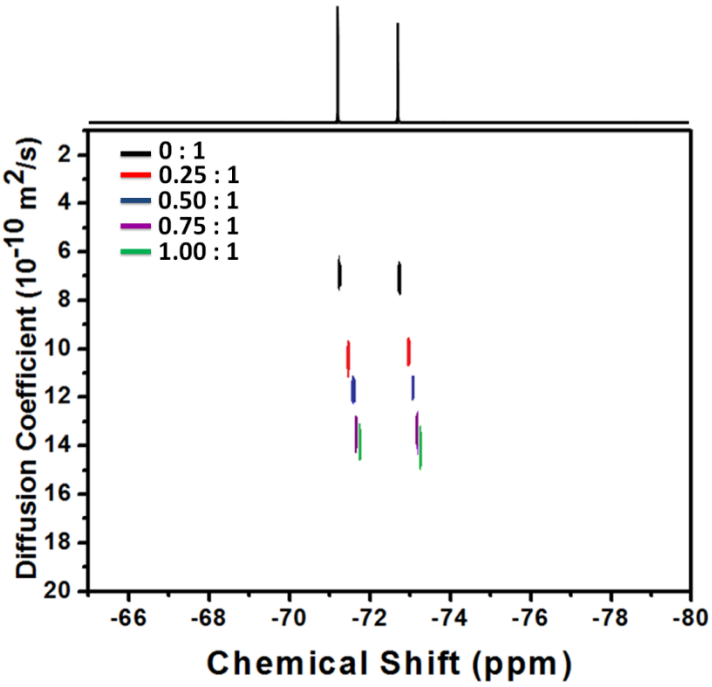

Figure 3.1. ^{19}F diffusion NMR spectra (DOSY processed and overlayed) for PF_6 anions in PF_6-BPh_4 ion-exchange experiment. The doublet centered at about -72 ppm was from fluorine of PF_6 anions. The ratios in graph represented the molar ratios of BPh_4 to PF_6 anions in each sample (The amount of PF_6 anions was 1.02×10^{-2} mmol in each sample, calculated from the weight of PMAECoPF_6 polymers in samples.)

According to these diffusion coefficients in **Table 3.1**, molar fractions of free ions and polymer-bound ions can be determined using **Equation (3.1)** with the assumption that the diffusion coefficients of small counterions would be the same with polymers if they associate with large polymers:[23-25]

$$D_{mean} = x \times D_{bound} + (1-x) \times D_{free} \qquad \textbf{Equation } (3.1)$$

where, x is the molar fraction of counterions bounded with polymers. $\boldsymbol{D}_{free}$ and $\boldsymbol{D}_{bound}$ are the diffusion coefficients for counterions dissociated and associated with

polymers respectively. The apparent D_{mean} is the weight-average diffusion coefficient of D_{free} and D_{bound}. According to the above assumption,[23-25] D_{bound} is the same as polymers and can be measured by diffusion ^{1}H NMR. According to **Table 3.1** and **Equation 3.1**, the molar fractions of associated and dissociated anions are summarized in **Table 3.2**.

$$[PMAECoPF_6]+[BPh_4] \Leftrightarrow [PMAECoBPh_4]+[PF_6] \qquad \textbf{Equation (3.2)}$$

$$K_e = \frac{[PMAECoBPh_4]\times[PF_6]}{[PMAECoPF_6]\times[BPh_4]} \qquad \textbf{Equation (3.3)}$$

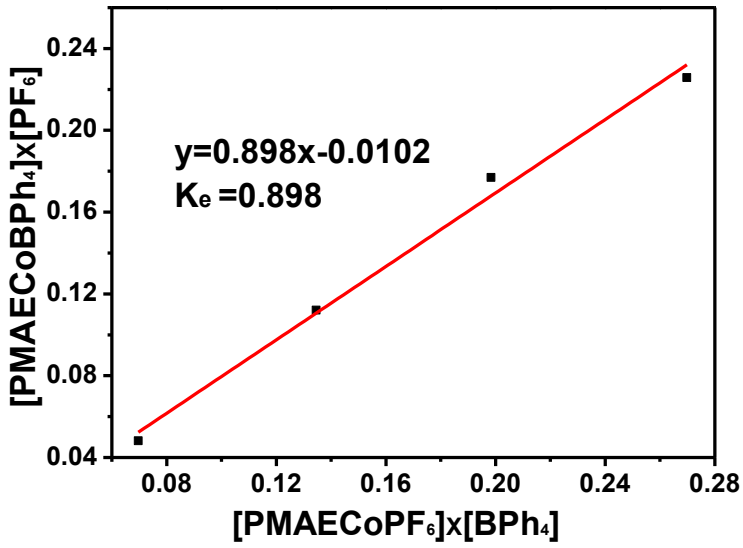

Figure 3.2. A plot to determine counterion exchange constant. The slope shows the constant: K_e=0.898.

The counterion exchange process is described by **Equation (3.2)**, where [PMAECoPF$_6$] and [PMAECoBPh$_4$] are molar fractions of PF$_6$ and BPh$_4$ anions associated with polymers, while [PF$_6$] and [BPh$_4$] are those of dissociated free anions. The anion exchange constant could be determined by **Equation (3.3)**. Based on the data in Table S2, [PMAECoPF$_6$]×[BPh$_4$] was plotted against [PMAECoBPh$_4$]×[PF$_6$]. As shown in **Figure 3.2**, there was a linear relationship observed. The slope of this plot,

equal to 0.898, represented the anion exchange constant, as described in **Equation (3.3)**. This constant was close to 1.0, indicating that PF_6 and BPh_4 anions have very similar association strength to complex with cobaltocenium cations and should have nearly equal exchange with each other in acetonitrile solvent.

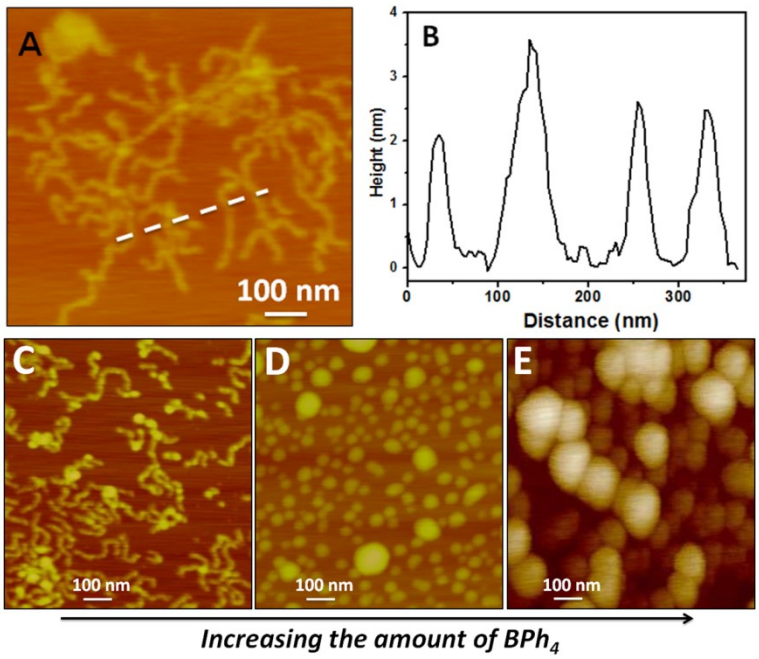

Figure 3.3. (A) AFM height image and (B) height profile for cobaltocenium-containing molecular brush with PF_6 anion; AFM height images for molecular brush with different molar ratios of BPh_4 and PF_6 anions: (C) 0.1 : 1.0 (D) 0.25 : 1.0 (E) 1.0 : 1.0.

The above quantitative analysis indicated that the exchange from small PF_6 and bulky BPh_4 anions might impart significant conformational change to cobaltocenium-containing polymers. Therefore, we designed an experimental system aiming to directly observe such effect. Considering the high grafting density of cobaltocenium cations and unique nanoscale unimolecular morphology with high persistence length, such cobaltocenium-containing molecular brushes may show a sensitive and drastic response toward anion exchange. In addition, molecular brushes could be imaged directly by

microscopy techniques due to their nanoscale sizes. We prepared the first cationic cobaltocenium-containing molecular brushes and studied their morphological response to the exchange of counterions. A cobaltocenium-containing brush polymer was synthesized *via* a 'graft from' technique by a combination of ring-opening metathesis polymerization (ROMP) and RAFT, as shown in **Scheme 3.2**. Norbornene-functionalized chain transfer agent was first synthesized to be used as monomer **1** (**Scheme 3.3**), which was polymerized by ROMP to produce the brush polymer backbone **2**. Then, a cobaltocenium-containing methacrylate monomer with PF_6 counterion MAECoPF6 was polymerized from the backbone *via* RAFT, yielding the final molecular brush **3**. ^{1}H NMR spectra (**Figure 3.5, 3.7** and **3.8**) coupled with many other characterizations of **1**, **2** and **3** demonstrated the successful execution for each synthetic step. These brushes were then dissolved in acetonitrile. A series of diluted solutions were drop-cast onto mica substrates. Tapping-mode AFM was subsequently used to image the morphologies of cobaltocenium-containing molecular brushes (**Figure 3.3**).

The molecular brush **3** deposited from pure acetonitrile exhibited an extended wormlike morphology with an average of height at 2.7 nm, very similar to many other molecular brushes,[1] primarily due to long persistent length imparted from densely grafted side chains. With the addition of BPh_4 anions into solution of these cobaltocenium-containing brushes, a conformational transition and change was clearly observed. As shown in Figure 3C, a more condensed, though still wormlike conformation was formed when only 10mol% BPh_4 anion (compared to overall PF_6 anion) was added. A sharp transition from wormlike morphology to spherical nanoparticles was observed when the amount of BPh_4 anion increased to 25mol% (**Figure 3.3D**). However, large aggregates

with an average of height at 17.1 nm were formed when BPh_4 was increased to 100mol%, compared to PF_6 anions (Figure **3.3E**). The gradual change of height profiles of these molecular brushes at different stages further confirmed that these brushes contracted, condensed and collapsed with the addition of bulky BPh_4 anions. According to a previous report,[22] acetonitrile is a good solvent for cobaltocenium-containing polymers with PF_6 anion, but a relatively poor solvent for polymers with BPh_4 anion. The exchange from PF_6 to BPh_4 would change solubility of these molecular brushes and thus enable them to respond by changing their conformation. Such change in morphology of molecular brushes in response to counterions is proposed in **Scheme 3.2B**.

Scheme 3.2. Synthesis of cationic cobaltocenium-containing molecular brushes and their proposed conformational response to counterion exchange.

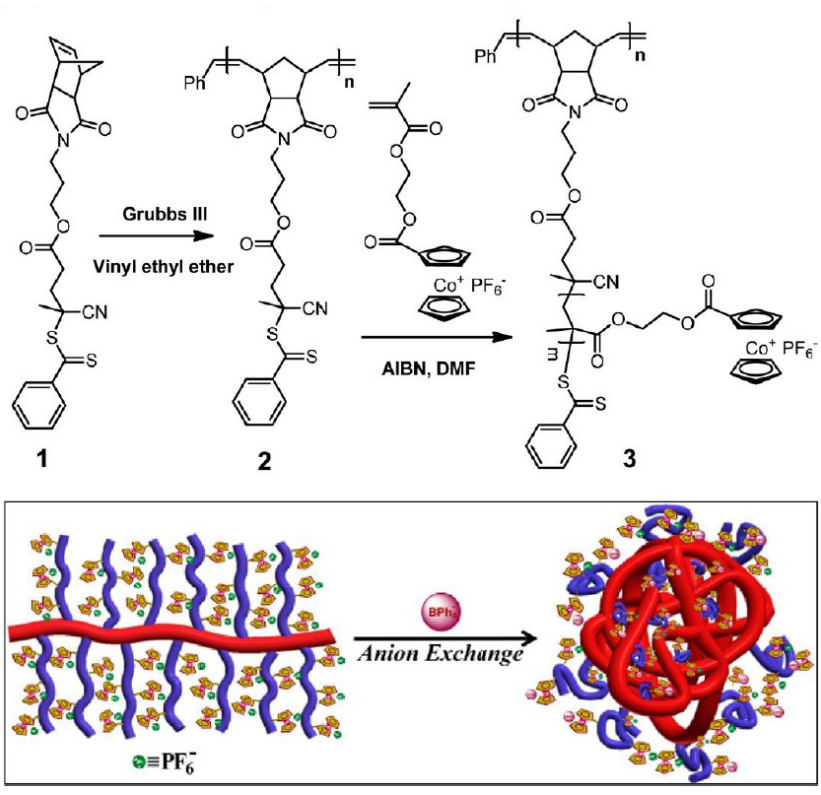

Table 3.1. Diffusion constant measured by ^{1}H and ^{19}F diffusion NMR at different ratios of BPh_4 to PF_6.

[BPh_4]/[PF_6]	D_{bound} **a**	D_{mean} **for BPh_4** **b**	D_{mean} **for PF_6** **c**
0.25 : 1	2.09×10^{-10} m^2/s **d**	6.16×10^{-10} m^2/s	9.77×10^{-10} m^2/s
0.50 : 1	2.00×10^{-10} m^2/s	6.61×10^{-10} m^2/s	11.7×10^{-10} m^2/s
0.75 : 1	2.05×10^{-10} m^2/s	7.16×10^{-10} m^2/s	13.5×10^{-10} m^2/s
1.00 : 1	2.00×10^{-10} m^2/s	7.74×10^{-10} m^2/s	14.4×10^{-10} m^2/s

a. $\boldsymbol{D}_{bound}$ is the diffusion coefficient for associated counterions, directly obtained from the diffusion coefficients of polymers;
b. $\boldsymbol{D}_{mean}$ is the average of diffusion coefficients for all counterions (dissociated and associated);
c. In the same polymer solution without $NaBPh_4$, the diffusion coefficients for PF_6 and polymers were also measured, which were 7.24 $\times10^{-10}$ m^2/s and 2.51 $\times10^{-10}$ m^2/s;
d. All diffusion coefficients were normalized by using diffusion coefficients of H_2O as internal standard.

Table 3.2. Normalized molar fractions for associated or dissociated BPh_4, PF_6 anions under different ratios of BPh_4 to PF_6.

[BPh_4]/[PF_6]	**0.25:1**	**0.50:1**	**0.75:1**	**1:1**
[$PMAECo^+BPh_4^-$] **a**	0.146 **c**	0.270	0.361	0.426
Free [BPh_4^-] **b**	0.104	0.230	0.389	0.574
[$PMAECo^+PF_6^-$] **a**	0.670	0.585	0.510	0.470
Free [PF_6^-] **b**	0.330	0.415	0.490	0.530

a. [PMAECo^{+}BPh$_4^{-}$] and [PMAECo^{+}PF$_6^{-}$] were the fractions of BPh$_4$, PF$_6$ anions associated with polymers;

b. [BPh$_4^{-}$] and [PF$_6^{-}$] were the molar fraction of free anion. Diffusion coefficients for free BPh$_4$ and PF$_6$ anions in acetonitrile were measured by ^{1}H and ^{19}F diffusion NMR, which were 12.0×10^{-10} m^2/s and 25.64×10^{-10} m^2/s respectively, similar to those in previous reports after correction; [26-27]

c. All the fractions were normalized by setting the total amount of PF$_6$ anions as 1.00.

Scheme 3.3. Synthesis of norbornene-functionalized chain transfer agent **1**.

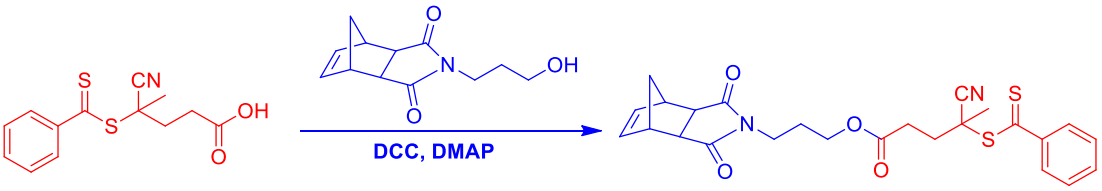

1

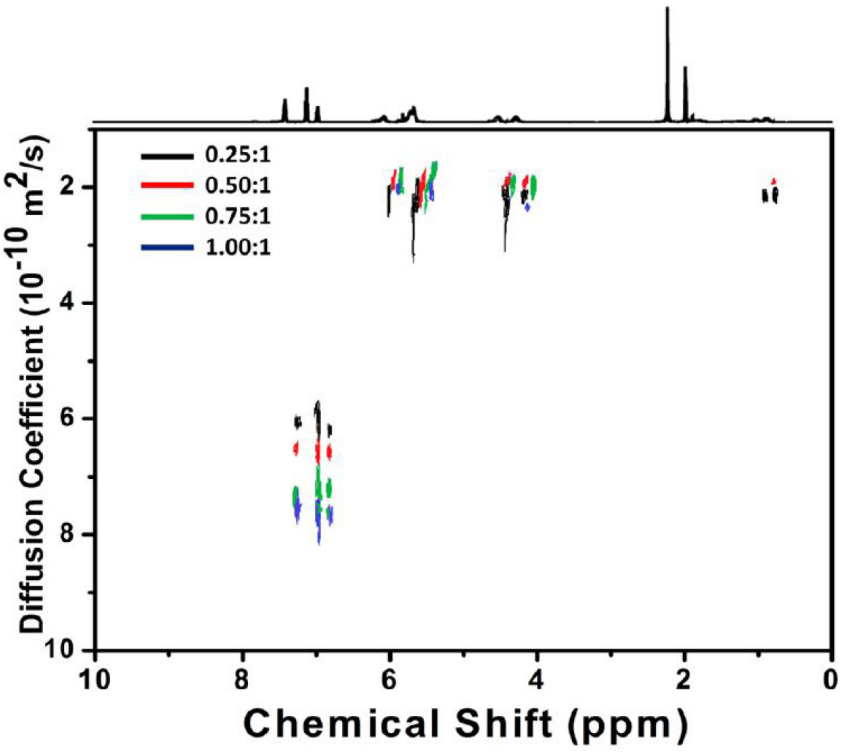

Figure 3.4. ^{1}H diffusion NMR spectra overlayed for cobaltocenium-containing polymers PMAECoPF$_6$ and BPh$_4$ anions. ^{1}H NMR spectra showed peaks at 5.75~6.20 ppm, 4.40 ppm, 4.61ppm and 0.80~1.10ppm from cobaltocenium polymers and peaks at 6.90~7.30 ppm were from BPh$_4$ anions. The ratios in the spectrum represented the molar ratios of BPh$_4$: PF$_6$ in each sample.

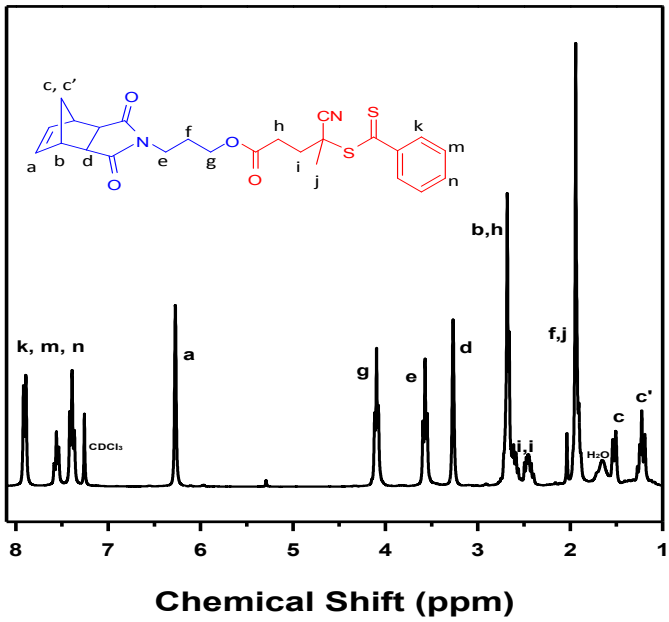

Figure 3.5. ^{1}H NMR spectrum for compound **1** in $CDCl_3$.

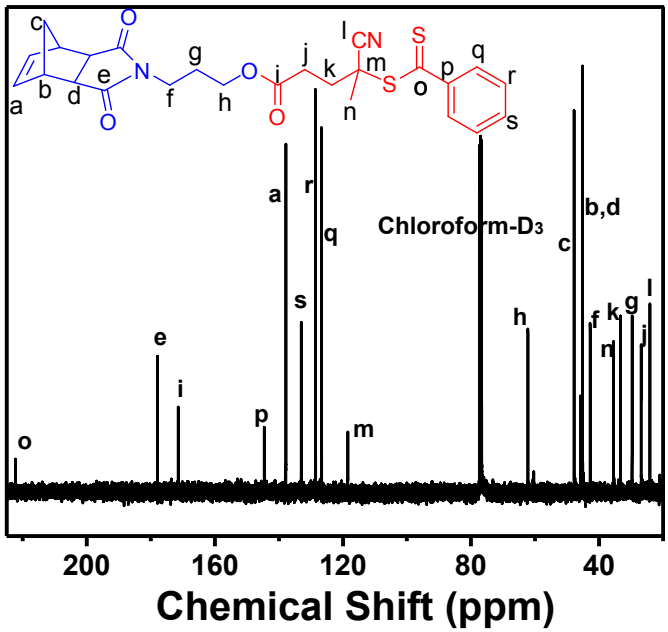

Figure 3.6. ^{13}C NMR spectrum for compound **1** in $CDCl_3$.

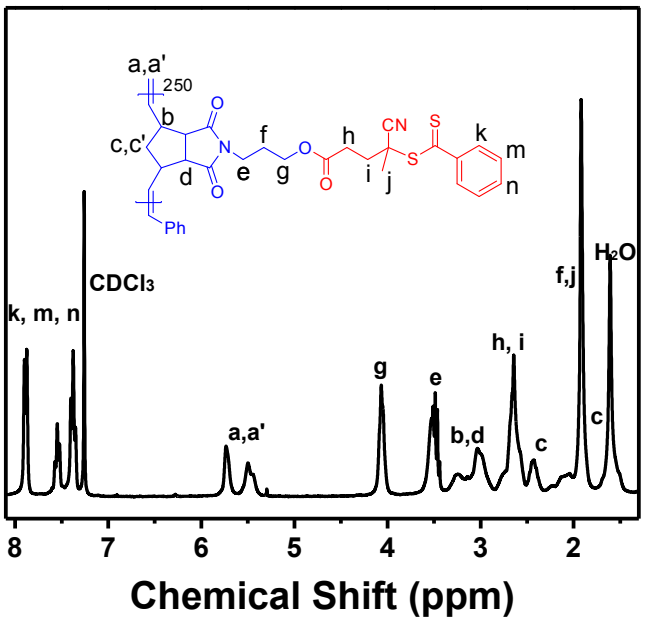

Figure 3.7. ^{1}H NMR spectrum for polymer **2** in $CDCl_3$.

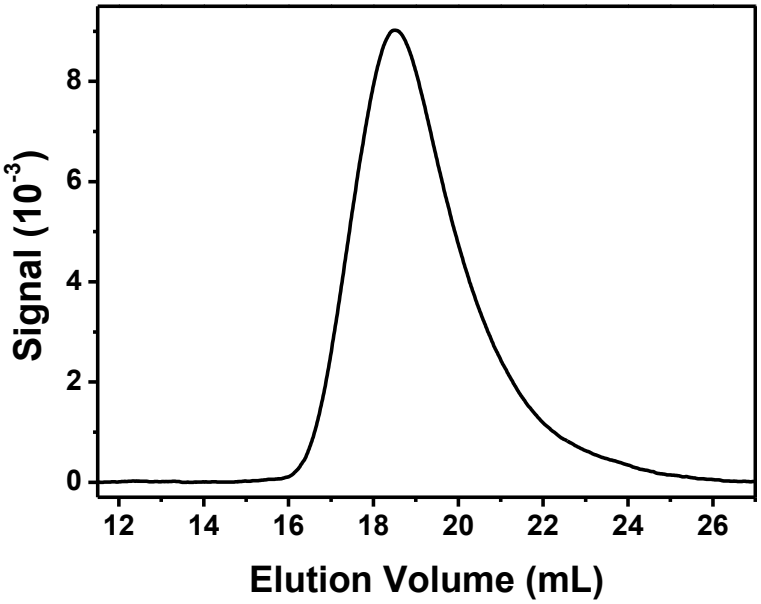

Figure 3.8. GPC trace for polymer **2**.

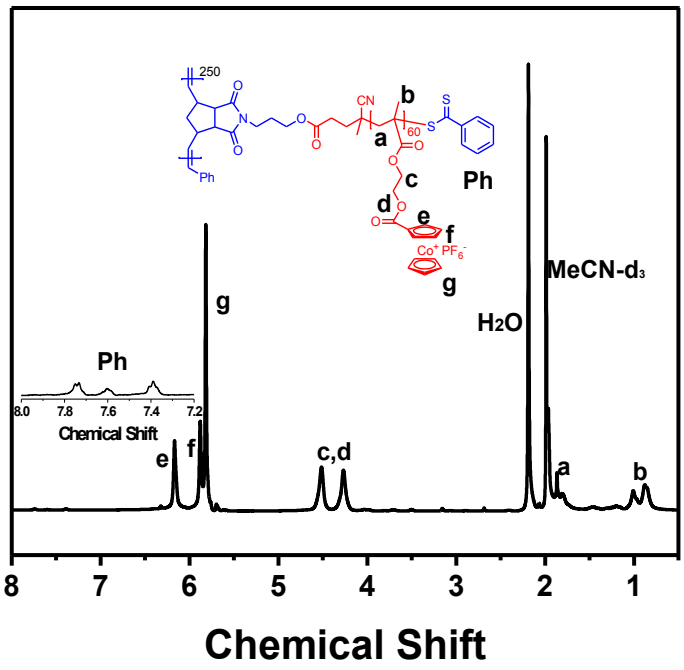

Figure 3.9. ^{1}H NMR spectrum for cobaltocenium-containing molecular brush **3** in acetonitrile-d_3. Insert: Phenyl protons from end groups.

3.4 EXPERIMENTAL

Materials. 4-Cyano-4-(phenylcarbonothioylthio) pentanoic acid (97%, CPPA) and ethyl vinyl ether (99%) were purchased from Aldrich, and used directly. Monomer (2-(methacrylolyoxy)ethyl cobaltoceniumcarboxylate hexafluorophosphate) ($MAECoPF_6$), side-chain cobaltocenium-containing methacrylate polymers ($PMAECoPF_6$, M_n = 22,000 g/mol, Mw/Mn= 1.24) and *N*-[3-hydroxylpropyl]-*cis*-5-norbornene-*exo*-2,3-dicarboximide (NPH) were synthesized according to our earlier reports.[14, 28] Grubbs catalyst, 3rd generation, was synthesized following a procedure reported in literature.[29] *N,N*-dimethylformamide (DMF) was dried and freshly distilled. Sodium tetraphenylborate (99%, $NaBPh_4$, Alfa Aesar) was used as received. All other reagents were from commercial sources and used as received.

Characterization. ^{1}H NMR (400 MHz) spectra were recorded on a Varian Mercury 400 MHz spectrometer with tetramethylsilane (TMS) as an internal reference. Diffusion NMR (bipolar pulse longitudinal eddy current delay, BBP-LED) experiments were carried out without spinning and under ambient temperature (298K).[30] A 500 MHz Bruker Avance III-HD spectrometer with a microprocessor-controlled gradient unit and a multinuclear probe with an actively shielded Z-gradient coil were used for all diffusion measurements. With duration of 1.00 ms, sine shaped gradient pulses were used in the experiments. In both the ^{1}H and ^{19}F BBP-LED experiments, the diffusion delay was set to 100 ms. The number of scans was set at 8 per increment with a recovery delay of 2s. All the spectra were acquired using 16 K points with a line broadening of 1 Hz. ^{1}H spectral width was -11.00 ppm and centered at 5.00 ppm, while ^{19}F window was 25 ppm with a center at -70 ppm. All spectra were processed with Bruker Topspin (version 3.2) using the standard DOSY routine to determine the diffusion coefficients. 16 spectra were collected with a range of 95% to 5% of the maximum gradient strength for each regression analysis. All diffusion coefficient measurements used H_2O as internal reference. Atomic force microscopy (AFM) was conducted on a Nanoscope V Multimode instrument, operating under tapping mode with a certain type of AFM tips (150KHz, 5N/m, length: 125 μm). . Polymer solutions in acetonitrile were drop-cast onto fresh-cleaved mica substrates. The samples were visualized by AFM after dryness. Gel permeation chromatography (GPC) was performed in 1% LiBr DMF solution at a flow rate of 0.8 mL/min on a Varian system equipped with a ProStar 210 pump and a Varian 356-LC RI detector and three Phenogel 5μ columns with narrow dispersed polystyrene as standards.

^{1}H and ^{19}F Diffusion NMR (BBP-LED) measurement for PF_6 and BPh_4. The counterion exchange between PF_6 and BPh_4 was studied *via* a titration experiment. 5.00 mg PMAECoPF_6 (1.02×10^{-2} mmol) was dissolved in 0.55 mL acetonitrile-d_3. 10.00 μL $NaBPh_4$ solution (2.55×10^{-3} mmol in acetonitrile-d_3) was then added to the polymer solution. The sample was then monitored by diffusion NMR. The diffusion coefficients for polymer and BPh_4 anion were recorded *via* ^{1}H diffusion NMR (**Figure 3.4**), while the PF_6 anion diffusion coefficient was monitored *via* ^{19}F diffusion NMR. Three other samples with different ratios of BPh_4 to PF_6 were measured by diffusion NMR. The diffusion coefficients are listed in **Table 3.1**.

Synthesis of *N*-[4-cyano-4-(phenylcarbonothioylthio) pentanoate]-*cis*-5-norbornene-*exo*-2, 3-dicarboximide (1). The norbornene-functionalized chain transfer agent **1** was synthesized *via* an esterification reaction between NPH and CPPA (**Scheme 3.3**). CPPA (0.600 g, 2.10 mmol), NPH (0.620 g, 2.80 mmol) and 4-dimethylaminopyridine (0.042 g, 0.34 mmol) were dissolved in dry dichloromethane (DCM) and cooled to 0 °C. Dicyclohexylcarbodiimide (0.440 g, 2.14 mmol) was first dissolved in 5 mL DCM and then added dropwise into reaction over 15 min. The reaction was stirred under room temperature for 24 hours. The solution was concentrated and then separated by column chromatograph (silica gel, eluent: ethyl acetate/hexane=4/6). The product was collected, concentrated and vacuum dried to give a viscous red compound (yield: 65%, 0.65g). ^{1}H NMR (**Figure 3.5**) ($CDCl_3$, δ, ppm): 7.90 (d, Ph, 2H), 7.55 (t, Ph, 2H), 7.41 (t, Ph, 2H), 6.24 (s, C*H*=C*H*, 2H), 4.11 (t, COOCH_2, 2H), 3.57 (t, NC$H_2$$CH_2$, 2H), 3.23 (t, C*H*CON, 2H), 2.72 (m, CH_2C*H*CH, CH_2COO, 4H), 2.49 and 2.52 (m, CH_2CH_2C, 2H), 1.96 (m, CH_2C$H_2$$CH_2$O, CNCC$H_3$, 5H), 1.50 and 1.23 (m, CHCH_2CH,

2H). ^{13}C NMR (**Figure 3.6**) ($CDCl_3$, δ, ppm): 221 (*C*=S), 177.9 (CH*C*ON), 171.4 (O*C*OCH_2), 144.5 (Ph), 137.8 (*C*H_2CHCH), 125-135 (Ph), 118.5 (*C*N), 62.2 (CH_2*C*H_2O), 47.8 (CH*C*H_2CH), 45.7 (CH_2*C*HCH), 45.2 (CH*C*HCO), 42.8 (N*C*$H_2$$CH_2$), 35.5 (*C*$CH_3$), 33.3 (C*C*$H_2$), 29.2 ($CH_2$*C*$H_2$$CH_2$), 26.8 (CO*C*$H_2$), 24.1 (C*C*$H_3$).

Synthesis of poly(*N*-[4-cyano-4-(phenylcarbonothioylthio) pentanoate]-*cis*-5-norbornene-*exo*-2,3-dicarboximide) (2) *via* ROMP. 0.10 mL Grubbs III catalyst solution (5.10×10^{-4} mmol in DCM) was charged into 0.5 mL dry DCM. Compound **1** (0.101 g, 0.210 mmol) was dissolved in 0.5 mL dry DCM and then added into reaction. The conversion of monomers was monitored by ^{1}H NMR by comparing the integration of peaks at 6.24 ppm with peaks at 7.40-8.00 ppm. The reaction was stopped after 11 min with a conversion of 63% The mixture was precipitated in diethyl ether three times, vacuum dried to yield red polymers (38 mg, 60%). ^{1}H NMR (**Figure 3.7**) ($CDCl_3$, δ, ppm): 7.94 (d, Ph, 2H), 7.53 (t, Ph, 2H), 7.46 (t, Ph, 2H), 5.50-5.50 (broad, C*H*=C*H*, 2H), 4.12 (t, COOC*H*$_2$, 2H), 3.57 (broad, NC*H*$_2$$CH_2$, 2H), 3.00-3.50 (broad, CH_2C*H*CH, C*H*CON, 4H), 2.70 (broad, C*H*$_2$COO, CH_2C*H*$_2$C, 4H), 2.46 and 1.52 (broad, $CHCH_2CH$, 2H), 1.95-2.05 (broad, CH_2C*H*$_2$$CH_2$O, CNCC*H*$_3$, 5H). Mn (NMR)= 120,500 (D.P.= 250). M_n (GPC) (**Figure 3.8**) = 153,000 g/mol, M_w/M_n= 1.28.

Synthesis of cationic cobaltocenium-containing molecular brush: poly(*N*-[4-cyano-4-(phenylcarbonothioylthio)pentanoate]-*cis*-5-norbornene-*exo*-2,3-dicarboximide)-g-poly(2-(methacrylolyoxy)ethyl cobaltoceniumcarboxylate hexafluorophosphate)) (3) *via* RAFT. The cobaltocenium-containing molecular brush was synthesized by a "graft from" approach using macroinitiator **2**. Polymer **2** (1.65 mg, 1.37×10^{-5} mmol), AIBN (0.17 mg, 1.04×10^{-3} mmol) and cobaltocenium-containing

methylacrylate monomer ($MAECoPF_6$, 0.25 g, 0.512 mmol) were dissolved by 0.35 ml dry DMF in Schlenk flask. The solution was purged by nitrogen gas for 30 min and then placed in 90 ^oC oil bath for 150 min. The conversion was determined from ^1H NMR by comparing the integrations of peaks from 6.10 ppm and peaks at 5.75~6.00 ppm. The polymerization was stopped with monomer conversion at 40%. The reaction mixture was precipitated in DCM three times, vacuum dried to yield yellow polymers (52 mg, 52%). ^1H NMR (**Figure 3.9**) (acetonitrile-d_3, δ, ppm): 6.24 (broad, Cp, 2H), 5.95 (broad, Cp, 2H), 5.81 (broad, Cp, 5H), 4.61 (broad, CH_2CH_2, 2H), 4.42 (broad, CH_2CH_2, 2H), 1.90~2.00 (broad, CH_2C, 2H), 0.80-1.10 (broad, CCH_3, 3H). Mn (^1H NMR)=7,440,500.

Response of molecular brushes toward counterions. Cobaltocenium-containing molecular brush (**3**, 1.0 mg) with PF_6 anions was dissolved in 1.0 mL acetonitrile. The solution was then diluted 20 times to make the polymer brush concentration to 0.05 mg/mL. Four samples were prepared. Each sample had 2 mL diluted polymer brush solution, which contained 2.05×10^{-4} mmol PF_6 anions. Then, four samples were added in 10 μL $NaBPh_4$ solution with different concentrations (0.00, 0.70, 1.75, and 7.00 mg/mL), which made the molar ratio of BPh_4 : PF_6 in each sample at 0 : 1, 0.10 : 1, 0.25 : 1 and 1 : 1 respectively. All samples were then characterized by AFM to investigate the response towards counterions.

3.5 CONCLUSIONS

In conclusion, the exchange of counterions (PF_6 and BPh_4) in cobaltocenium-containing polyelectrolytes was quantitatively studied by diffusion NMR, which determined the level of ions both in the free state and at the complexation and therefore the ion exchange constant. We have designed and prepared cationic cobaltocenium-

containing molecular brushes. The imaging of individual brushes by AFM allowed the direct observation of the impact of counterion exchange on macromolecular conformations. This quantitative approach could provide a foundation to study many other metallocene-based polyelectrolytes and to guide a variety of applications that are involved with ion-exchange.

3.6 ACKNOWLEDGMENT

The support from the University of South Carolina (start-up funds) and National Science Foundation (CHE-1151479) is acknowledged.

3.7 REFERENCES

1. D. T. Haynie, L. Zhang, J. S. Rudra, W. H. Zhao, Y. Zhong and N. Palath, *Biomacromolecules* **2005**, *6*, 2895-2913.
2. Y. H. Kim, Y. M. Lee, J. Park, M. J. Ko, J. H. Park, W. Jung and P. J. Yoo, *Langmuir* **2010**, *26*, 17756-17763.
3. E. N. Peleka and K. A. Matis, *Ind. Eng. Chem. Res.* **2011**, *50*, 421-430.
4. J. A. Lichter, K. J. Van Vliet and M. F. Rubner, *Macromolecules* **2009**, *42*, 8573-8586.
5. M. F. Z. Kadir, S. R. Majid and A. K. Arof, *Electrochim. Acta.* **2010**, *55*, 1475-1482.
6. J. E. Wong, H. Zastrow, W. Jaeger and R. von Klitzing, *Langmuir* **2009**, *25*, 14061-14070.
7. Y. Akgol, C. Cramer, C. Hofmann, Y. Karatas, H. D. Wiemhofer and M. Schonhoff, *Macromolecules* **2010**, *43*, 7282-7287.
8. C. Combellas, F. Kanoufi, S. Sanjuan, C. Slim and Y. Tran, *Langmuir* **2009**, *25*, 5360-5370.
9. J. A. Jaber and J. B. Schlenoff, *Chem Mater* **2006**, *18*, 5768-5773.
10. U. F. J. Mayer, J. B. Gilroy, D. O'Hare and I. Manners, *J Am Chem Soc* **2009**, *131*, 10382-10383.
11. L. X. Ren, C. G. Hardy and C. B. Tang, *J Am Chem Soc* **2010**, *132*, 8874-8875.
12. G. R. Whittell and I. Manners, *Adv. Mater.* **2007**, *19*, 3439-3468.
13. P. Nguyen, P. Gomez-Elipe and M. I, *Chem. Rev.* **1999**, *99*, 1515-1548.
14. J. Y. Zhang, L. X. Ren, C. G. Hardy and C. B. Tang, *Macromolecules* **2012**, *45*, 6857-6863.
15. F. Noor, A. Wustholz, R. Kinscherf and N. Metzler-Nolte, *Angew Chem Int Edit* **2005**, *44*, 2429-2432.

16. L. X. Ren, J. Y. Zhang, C. G. Hardy, S. G. Ma and C. B. Tang, *Macromol Rapid Comm* **2012**, *33*, 510-516.
17. B. K. Bennett, R. G. Harrison and T. G. Richmond, *J Am Chem Soc* **1994**, *116*, 11165-11166.
18. I. Philip and A. E. Kaifer, *J. Org. Chem.* **2005**, *70*, 1558-1564.
19. H. B. Qiu, J. B. Gilroy and I. Manners, *Chem. Commun.* **2012**.
20. P. S. Pregosin, *Prog. Nucl. Mag. Res. Sp.* **2006**, *49*, 261-288.
21. D. H. Wu, A. D. Chen and C. S. Johnson, *J. Magn. Reson. Ser. A* **1995**, *115*, 260-264.
22. L. X. Ren, C. G. Hardy, S. F. Tang, D. B. Doxie, N. Hamidi and C. B. Tang, *Macromolecules* **2010**, *43*, 9304-9310.
23. L. Fielding, *Tetrahedron* **2000**, *56*, 6151-6170.
24. R. Wimmer, F. L. Aachmann, K. L. Larsen and S. B. Petersen, *Carbohyd. Res.* **2002**, *337*, 841-849.
25. J. H. Ma, C. Guo, Y. L. Tang, H. Zhang and H. Z. Liu, *J. Phys. Chem. B.* **2007**, *111*, 13371-13378.
26. A. Moreno, P. S. Pregosin, L. F. Veiros, A. Albinati and S. Rizzato, *Chem-Eur. J.* **2008**, *14*, 5617-5629.
27. D. Schott, P. S. Pregosin, N. Jacques, M. Chavarot, F. Rose-Munch and E. Rose, *Inorg. Chem.* **2005**, *44*, 5941-5948.
28. L. X. Ren, J. Y. Zhang, X. L. Bai, C. G. Hardy, K. D. Shimizu and C. B. Tang, *Chem. Sci.* **2012**, *3*, 580-583.
29. M. S. Sanford, J. A. Love and R. H. Grubbs, *Organometallics* **2001**, *20*, 5314-5318.
30. D. H. Wu, A. D. Chen and C. S. Johnson, *J. Magn. Reson. Ser. A* **1995**, *115*, 260-264.

CHAPTER 4

CHARGED METALLOPOLYMERS AS UNIVERSAL PRECURSORS FOR VERSATILE COBALT MATERIALS [†]

[†] J. Zhang, Y. Yan, M. W. Chance, J. H. Chen, J. Hayat, S. G. Ma and C. Tang, *Angew. Chem. Int. Ed.* **2013**, *52*, 13387-13391. Reprinted here with permission of publisher.

4.1 ABSTRACT

A facile phase transfer ion-exchange strategy was used to prepare cationic cobaltocenium-containing polyelectrolytes with different counterions. These cobalt-containing homopolymers, block copolymers and polymer brushes were used as universal precursors to prepare versatile inorganic cobalt-based materials, including cobalt metal, cobalt phosphide, cobalt monoxide, cobalt-iron alloy and cobalt ferrite. Based on self-assembly of block copolymers and the unique architecture of polymer brushes, cobalt-based nanoparticles and nanowires were conveniently obtained from these nanoscale precursors.

4.2 INTRODUCTION

Inorganic metal-based materials have been widely utilized in catalytic chemistry, life science and engineering.[1-5] Among these metal-related materials, cobalt-related materials, including metallic cobalt,[6-7] cobalt oxide,[8] cobalt alloy[9] and cobalt phosphide[10-11] have been broadly used in magnetic materials, aerospace engineering and energy storage. With the development of modern nanoelectronic technology and the increasing demand for nanostructured materials, [12] the preparation of nanostructured inorganic cobalt-containing materials has become a crucial technological challenge for industry. Various methods have been developed to prepare nanoscale inorganic cobalt-containing materials, including electrodeposition,[13] polymeric precursor synthesis,[14-16] solvothermal/hydrothermal methods,[11, 17] and sol/gel precipitation.[18-19] Among them, the utilization of metal-containing polymer precursors to prepare nanostructured cobalt-based materials has been broadly used particularly used due to many distinguished advantages, including controlled molecular weight and architectures from well-

established controlled/living synthetic methods, various morphologies from polymer self-assembly[20] and facile manipulation of polymers.[21-23] As a result, various types of metal-containing polymer precursors, such as polymer thin films, micelles and fibers, have been designed and utilized for funtional inorganic materials.[14-16]

However, metal-containing polyelectrolytes or charged metallopolymers were much less studied as precursors to prepare inorganic metal-based materials.[24-26] Compared with neutral metal-containing polymers, the existence of counterions in charged metallopolymers has several advantages as novel precursors, such as ion-dependent solubility,[27-28] ion-induced self-assembly[29] and various chemical elements. Thus these polyelectrolytes could be 'universal' precursors for access to multifunctional inorganic materials. Unfortunately, it is challenging to perform facile exchange of counterions for charged metallopolymers. Most studies have been limited to specific systems (usually small molecules[30] or super-macromolecules[31]), thus severely restricting the diversity of charged metallopolymers .

Phase transfer has been applied in various organic reactions[32] and utilized in applications such as ionic self-assembly,[33-34] heterogeneous catalysts[32, 35] and ionic liquids.[36-37] However, the utilization of phase transfer to tune metal-associated counterions for charged metallopolymers is much less explored.[29, 34] We have recently demonstrated ion exchange between hexafluorophosphate (PF_6^-) and tetraphenyl borate (BPh_4^-) ions in cationic cobaltocenium-containing monomers/polymers, which was clearly a phase transfer-driven reaction.[28, 38] But this specific reaction was only limited for BPh_4^- anions. It is still challenging to apply a powerful technique to access other types of counterions for cobaltocenium-containing polymers.

Herein, we report a facile phase transfer ion-exchange method to prepare cationic cobaltocenium-containing polyelectrolytes with diverse counterions *via* the use of tetrabutylammonium salts (**Scheme 4.1**). These cobalt-containing polyelectrolytes were further utilized as a class of 'universal' precursors to prepare versatile inorganic cobalt materials (**Scheme 4.2**). Cobalt monoxide, cobalt metal and cobalt phosphide were obtained from the same polymeric frameworks by simply changing the counterions. Furthermore, diverse cobalt nanomaterials (including nanoparticles and 1D nanowires) were produced by integrating these polyelectrolytes into nanoscale precursors.

Scheme 4.1. Facile phase transfer ion-exchange to prepare cationic cobaltocenium-containing polyelectrolytes with different counterions *via* the use of tetrabutylammonium salts (TBAX, X as anion).

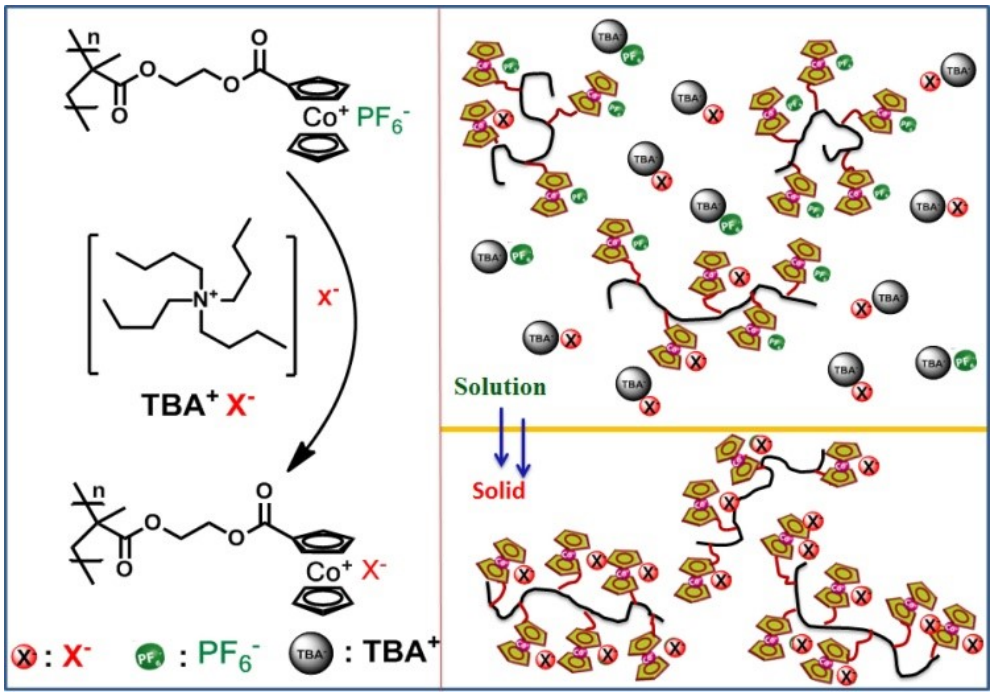

4.3 Results and Discussion

Scheme 4.2. Robust precursors to prepare versatile cobalt-based bulk materials, nanoparticles and 1D nanowires from cationic cobaltocenium-containing homopolymers, block copolymers and polymer brushes.

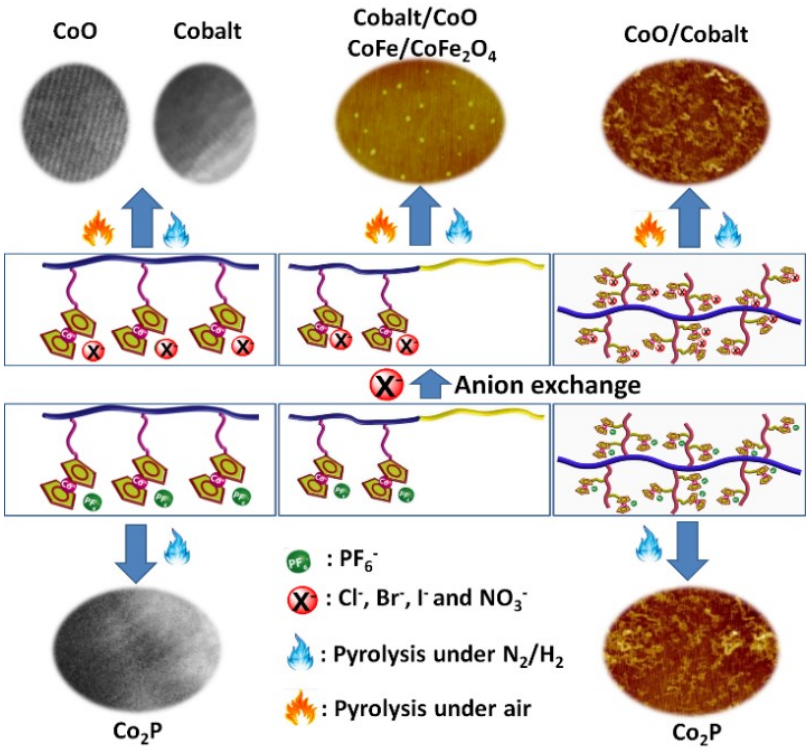

Hexafluorophosphate (PF_6^-) paired cobaltocenium-containing methacrylate polymer, poly(2-(methacrylolyoxy)ethyl cobaltoceniumcarboxylate hexafluorophosphate) (PMAECoPF$_6$, M_n = 22,000 g/mol, M_w/M_n = 1.25), was synthesized according to our previous work.[39] PF_6^--paired cobaltocenium-containing polymers showed good solubility in acetonitrile that is also a good solvent for a variety of tetrabutylammonium salts (TBAX, X as anion). Anion exchange process occurred immediately when PF_6^--paired polymer solution was added into TBAX solution, as shown in **Scheme 4.1**. X anions in TBAX salts firstly diffused into acetonitrile solution and then exchanged with PF_6^- that is associated with the cobaltocenium moiety. Due to the limited solubility of X anion-associated cobaltocenium polymers in acetonitrile, these polymers immediately

precipitated out of the solution. The driving force for quantitative counterion exchange was irreversible phase separation between cobaltocenium-containing polyelectrolytes and the solvent. Due to the strong phase separation, complete ion exchange was achieved in only a few minutes. In comparison, anion exchange for PF_6^--paired cobaltocenium-containing small molecules was limited, probably due to relatively good solubility of X anion-associated small molecules and therefore much-reduced phase separation.

^{19}F (**Figure 4.6**) and ^1H NMR (**Figure 4.7**) spectra demonstrated that several different anions, including F^-, Cl^-, Br^-, I^-, NO_3^- and Ac^-were able to perform quantitative anion exchange with PF_6^--paired cobaltocenium-containing polyelectrolyte *via* TBAX salts. As shown in **Figure 4.6a**, PF_6^--paired polymers had two symmetry peaks centered at -71.5 ppm.[28] After exchanging with TBAF, the obtained F^--paired polymers showed one broad peak at -125.0 ppm and one sharp peak at -129.3 ppm in deuterated water (**Figure 4.6b**), while in deuterated methanol, only one peak was observed at -152.3 ppm (**Figure 4.8**). The peak in D_2O at -125.0 ppm was from fluorine bonded with D_2O and the peak at -129.3 ppm was from free fluoride anions.[40] In addition, no fluorine signal was observed in ^{19}F NMR spectra after exchanging with Cl^-, Br^-, I^-, NO_3^- and Ac^- anions, indicating the complete removal of PF_6^- anions. The general properties of these new cobaltocenium-containing polymers were summarized in **Table 4.1, Figures 4.9, 4.10 and 4.11**). ^1H NMR spectrum (**Figure 4.7**) demonstrated that the exchange processes of Cl^-, Br^-, I^-, and NO_3^- for cobaltocenium-containing polyelectrolytes did not affect the polymer framework.

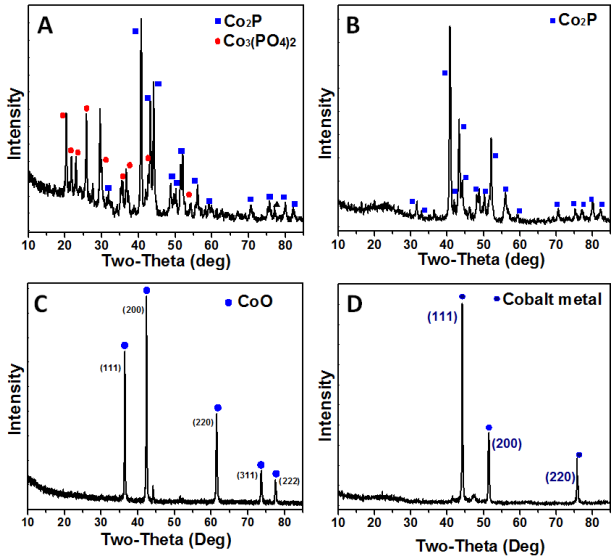

Figure 4.1. XRD patterns for inorganic cobalt-containing materials from cobaltocenium-containing polyelectrolytes with different counterions. (A) UV/Ozonolysis and pyrolysis of PF_6^--paired polymers under air at 800 ^oC; (B) Pyrolysis of PF_6^--paired polymers under H_2/N_2 atmosphere at 800 ^oC; (C) UV/Ozonolysis and pyrolysis of I^--paired polymers under air at 800 ^oC; (D) Pyrolysis of I^--paired polymers under H_2/N_2 atmosphere at 800 ^oC.

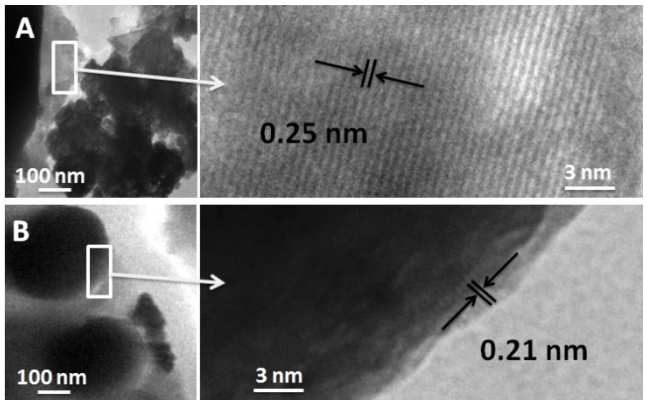

Figure 4.2. TEM images: (A) cobalt monoxide (CoO) and (B) cobalt metal prepared by templating synthesis of cobaltocenium-containing polyelectrolytes with iodide as counterions. Right pictures are HR-TEM images.

The utilization of cobaltocenium-containing polymers as precursors to prepare cobalt-based materials by UV/Ozonolysis and further pyrolysis under air was reported recently.[16] However, the resultant cobalt-containing materials prepared from PF_6^--paired cobaltocenium-containing polymers could not avoid the binding with phosphorus and oxygen to produce a mixture of cobalt-containing materials (**Figure 4.1A**). To obtain

pure inorganic materials, the above PF_6^--paired cobaltocenium-containing homopolymers were directly pyrolyzed at 800 ^oC under reductive H_2/N_2 atmosphere (5v/v% H_2) (**Scheme 4.2**). As shown in Figure 2B, X-ray diffraction (XRD) pattern indicated the formation of high quality of Co_2P, a class of transition-metal phosphides.[10-11],[41] The material was also confirmed by high resolution transmission electron microscopy (HR-TEM) (**Figure 4.12A and 4.12B**) and selected area electron diffraction (SAED) pattern (**Figure 4.12C**). Compared with traditional air sensitive, highly reactive and toxic phosphide precursors to prepare cobalt phosphide,[10, 41] PF_6^--paired cobaltocenium-containing polymers with phosphorus and cobalt elements provide a new and convenient method for preparation of cobalt phosphide.

However, considering the difficulty to remove phosphorus from pyrolyzed products of PF_6^--paired cobaltocenium-containing polymers,[16] synthesis of other cobalt-based materials was still restricted. The phase transfer counterion exchange via TBAX salts offered an opportunity to greatly improving the synthesis of diverse cobalt-containing materials (**Scheme 4.2**). Cl^-, Br^-, I^-, and NO_3^- paired cobaltocenium-containing polymers were prepared as stable precursors *via* TBAX anion exchange. Through UV/Ozonolysis and further pyrolysis in air at 800 ^oC, all of these precursors produced cobalt monoxide, which was confirmed by XRD pattern (**Figure 4.1C**),[42] HR-TEM (**Figure 4.2A**) and SAED pattern (**Figure 4.13A**). However, direct pyrolysis of these anions paired polymers under reductive H_2/N_2 atmosphere (5v/v% H_2) at 800 ^oC led to the formation of cobalt metal, which was also respectively verified by XRD pattern,[43-44] HR-TEM and SAED pattern (**Figure 4.1D, Figure 4.2B and Figure 4.13B**). The composition and yield of inorganic cobalt materials from iodide-paired cobaltocenium-

containing polymers was determined by thermogravimetric analysis (TGA) (**Figure 4.26** and **Table 4.2**). For PF_6-polymers pyrolysis under reductive atmosphere at 800 ^oC, the yield was about 48%. For iodide-paired polymers, the yield was about 38%. While for materials obtained from iodide-polymers under air, the weight percentage of final left materials was decreased to 22%. However, the final left weight percentage should be around 15% if only pure inorganic cobalt compounds were obtained. The higher final left weight percentage should be mostly contributed by carbons due to the large content of carbon in polymers, which was indicated by XRD spectra (**Figure 4.1B** and **Figure 4.1D**, the broad peak at about 24^o).[45] Inductively coupled plasma mass spectrometry (ICP-MS) was further used to characterize the cobalt content in final inorganic materials. As shown in **Table 4.2**, the weight percentage of cobalt element in final materials was around 50% (pyrolysis under air) and 30% (pyrolysis under H_2/N_2) (summarized in **Table 4.2**). These data demonstrated that for final materials, the inorganic cobalt materials were embedded in a matrix. And the matrix was constituted by carbon materials, which were consistent with previous reports. [22, 46]

The simple and robust access to various bulk cobalt-based materials from cobaltocenium homopolymers with different counterions could be further extended to make similar inorganic materials in nanoscale by designing nanostructured precursors (**Scheme 4.3**). PF_6^--paired cobaltocenium-containing diblock copolymers with *tert*-butyl acrylate (tBA) as the second block were synthesized according to our previous work (PMAECoPF$_6$-*b*-PtBA, block ratio: PMAECoPF$_6$:PtBA = 62:43, M_n = 35,800 g/mol).[39] $TBANO_3$ was then used to replace PF_6^- anions by NO_3^- anions. ^1H and ^{19}F NMR spectra (**Figure 4.14**) demonstrated the successful synthesis and counterion exchange. After

exchanging the anions, the PF_6^--paired hydrophobic cobaltocenium block was converted into hydrophilic NO_3^--paired block (PMAECoNO$_3$). With the presence of hydrophobic PtBA block, the new amphiphilic diblock copolymers self-assembled into nanoscale micelles in aqueous solution. As shown in AFM (**Figure 4.3A**) and TEM image (**Figure 4.15**), cobaltocenium-containing diblock copolymers self-assembled into spherical micelles with an average diameter about 70 ± 10 nm. After pyrolysis in air at 800 ^oC, the removal of organic polymer framework and the decomposition of nitrate anions converted the micelles into inorganic cobalt monoxide nanoparticles with a much reduced diameter about 15 ± 5 nm (**Figure 4.3B**).

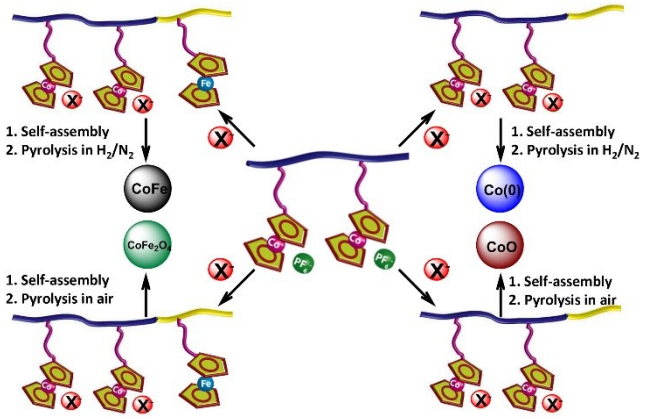

Scheme 4.3. Robust precursors to prepare versatile nanostructured cobalt-based materials via cationic cobaltocenium-containing block copolymer micelles: X^- = Cl^-, Br^-, I^-, and NO_3^-.

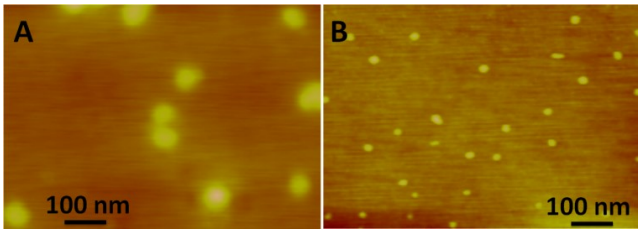

Figure 4.3. AFM height images: (A) micelles before pyrolysis and (B) after pyrolysis under air at 800 ^oC from self-assembled micelles of cobaltocenium-containing diblock copolymers (PMAECoNO$_3$-b-PtBA) in water.

Similar to bulk cobalt-containing materials produced by cobaltocenium-containing homopolymers, PMAECoNO$_3$-*b*-PtBA block copolymer micelles were converted into cobalt monoxide (by UV/Ozonolysis and pyrolysis under air at 800 ºC) or elemental cobalt metal (by pyrolysis under H_2/N_2 atmosphere at 800 ºC) nanoparticles, which were confirmed by XRD (**Figure 4.17A**) and X-ray photoelectron spectroscopy (XPS) (**Figure 4.18**, black curve). For nanoparticles obtained by pyrolysis in air, the XRD pattern indicated the formation of crystalline CoO nanoparticles.[42, 47-48] However, when micelles were pyrolyzed under H_2/N_2 atmosphere, cobalt metal nanoparticles were obtained, as demonstrated by XRD (**Figure 4.16B**) and XPS (**Figure 4.18**, red curve).[43-44] Additional peak at 26.13 º in XRD also indicated the existence of amorphous carbon and carbon nanotubes[45] in these nanoparticles, which was identified by Raman spectrum (**Figure 4.17**).[49] Details of these carbon materials are beyond the current study.

A heterobimetallic diblock copolymer, PMAECoPF$_6$-*b*-PMAEFc (PMAEFc = poly(2-(methacrylolyoxy)ethyl ferrocenecarboxylate), block ratio =45:30, M_n = 32,800 g/mol), was synthesized according to our previous work,[39] which could be used as precursors for preparation of nanostructured cobalt/iron hybrid materials. Counterion exchange with TBAI was used to replace PF_6^- anions. As shown in **Figure 4.20**, ^{1}H and ^{19}F NMR spectra demonstrated the successful synthesis and complete anion exchange for the heterobimetallic diblock copolymer. With iodide as the counterion, the cobaltocenium-containing block (PMAECoI) was turned into hydrophilic with the presence of hydrophobic ferrocene-containing block, which formed micelles with ferrocene in the core and cobaltocenium in the shell in aqueous solution (**Scheme 4.4**).

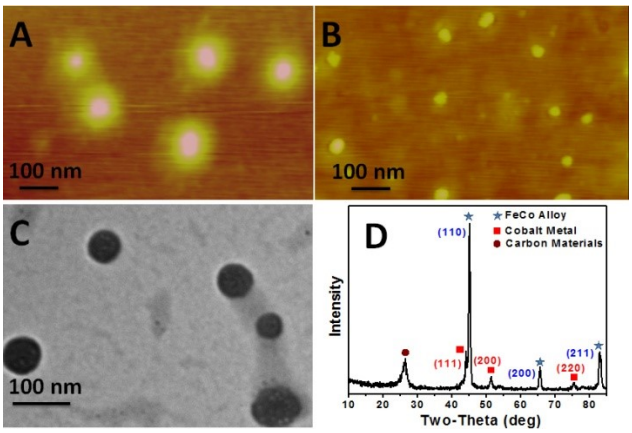

Figure 4.4. (A) AFM height image and (C) TEM image of I^- paired cobaltocenium-containing block copolymer micelles (PMAECoI-b-PMAEFc); (B) AFM height image of pyrolyzed micelles; (D) XRD pattern of pyrolyzed micelles under reductive atmosphere (H_2/N_2) at 800 ^oC.

As shown in **Figures 4.4A** (AFM) and **4.4C** (TEM), spherical micelles of self-assembled diblock copolymers with a diameter of about 70±15 nm were observed. **Figure 4.4B** showed the nanoparticles (size: 40±10 nm) after pyrolysis of micelles. XRD pattern (**Figure 4.4D**) showed that FeCo hybrid, a class of soft magnetic materials, [9, 50] was obtained when pyrolyzed under reductive atmosphere (H_2/N_2) at 800 ^oC.[50] Considering excess cobalt element in block copolymers, insignificant cobalt metal was also identified.[43] Additionally, amorphous carbon and carbon nanotubes were again observed for the materials in reductive atmosphere as a matrix. However, after UV/Ozonolysis followed by pyrolysis in air at 800 ^oC, the XRD (**Figure 4.21**) showed the formation of cobalt ferrite ($CoFe_2O_4$),[51] which is a well-known hard magnetic material.[52] Peaks at 36.6^o, 42.5^o, 61.6^o and 73.7^o indicated the existence of cobalt monoxide.[42] XPS spectrum (**Figure 4.22**) further demonstrated those materials. The iodide anions in the hydrophilic cobaltocenium-containing block were removed and led to the formation of cobalt-iron nanoalloy or nanoscale cobalt ferrite hybride materials.

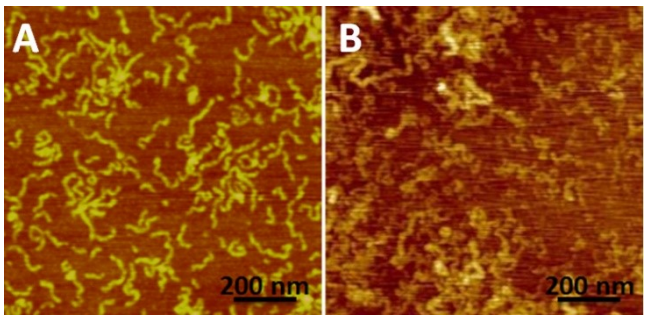

Figure 4.5. AFM height images for PF_6^--paired cobaltocenium-containing polymer brushes: (A) before pyrolysis and (B) after pyrolysis under H_2/N_2 at 800 ºC.

Worm-like metal-containing polymer brushes have been utilized to prepare 1D inorganic nanowires for decades due to their ability to form extended chain conformations and their unique solution and bulk properties.[24, 26] Considering the advantages of facile TBAX anion exchange, cationic cobaltocenium-containing polymer brush may be a versatile precursor for preparation of inorganic cobalt-based 1D nanowires (**Scheme 4.2**).

Cobaltocenium-containing polymer brush (poly(*N*-[4-cyano-4-(phenylcarbonothioylthio)-pentanoate]-cis-5-norbornene-exo-2,3-dicarboximide)-*g*-poly-(2 (methacrylolyoxy) ethyl cobaltoceniumcarboxylate hexafluorophosphate)) was synthesized according to our previous work (M_n = 3,083,400 g/mol).[38] TBAI was utilized to perform anion exchange to replace PF_6^- anions with iodide ions (**Scheme 4.5**). Both PF_6^--paired and I^--paired cobaltocenium-containing polymer brushes showed worm-like structure with a length at about 130-200 nm (**Figure 4.5A** and **Figure 4.24A**). Considering the high grafting density of cobaltocenium side chains in the polymer brush, such cylindrical metal-containing brush was then used as a precursor for the formation of 1D cobalt-based nanowire. After pyrolysis, cobalt-based 1D nanowires were observed

from PF_6^--paired (**Figure 4.5B** and **Figure 4.23B**) and I^--paired cobaltocenium-containing polymer brushes (**Figure 4.25B**).

By pyrolysis under H_2/N_2 atmosphere at 800 ^oC, PF_6^--paired cobaltocenium-containing polymer brushes were converted into 1D cobalt phosphide nanowires, which were identified by XRD (**Figure 4.25A**). While for I^--paired brushes, nanowires of elemental cobalt metal (by pyrolysis under H_2/N_2 atmosphere at 800 ^oC) and nanowires of cobalt monoxide (by UV/Ozonolysis and pyrolysis under air) were produced. These materials were confirmed by XRD (**Figure 4.25B** and **4.25C**), which showed the same peaks as those in bulk and in nanoparticle, as discussed above. TGA curves (**Figure 4.26**) for those polymer brushes indicated that the above mentioned mentioned carbon materials helped these cobalt element to construct inorganic nanowires.

4.4 EXPERIMENTAL

Materials. Chain transfer agent cumyl dithiobenzoate (97%, CDB) was purchased from Aldrich, and used directly. Cobaltocenium-containing methacrylate polymers with hexafluorophosphate anion (poly(2-(methacrylolyoxy)ethyl cobaltoceniumcarboxylate hexafluorophosphate)) were synthesized according to our earlier reports (M_n = 22,000 g/mol, M_w/M_n = 1.25).[39] Cobaltocenium-containing polymer brush (poly(*N*-[4-cyano-4-(phenylcarbonothioylthio)-pentanoate]-cis- 5-norbornene-exo-2,3-dicarboximide)-g-poly(2-(methacrylolyoxy)ethyl cobaltoceniumcarboxylate hexafluorophosphate)) was synthesized according to our previous report (M_n = 3,083,400 g/mol).[38] All tetrabutylammonium salts with different anions were purchased from Sigma Aldrich and used as received. All other chemicals were from commercial sources and used as received.

Characterization. ^{1}H NMR (400 MHz) spectra were recorded on a Varian Mercury 400 spectrometer with tetramethylsilane (TMS) as an internal reference. ^{19}F NMR (376 MHz) spectra were recorded on a Varian Mercury 400 spectrometer with CHF_3 as an internal reference. Transmission electron microscopy (TEM) samples were conducted using a Zeiss Libra 120. TEM experiments were performed at 120kV with an emission current of 6μA in order to minimize electron-beam-induced nanoparticle change or damage. UV/Ozonolysis was conducted on a 42 A UVO cleaner (Jellght Company Inc.). Atomic force microscopy (AFM) was conducted on a Nanoscope V Multimode instrument, operating under tapping mode. Solution samples were drop-cast on silicon wafer substrates. The samples were visualized by AFM after dryness. X-ray photoelectron spectroscopy (XPS) measurements were conducted using a Kratos AXIS Ultra DLD XPS system equipped with a monochromatic Al Kα source. The energy scale of the system is calibrated using an Au foil with Au4f scanned for the Al radiation and a Cu foil with Cu2p scanned for Mg radiation resulting in a difference of 1081.70 ± 0.025 eV between these two peaks. The binding energy is calibrated using an Ag foil with $Ag3d_{5/2}$ set at 368.21 ± 0.025 eV for the monochromatic Al X-ray source. The monochromatic Al Kα source was operated at 15 keV and 120 W. The pass energy was fixed at 40 eV for the detailed scans. A charge neutralizer (CN) was used to compensate for the surface charge. Samples were not conductive and C1s was used as the peak reference. The binding energy (BE eV) was corrected with the C1s (284.8 eV) as standard. Lindberg bluem furnace was used to pyrolyze polymers under H_2/N_2 (H_2, 5% volume) flow or under air flow at 800 ^{o}C. X-ray diffraction (XRD) measurements were conducted on a Rigaku D/Max 2100 Powder X-Ray Diffractometer (Cu Kα radiation)

instrument and scanned from 10° to 85° with a step size of 0.005° and a step rate of 6 s. The data were collected at the second scan. TGA was conducted on a TA Instruments Q5000 with a heating rate of 10 °C /min from 10 to 850 °C under constant air flow or reductive flow (H_2/N_2, 5v/v% H_2).

General procedure of counterion exchange experiment *via* tetrabutylammonium salts. 1 mL PF_6^--paired cobaltocenium-containing polymer solution (30 mg/mL in acetonitrile) was slowly dropped into 5 mL tetrabutylammonium salt solution (in acetonitrile) under vigorous stirring. The concentrations for each salt were summarized in **Table 4.1**. After stirring for 3~5 minutes, the precipitated polymers were collected and washed by acetonitrile three times to remove PF_6^- anions and excess tetrabutylammonium salts. The solid polymers were then vacuum-dried and collected. ^{1}H NMR (**Figure 4.6**, for Cl^-, Br^-, I^-, and NO_3^- paired polymers) (D_2O, δ, ppm): 6.14 (broad, Cp, 2H), 5.85 (broad, Cp, 2H), 5.73 (broad, Cp, 5H), 4.43 (broad, C*H*$_2$CH$_2$, 2H), 4.15 (broad, CH$_2$C*H*$_2$, 2H), 1.50~1.80 (broad, C*H*$_2$C, 2H), 0.50-1.00 (broad, CC*H*$_3$, 3H). M_n (^{1}H NMR) = 17,000 g/mol (Cl^-), 19,000 g/mol (Br^-), 21,200 g/mol (I^-) and 18,200 g/mol (NO_3^-). ^{19}F NMR (**Figure 4.1c**) showed no fluorine signal for Cl^-, Br^-, I^-, NO_3^- and Ac^- paired polymers. ^{19}F NMR (**Figure 4.6**) for F^- paired polymer (CD_3OD, δ, ppm): -152.3 (Cp_2CoF). ^{1}H NMR spectrum (**Figure 4.9**) for F^- paired cobaltocenium-containing polymers, (D_2O, δ, ppm): 6.14 (broad, Cp, 2H), 5.87 (m and broad, Cp, 2.5H), 5.74 (broad, Cp, 5H), 5.63 (m, Cp, 0.5H), 5.60 (m, Cp, 1.2H), 4.43 (broad, C*H*$_2$CH$_2$, 2H), 4.15 (broad, CH$_2$C*H*$_2$, 2H), 3.91 (broad, C*H*$_2$CH$_2$OH, 1.3H), 3.64 (broad, CH$_2$C*H*$_2$OH, 1.3H), 1.50~1.80 (broad, C*H*$_2$C, 2.5H), 0.50-1.00 (broad, CC*H*$_3$, 3.8H). ^{1}H NMR spectrum (**Figure 4.8**) for Ac^- paired cobaltocenium-containing polymers, (D_2O, δ, ppm): 6.14

(broad, Cp, 2H), 5.85 (m and broad, Cp, 2H), 5.74 (broad, Cp, 5H), 4.43 (broad, C*H*$_2$CH$_2$, 2H), 4.15 (broad, CH$_2$C*H*$_2$, 2H), 3.86 (broad, C*H*$_2$CH$_2$OH, 0.1H), 3.62 (broad, CH$_2$C*H*$_2$OH, 0.1H), 1.50~1.80 (broad, C*H*$_2$C, 2H), 0.50-1.00 (broad, CC*H*$_3$, 3H).

General procedure to prepare bulk cobalt-based materials from cobaltocenium-containing homopolymers. Two different conditions were applied to prepare different cobalt-containing inorganic materials. 50 mg cobaltocenium-containing homopolymers were first UV/Ozonolyzed for two hours and then pyrolyzed under air at 800 ^{o}C. On the other hand, reductive atmosphere was used to pyrolyze these different anions-paired cobaltocenium-containing homopolymers. 50 mg homopolymers were pyrolyzed for 4 hours at 800 ^{o}C under reducing atmosphere (H_2/N_2, 5v/v% H_2). Black powder was then collected to characterize by XRD.

TBAX counterion exchange for cobaltocenium-containing diblock copolymers with tert-butyl acrylate (PtBA) as the second block. Diblock copolymers (PMAECoPF$_6$-*b*-PtBA) were synthesized according to the previous work (block ratio: PMAECoPF$_6$: PtBA = 62 : 43, M_n = 35,800 g/mol).[39] TBANO$_3$ was used to perform anion exchange with the diblock copolymer. The procedure was the same as the ion-exhcnage conducted for homopolymers. ^{1}H NMR (**Figure 4.15**) (DMSO-D$_6$, δ, ppm): 6.31 (broad, Cp from Cp$_2$Co, 2H), 6.00-5.90 (broad, Cp from Cp$_2$Co, 6.8H), 4.30-4.50 (broad, C*H*$_2$CH$_2$O, 2H), 4.10-4.20 (broad, CH$_2$C*H*$_2$O, 2H), 1.20-1.50 (broad, C(C*H*$_3$)$_3$, CC*H*$_2$, 4H), 0.80-1.00 (broad, CC*H*$_3$, 3H).

TBAX counterion exchange for heterobimetallic cobaltocenium-*b*-ferrocene diblock copolymers. Diblock copolymers (PMAECoPF$_6$-*b*-PMAEFc) were synthesized

via chain extension according to our previous work (block ratio, PMAECoPF$_6$: PMAEFc = 45 : 30, M_n = 32,800 g/mol).[39] The procedure of counterion exchange with TBAI for diblock copolymers was the same as counterion exchange for homopolymers. According to the integration in ^{1}H NMR spectrum (**Figure 4.21**), the ratio of the cobaltocenium-containing block to ferrocene-containing block was about 45 : 30. ^{1}H NMR (**Figure 4.21**) (DMSO-D$_6$, δ, ppm): 6.31 (broad, Cp from Cp_2Co, 2H), 6.00-5.90 (broad, Cp from Cp_2Co, 6.7H), 4.81 (broad, Cp from Cp_2Fe, 1.0H), 4.20-4.59 (broad, O*C*H_2*C*H_2O and Cp_2Fe, 7.2H), 2.09 (broad, CH_2C), 0.60-1.00 (s, CH_3).

Solution self-assembly for diblock copolymers (PMAECoNO$_3$-*b*-PtBA) with NO_3^- as counterions and synthesis of inorganic cobalt-containing nanoparticles. 2 mg PMAECoNO$_3$-*b*-PtBA was first dissolved in 1 mL water and stirred overnight. The solution was then used for TEM and AFM characterization. AFM sample was further pyrolyzed for imaging inorganic nanoparticles. Two different ways were applied to collect inorganic cobalt-containing materials from these micelles. Some samples were first UV-Ozonolyzed for two hours and then pyrolyzed under air at 800 ^{o}C for 5 minutes. Other samples were pyrolyzed for 4 hours at 800 ^{o}C under reducing atmosphere (H_2/N_2, 5v/v% H_2). All samples were then characterized by XPS and XRD.

Solution self-assembly for heterobimetallic diblock copolymers (PMAECoI-*b*-PMAEFc) with I^- as counterions and synthesis of cobalt-iron hybrid inorganic nanoparticles. Solution self-assembly of PMAECoI-*b*-PMAEFc diblock copolymers was performed in aqueous solution. 1 mg diblock copolymers were first dissolved in 1 mL water and then purged with nitrogen for 30 minutes. The solution was sealed and stirred overnight and then used for TEM and AFM characterization. Two different ways were

also used to collect inorganic cobalt-containing materials from heterometallic micelles. Some samples were UV/Ozonolyzed for two hours and then pyrolyzed under air at 800 ^{o}C for 5 minutes. Other samples were pyrolyzed for 4 hours at 800 ^{o}C under reducing atmosphere (H_2/N_2, 5v/v% H_2). Inorganic cobalt-containing materials were collected for XPS and XRD characterization.

Synthesis of inorganic cobalt-based 1D nanowires from cobaltocenium-containing polymer brushes. PF_6^--paired cobaltocenium-containing polymer brushes were obtained according to our previous report. (M_n = 3,083,400 g/mol). I^--paired cobaltocenium-containing polymer brushes were prepared by following the same procedure of cobaltocenium-containing homopolymers (confirmed by ^{1}H NMR and ^{19}F NMR). 1 mg PF_6^--paired polymer brushes were dissolved in 1 mL acetonitrile and then diluted to 0.05mg/mL, while for I^--paired cobaltocenium-containing polymer brushes, they were dissolved in water and kept concentration at 0.05 mg/mL. Both of the samples were then used for AFM and TEM characterization. Two different ways were also used to collect inorganic cobalt-containing materials from cobalt-containing polymer brushes. One was UV/Ozonolyzed for two hours and then pyrolyzed under air at 800 ^{o}C for 5 minutes. The other one was directly pyrolyzed for 4 hours at 800 ^{o}C under reducing atmosphere (H_2/N_2, 5v/v% H_2). Inorganic cobalt-containing materials were collected for XRD characterization.

Inductively Coupled Plasma−Mass Spectrometry Analysis for cobalt-based inorganic materials. Inductively coupled plasma−mass spectrometer (ICP-MS) samples were prepared by digesting the samples in 2 mL of aqua regia. The concentrations of cobalt in cobalt monoxide, cobalt phosphide and cobalt metal were detected by a

Thermo-Finnigan Element XR ICP-MS. The instrument was calibrated for element Co (59). The calibration range was from 1.0 to 60 ppb. The R squared value for the initial calibration curve was greater than 0.99. The samples were analyzed immediately after the initial calibration, and the target element results were within the calibration range.

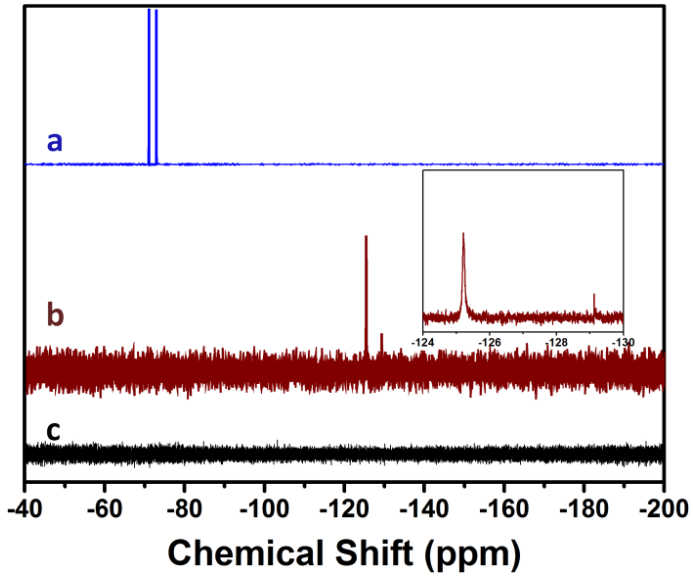

Figure 4.6. ^{19}F NMR spectra of cobaltocenium-containing polyelectrolytes with different counterions in D_2O: (a) PF_6^-; (b) F^-, insert is an enlarged part of peaks; (c) Cl^-, Br^-, I^-, NO_3^- or Ac^-.

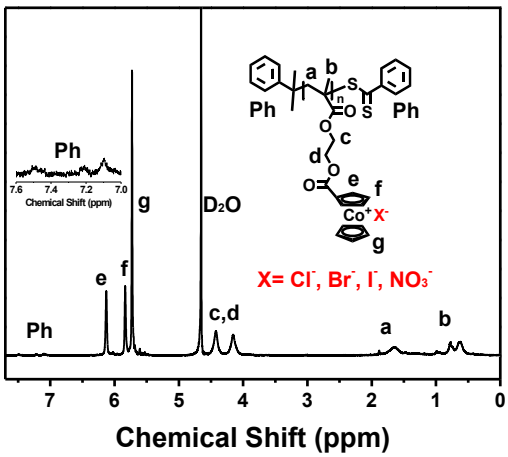

Figure 4.7. ^1H NMR spectrum of cobaltocenium-containing polyelectrolytes with Cl^-, Br^-, I^-, or NO_3^- as counterions.

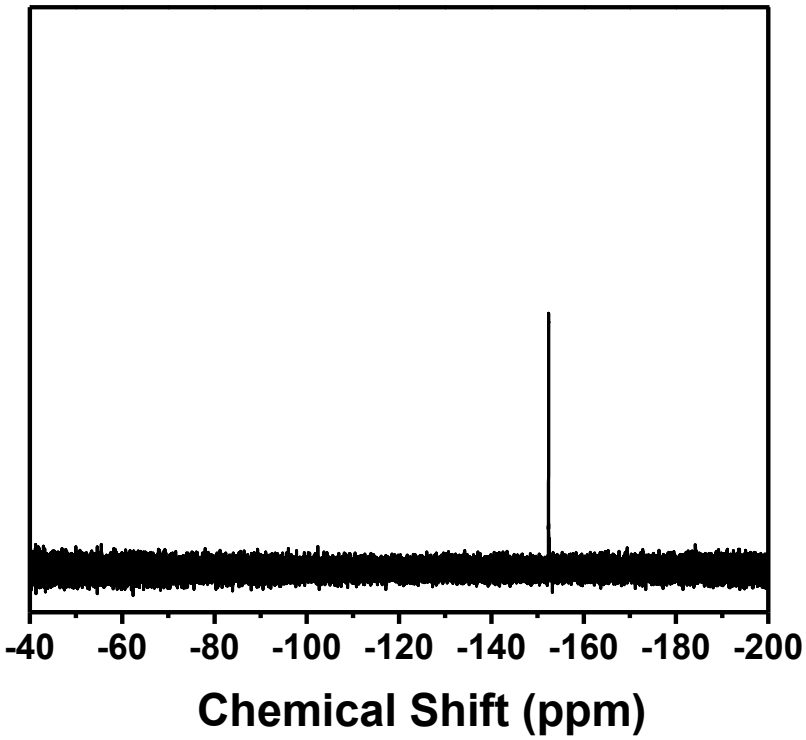

Figure 4.8. ^{19}F NMR spectrum of F^--paired cobaltocenium-containing polymer in CD_3OD.

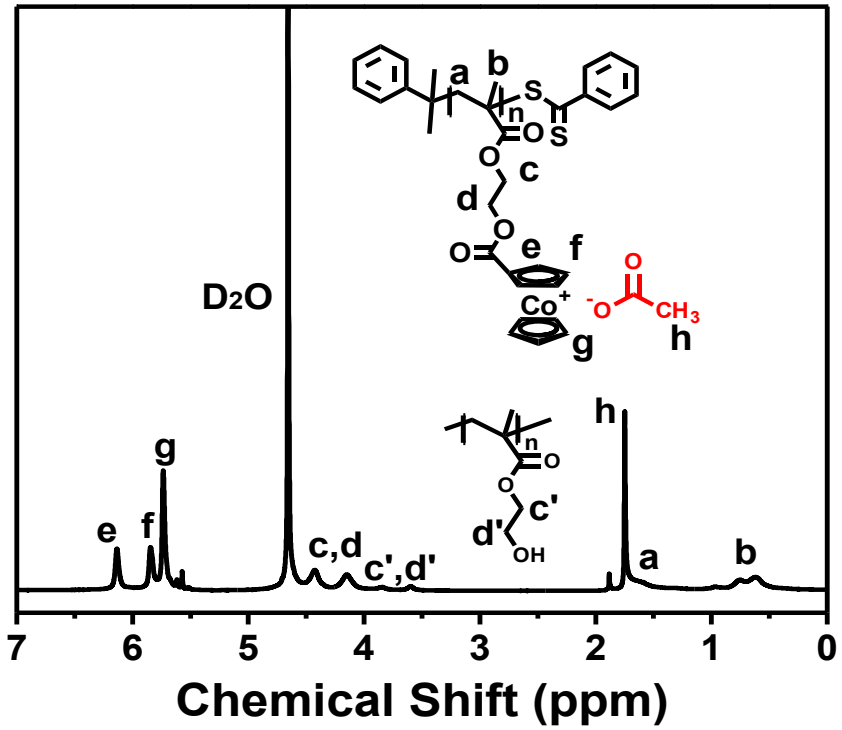

Figure 4.9. ^1H NMR spectrum of Ac^--paired cobaltocenium-containing polymer.

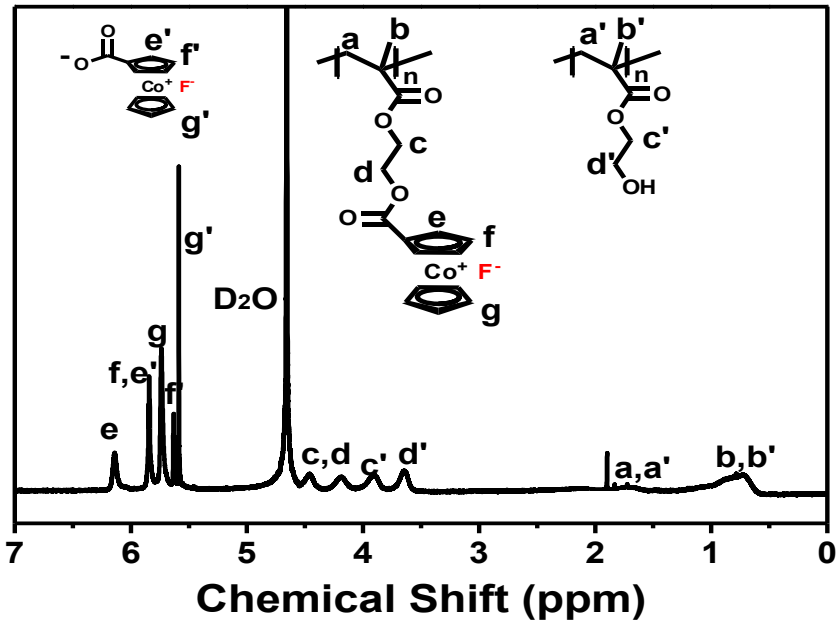

Figure 4.10. ^{1}H NMR spectrum of F^--paired cobaltocenium-containing polymer. Part of cobaltocenium units were cleaved from polymers.

Table 4.1. Some properties of cationic cobaltocenium-containing polymers after TBAX counterion exchange.

Anions	Concentration[a] (mg/mL)	Stability	Hydroscopic	Yield (%)
F^-	20[b]	×	Very Strong	40
Cl^-	30-50	√	Weak	71
Br^-	30-40	√	Weak	81
I^-	30-50	√	Very Weak	88
NO_3^-	30-50	√	Very Weak	92
Ac^-	20[b]	×	Strong	45

a. This concentration range of TBAX salt was enough to have complete exchange and did not affect polymer frameworks.

b. For TBAF and TBAAc, the concentration was 20 mg/mL. High concentration of TBAF and TBAAc led to the partial cleavage of ester groups (Figure 4.9 and Figure 4.10). There were about 35% and 5% of ester group cleaved after exchanging with F^- and Ac^- respectively. This might be due to the basicity of F^- and Ac^- anions, which could cleave the ester groups.

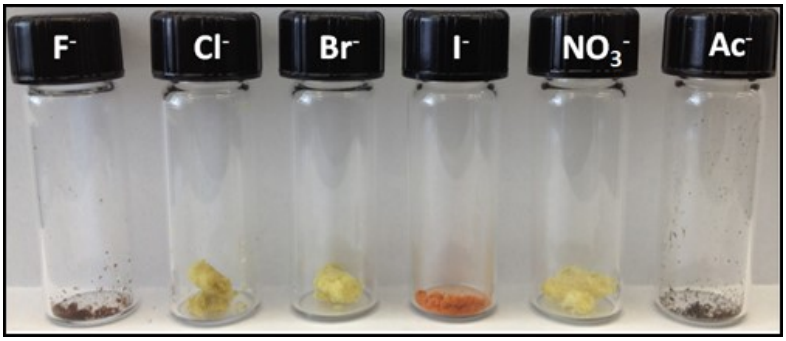

Figure 4.11. Different colors observed for F^-, Cl^-, Br^-, I^-, NO_3^- and Ac^- paired cobaltocenium-containing polyelectrolytes. F^- and Ac^- based polymers were deep brown, while Br^- and NO_3^- showed similar bright yellow. Dark yellow and orange were observed for Cl^- and I^- paired cobaltocenium-containing polymers respectively.

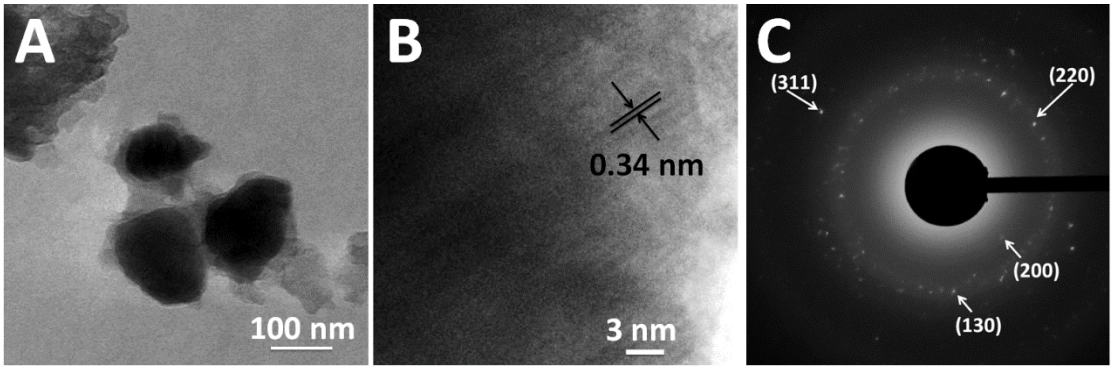

Figure 4.12. (A) TEM image, (B) high resolution TEM image, and (C) SAED pattern of Co_2P prepared by cobaltocenium-containing polyelectrolytes with PF_6^- anions.

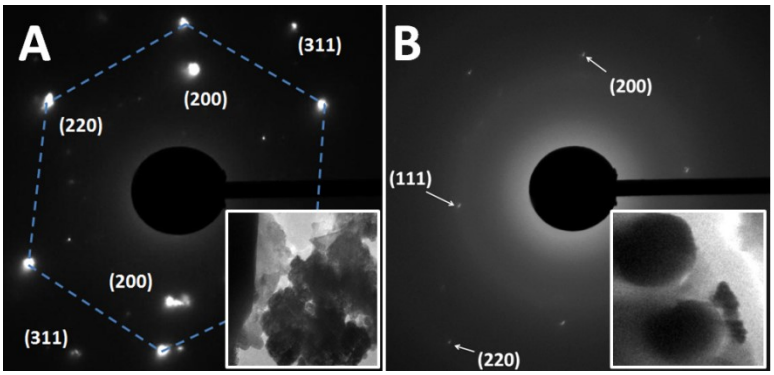

Figure 4.13. Selected area electron diffraction (SAED) patterns for CoO (A) and cobalt metal (B) from cobaltocenium-containing polyelectrolytes with Cl^-, Br^-, I^- and NO_3^- anions. Insert are TEM images of selected area.

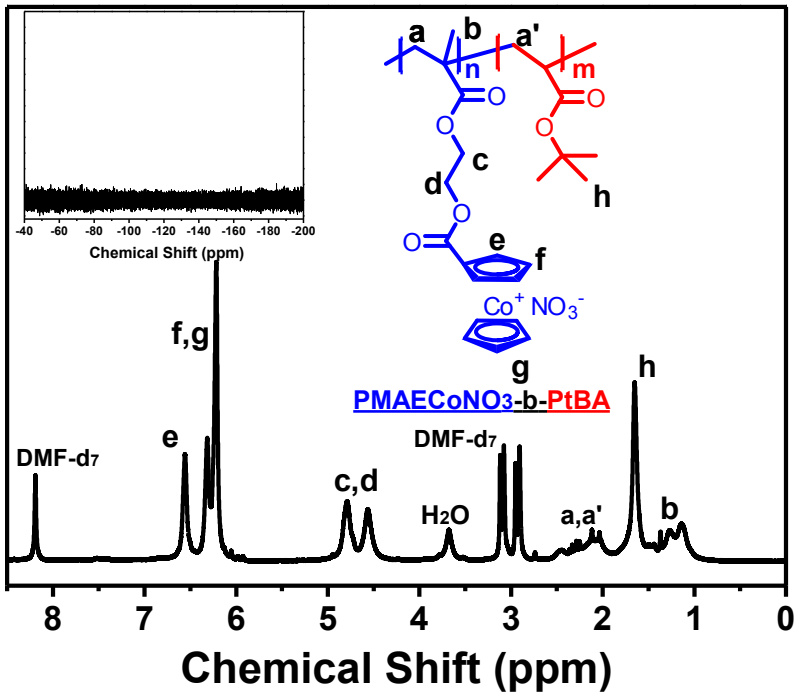

Figure 4.14. ^{1}H NMR spectrum of cobaltocenium-containing diblock copolymer (PMAECoNO$_3$-*b*-PtBA). Insert is ^{19}F NMR spectrum for this diblock copolymer (No fluorine signal was observed).

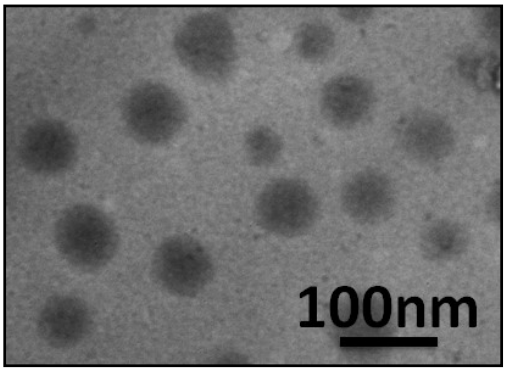

Figure 4.15. TEM image of self-assembled micelles from cobaltocenium-containing diblock copolymers (PMAECoNO$_3$-*b*-PtBA) in water.

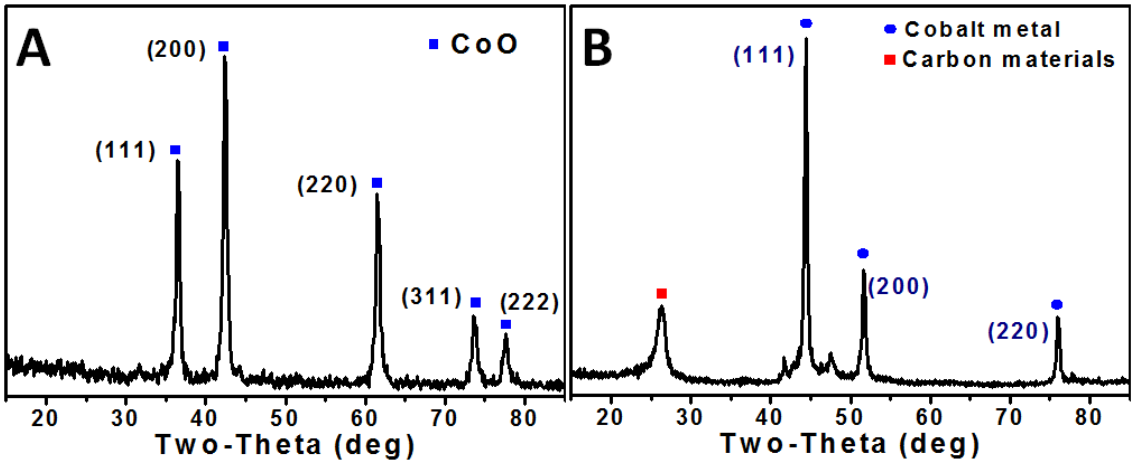

Figure 4.16. XRD patterns: (A) UV/Ozonolyzed and pyrolyzed micelles of PMAECoNO$_3$-*b*-PtBA under air at 800 ºC; (B) pyrolyzed micelles under H_2/N_2 atmosphere at 800 ºC.

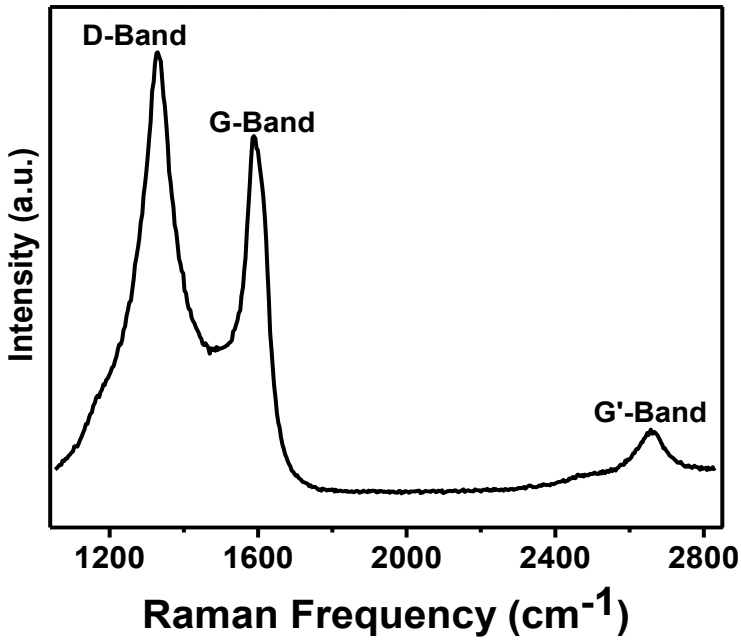

Figure 4.17. Raman spectrum for pyrolyzed micelles (under H_2/N_2 atmosphere at 800 ºC) from cobaltocenium-containing diblock copolymers (PMAECoNO$_3$-*b*-PtBA). D-Band, G-Band and G'-Band at 1300, 1570 and 2660 cm^{-1} indicated the existence of carbon nanotubes. The ratio of the area for peaks at D-band and G-band (I_D/I_G) showed the ratio of amorphous carbon and carbon nanotubes in carbon materials.

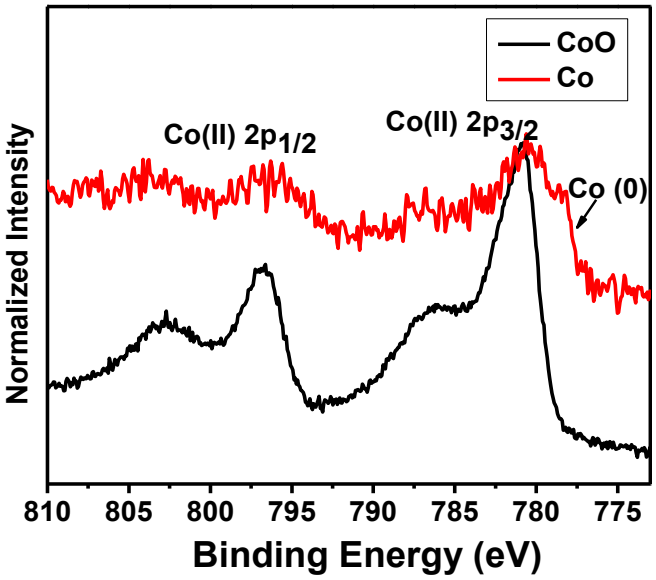

Figure 4.18. XPS spectra of pyrolyzed micelles of cobaltocenium-containing diblock copolymer PMAECoNO$_3$-*b*-PtBA. Black curve (UV/Ozonolysis and pyrolyzed under air at 800 ^{o}C) and red curve(pyrolyzed under H_2/N_2 atomosphere at 800 ^{o}C, relatively poor quality due to strong magnetic response of cobalt metal when characterized by XPS). Black curve showed Co ($2p_{1/2}$) and Co ($2p_{3/2}$) peaks at 796.70 eV and 780.81 eV with two strong shake-up peaks at 5eV higher, which was in good agreement with crystalline CoO reported in literature.[47-48] Red curve showed one additional peak at 778.12 eV, indicating the formation of elemental cobalt.[53]

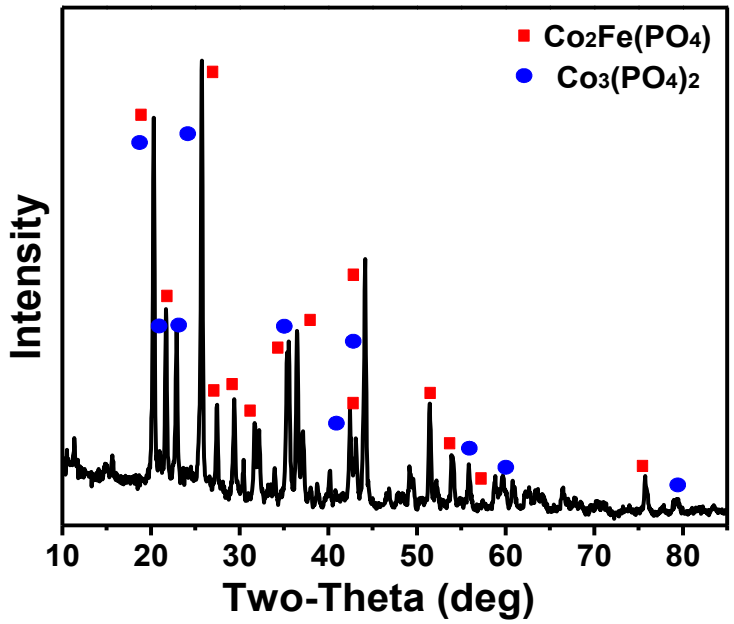

Figure 4.19. XRD pattern of PF_6^--paired heterobimetallic diblock copolymers (PMAECoPF$_6$-*b*-PMAEFc) with cobaltocenium and ferrocene blocks after UV/Ozonolysis and pyrolysis in air.

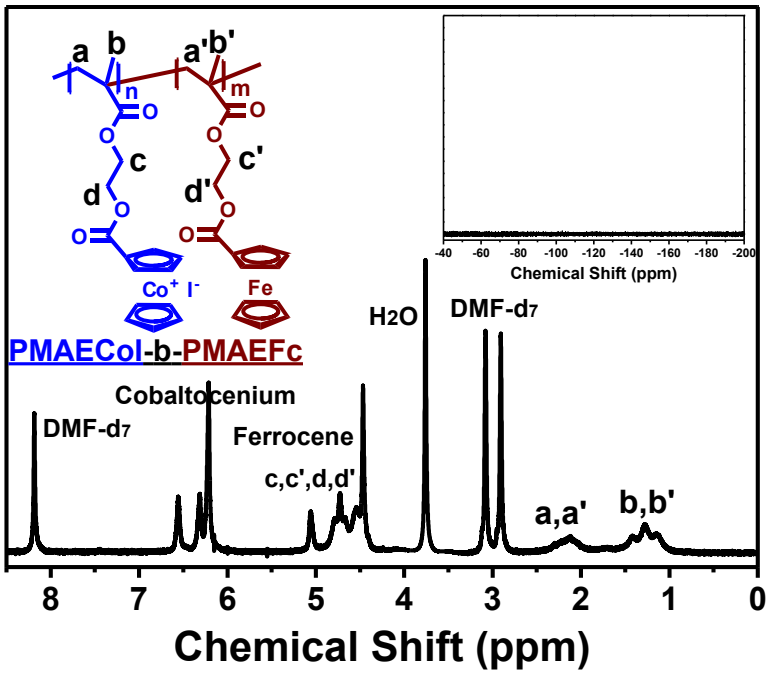

Figure 4.20. ^{1}H NMR spectrum of heterobimetallic diblock copolymers PMAECoI-*b*-PMAEFc. Insert is ^{19}F NMR spectrum of this diblock copolymer (no fluorine signal was observed).

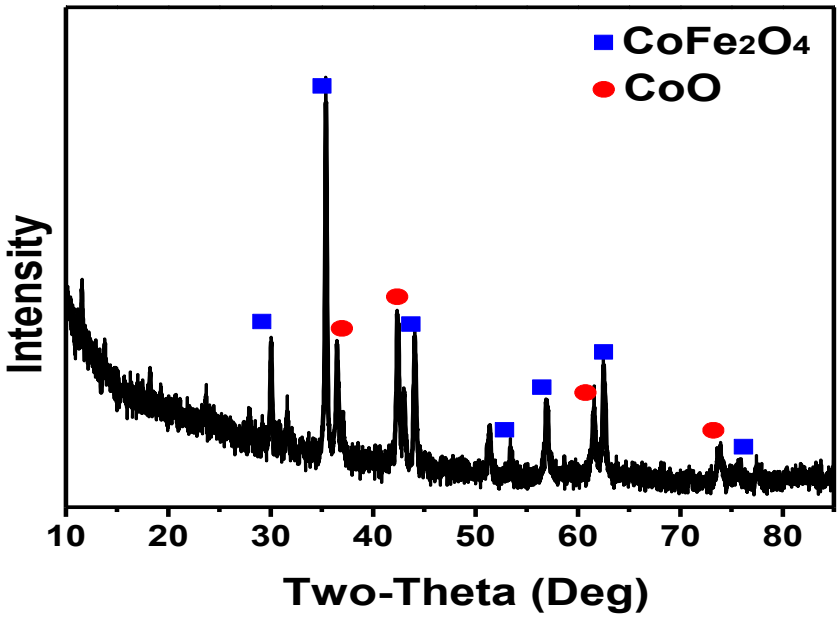

Figure 4.21. XRD pattern of UV/Ozonolyzed and pyrolyzed micelles from iodide-paired heterobimetallic diblock copolymer PMAECoI-*b*-PMAEFc in air at 800 ºC.

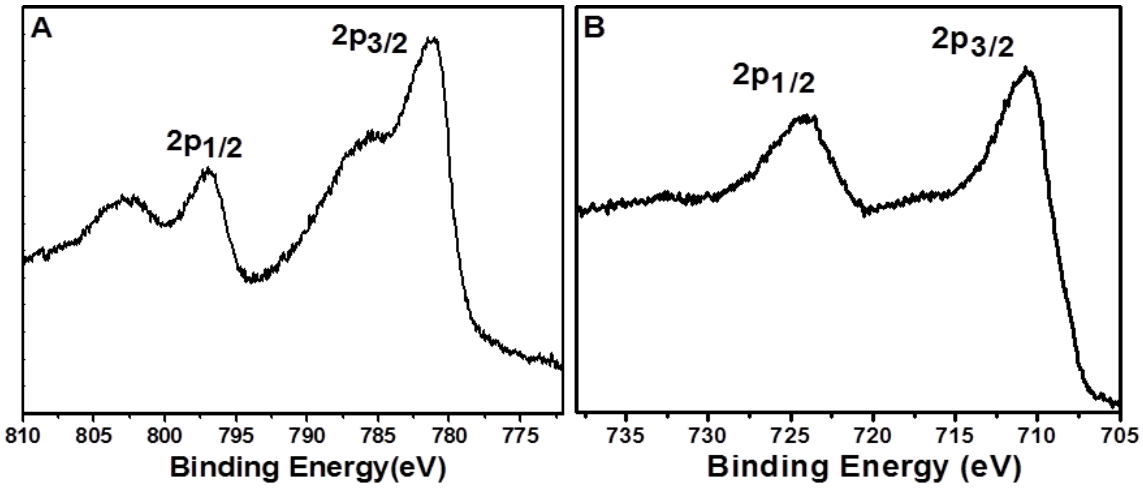

Figure 4.22. XPS spectra of UV/Ozonolyzed and pyrolyzed micelles from iodide-paired heterobimetallic diblock copolymer PMAECoI-*b*-PMAEFc in air at 800 ºC: (A) cobalt, (B) iron. Figure A showed peaks at 796.86 eV and 781.04 eV with two shake-up peaks at ~5 eV higher, corresponding to cobalt oxidation state (Co(II)).[51, 54] Another two peaks in Figure B at 724.15 eV and 710.64 eV with two weak shake-up peaks (~7.5 eV higher) indicated the state of iron element in $CoFe_2O_4$.[54-55]

Scheme 4.5. Counterion exchange of cobaltocenium-containing polymer brush *via* TBAI.

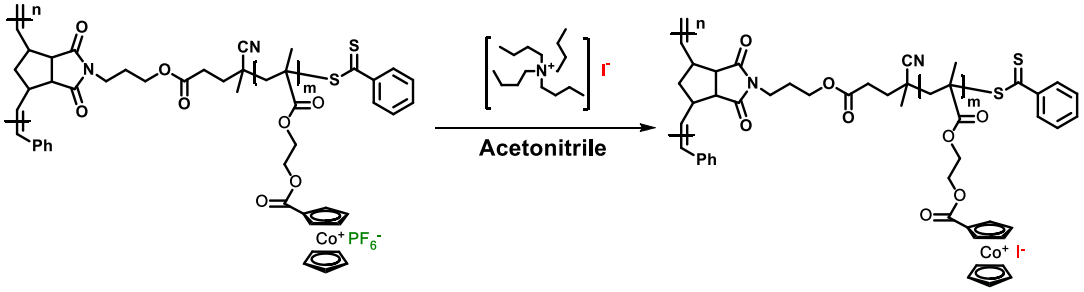

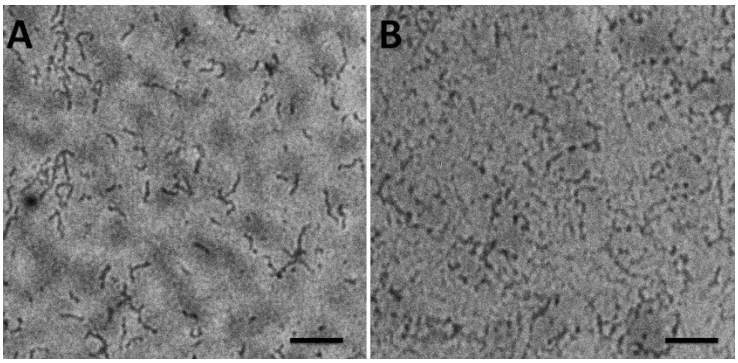

Figure 4.23. TEM images for PF_6^--paired cobaltocenium-containing polymer brushes before UVO/pyrolysis (A) and after UVO/pyrolysis (B). Scale bar: 250 nm.

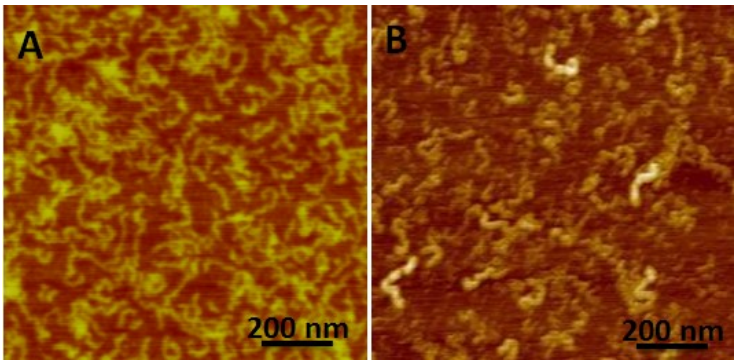

Figure 4.24. AFM height images for I^--paired cobaltocenium-containing polymer brushes: (A) before pyrolysis; (B) after pyrolysis in air at 800 °C.

Scheme 4.4. Counterion exchange of heterobimetallic diblock copolymer ($PMAECoPF_6$-*b*-PMAEFc) and its solution self-assembly.

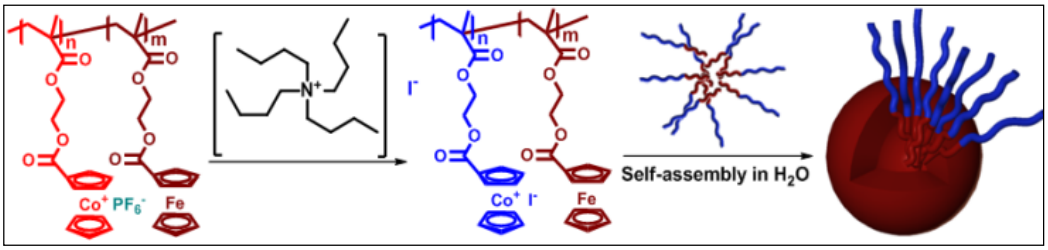

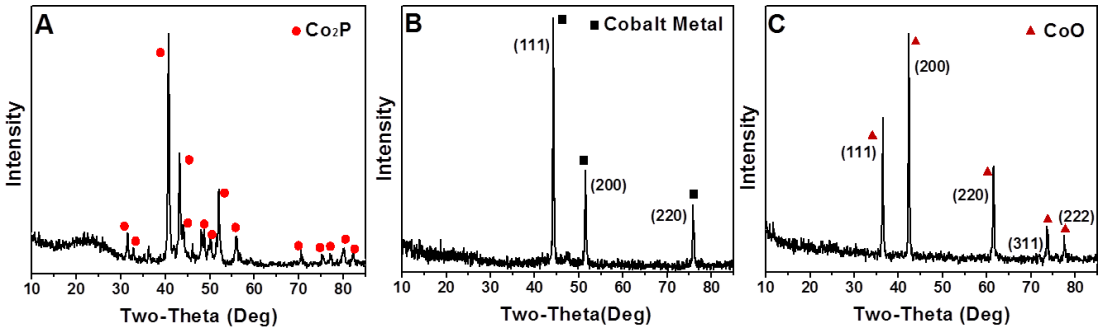

Figure 4.25. XRD patterns: (A) pyrolyzed PF_6^--paired cobaltocenium-containing polymer brushes under H_2/N_2 atmosphere at 800 °C; (B) pyrolyzed I^--paired cobaltocenium-containing polymer brushes under H_2/N_2 atmosphere at 800 °C; and (C) UV/Ozonolyzed and pyrolyzed I^--paired cobaltocenium-containing polymer brushes in air at 800 °C.

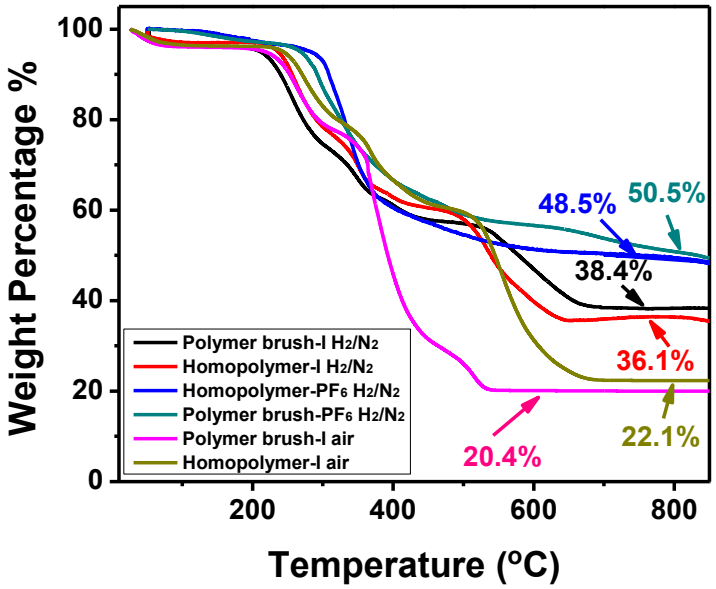

Figure 4.26. TGA curves for iodide and PF_6^- paired cobaltocenium-containing homopolymers and polymer brushes under air and under reductive atmosphere (H_2/N_2, 5v/v%). All polymers started to decompose at 190 °C and the stable curves started from about 700 °C.

Table 4.2. Yield and cobalt content about inorganic cobalt-based materials prepared by pyrolysis of cobaltocenium-containing polymers.

	Cobalt monoxide [a]	Cobalt Phosphide [a]	Cobalt Metal [a]
Yield [b]	22.1%	48.5%	36.1%
Cobalt% [c]	52.4%	26.9%	28.1%

a. Cobalt monoxide was collected after TGA under air from cobaltocenium-containing homopolymers. While cobalt phosphide and cobalt metal were collected after TGA under reductive atmosphere (H_2/N_2, 5v/v%) from cobaltocenium-containing homopolymers.
b. Yields were determined by the weight percentage of final inorganic materials from TGA of homopolymers. Yields for polymer brushes were similar as homopolymer (**Figure 4.26**).
c. Cobalt% was the weight percentage of cobalt element in final materials from homopolymers, which was determined by ICP-MS. Theoretical values were 78.7%, 79.1% and 100% for pure cobalt monoxide, cobalt phosphide and cobalt metal.

4.5 Conclusions

In conclusion, a facile phase transfer ion-exchange strategy was applied to prepare charged cobalt-containing polyelectrolytes with various types of counterions, including F^-, Cl^-, Br^-, I^-, NO_3^- and Ac^-. With this convenient counterion exchange method, functional materials of cobalt metal, cobalt monoxide, cobalt-iron nanoalloy and cobalt ferrite nanoparticles were obtained from versatile cobaltocenium-containing polymeric

precursors under different conditions. Through a similar procedure, inorganic cobalt-based 1D nanowires (including cobalt phosphide, cobalt monoxide and cobalt metal) were prepared by using cobaltocenium-containing polymer brushes as precursors. Such cobalt-containing polymeric materials with a convenient and fast phase transfer method could open a facile way toward the preparation of advanced cobalt-containing materials.

4.6 ACKNOWLEDGEMENTS

The support from National Science Foundation (CHE-1151479) is acknowledged. A portion of this research was conducted at the Center for Nanophase Materials Sciences, which is sponsored at Oak Ridge National Laboratory by the Division of Scientific User Facilities, Office of Basic Energy Sciences, U.S. Department of Energy.

4.7 REFERENCES

1. T. M. Trnka, J. P. Morgan, M. S. Sanford, T. E. Wilhelm, M. Scholl, T. L. Choi, S. Ding, M. W. Day and R. H. Grubbs, *J Am Chem Soc* **2003**, *125*, 2546-2558.
2. G. R. Whittell and I. Manners, *Adv. Mater.* **2007**, *19*, 3439-3468.
3. F. H. Schacher, P. A. Rupar and I. Manners, *Angew Chem Int Edit* **2012**, *51*, 7898-7921.
4. X. S. Wang, K. Cao, Y. B. Liu, B. Tsang and S. Liew, *J Am Chem Soc* **2013**, *135*, 3399-3402.
5. F. Jakle, *Chem Rev* **2010**, *110*, 3985-4022.
6. M. A. Zalich, V. V. Baranauskas, J. S. Riffle, M. Saunders and T. G. St Pierre, *Chem Mater* **2006**, *18*, 2648-2655.
7. G. H. Jeong, A. Yamazaki, S. Suzuki, H. Yoshimura, Y. Kobayashi and Y. Homma, *J Am Chem Soc* **2005**, *127*, 8238-8239.
8. P. Y. Keng, B. Y. Kim, I. B. Shim, R. Sahoo, P. E. Veneman, N. R. Armstrong, H. Yoo, J. E. Pemberton, M. M. Bull, J. J. Griebel, E. L. Ratcliff, K. G. Nebesny and J. Pyun, *Acs Nano* **2009**, *3*, 3143-3157.
9. G. S. Chaubey, C. Barcena, N. Poudyal, C. B. Rong, J. M. Gao, S. H. Sun and J. P. Liu, *J Am Chem Soc* **2007**, *129*, 7214-7215.
10. B. M. Barry and E. G. Gillan, *Chem Mater* **2008**, *20*, 2618-2620.
11. A. E. Henkes, Y. Vasquez and R. E. Schaak, *J Am Chem Soc* **2007**, *129*, 1896-1897.
12. J. H. Fendler, *Chem Mater* **1996**, *8*, 1616-1624.
13. I. G. Casella, *J Electroanal Chem* **2002**, *520*, 119-125.

14. Z. M. Al-Badri, R. R. Maddikeri, Y. P. Zha, H. D. Thaker, P. Dobriyal, R. Shunmugam, T. P. Russell and G. N. Tew, *Nat Commun* **2011**, *2*, 482.
15. A. G. MacDiarmid, *Angew Chem Int Edit* **2001**, *40*, 2581-2590.
16. L. Ren, J. Zhang, C. G. Hardy, S. Ma and C. Tang, *Macromol Rapid Comm* **2012**, *33*, 510-516.
17. N. Du, H. Zhang, B. Chen, J. B. Wu, X. Y. Ma, Z. H. Liu, Y. Q. Zhang, D. Yang, X. H. Huang and J. P. Tu, *Adv. Mater.* **2007**, *19*, 4505-4509.
18. U. Schubert, N. Husing and A. Lorenz, *Chem Mater* **1995**, *7*, 2010-2027.
19. H. Tuysuz, Y. Liu, C. Weidenthaler and F. Schuth, *J Am Chem Soc* **2008**, *130*, 14108-14110.
20. J. B. Beck and S. J. Rowan, *J Am Chem Soc* **2003**, *125*, 13922-13923.
21. J. R. Capadona, K. Shanmuganathan, D. J. Tyler, S. J. Rowan and C. Weder, *Science* **2008**, *319*, 1370-1374.
22. K. Liu, S. B. Clendenning, L. Friebe, W. Y. Chan, X. B. Zhu, M. R. Freeman, G. C. Yang, C. M. Yip, D. Grozea, Z. H. Lu and I. Manners, *Chem Mater* **2006**, *18*, 2591-2601.
23. G. Riess, *Prog Polym Sci* **2003**, *28*, 1107-1170.
24. M. Mullner, T. Lunkenbein, J. Breu, F. Caruso and A. H. E. Muller, *Chem Mater* **2012**, *24*, 1802-1810.
25. X. Y. Shi, M. W. Shen and H. Mohwald, *Prog Polym Sci* **2004**, *29*, 987-1019.
26. J. Y. Yuan, F. Schacher, M. Drechsler, A. Hanisch, Y. Lu, M. Ballauff and A. H. E. Muller, *Chem Mater* **2010**, *22*, 2626-2634.
27. J. P. Magnusson, A. Khan, G. Pasparakis, A. O. Saeed, W. X. Wang and C. Alexander, *J Am Chem Soc* **2008**, *130*, 10852-10853.
28. L. Ren, C. G. Hardy, S. Tang, D. B. Doxie, N. Hamidi and C. Tang, *Macromolecules* **2010**, *43*, 9304-9310.
29. R. Ahmed, S. Patra, I. Hamley, I. Manners and C. F. Faul, *J Am Chem Soc* **2013**, *135*, 2455-2458.
30. L. Alaerts, J. Wahlen, P. A. Jacobs and D. E. De Vos, *Chem Commun* **2008**, 1727-1737.
31. M. J. M. Munoz and G. Fernandez, *Chem Sci* **2012**, *3*, 1395-1398.
32. P. G. Jessop, T. Ikariya and R. Noyori, *Chem Rev* **1999**, *99*, 475-493.
33. Z. C. Wang, K. C. J. Ho, C. J. Medforth and J. A. Shelnutt, *Adv. Mater.* **2006**, *18*, 2557-2560.
34. F. C. Shen, J. Yang, C. F. Wang, L. Chen and S. Chen, *J Inorg Organomet P* **2011**, *21*, 570-575.
35. A. Baiker, *Chem Rev* **1999**, *99*, 453-473.
36. H. Itoh, K. Naka and Y. Chujo, *J Am Chem Soc* **2004**, *126*, 3026-3027.
37. G. T. Wei, Z. S. Yang, C. Y. Lee, H. Y. Yang and C. R. C. Wang, *J Am Chem Soc* **2004**, *126*, 5036-5037.
38. J. Zhang, P. J. Pellechia, J. Hayat, C. G. Hardy and C. Tang, *Macromolecules* **2013**, *46*, 1618–1624.
39. J. Zhang, L. Ren, C. G. Hardy and C. Tang, *Macromolecules* **2012**, *45*, 6857-6863.
40. J. H. Clark, E. M. Goodman, D. K. Smith, S. J. Brown and J. M. Miller, *J Chem Soc Chem Comm* **1986**, 657-658.

41. H. T. Zhang, D. H. Ha, R. Hovden, L. F. Kourkoutis and R. D. Robinson, *Nano Lett* **2011**, *11*, 188-197.
42. D. Barreca, C. Massignan, S. Daolio, M. Fabrizio, C. Piccirillo, L. Armelao and E. Tondello, *Chem Mater* **2001**, *13*, 588-593.
43. D. L. Leslie-Pelecky, M. Bonder, T. Martin, E. M. Kirkpatrick, Y. Liu, X. Q. Zhang, S. H. Kim and R. D. Rieke, *Chem Mater* **1998**, *10*, 3732-3736.
44. Z. H. Wang, C. J. Choi, B. K. Kim, J. C. Kim and Z. D. Zhang, *Carbon* **2003**, *41*, 1751-1758.
45. S. H. Lim, Z. T. Li, C. K. Poh, L. F. Lai and J. Y. Lin, *J Power Sources* **2012**, *214*, 15-20.
46. A. Berenbaum, M. Ginzburg-Margau, N. Coombs, A. J. Lough, A. Safa-Sefat, J. E. Greedan, G. A. Ozin and I. Manners, *Adv. Mater.* **2003**, *15*, 51-55.
47. A. Gulino, P. Dapporto, P. Rossi, G. Anastasi and I. Fragala, *J Mater Chem* **2004**, *14*, 2549-2553.
48. G. J. Yang, D. Q. Gao, Z. H. Shi, Z. H. Zhang, J. Zhang, J. L. Zhang and D. S. Xue, *J Phys Chem C* **2010**, *114*, 21989-21993.
49. A. A. Koos, R. J. Nicholls, F. Dillon, K. Kertesz, L. P. Biro, A. Crossley and N. Grobert, *Carbon* **2012**, *50*, 2816-2823.
50. A. L. Elias, J. A. Rodriguez-Manzo, M. R. McCartney, D. Golberg, A. Zamudio, S. E. Baltazar, F. Lopez-Urias, E. Munoz-Sandoval, L. Gu, C. C. Tang, D. J. Smith, Y. Bando, H. Terrones and M. Terrones, *Nano Lett* **2005**, *5*, 467-472.
51. C. H. Kim, Y. Myung, Y. J. Cho, H. S. Kim, S. H. Park, J. Park, J. Y. Kim and B. Kim, *J Phys Chem C* **2009**, *113*, 7085-7090.
52. X. S. Gao, L. F. Liu, B. Birajdar, M. Ziese, W. Lee, M. Alexe and D. Hesse, *Adv Funct Mater* **2009**, *19*, 3450-3455.
53. M. C. Biesinger, B. P. Payne, A. P. Grosvenor, L. W. M. Lau, A. R. Gerson and R. S. Smart, *Appl Surf Sci* **2011**, *257*, 2717-2730.
54. Z. P. Zhou, Y. Zhang, Z. Y. Wang, W. Wei, W. F. Tang, J. Shi and R. Xiong, *Appl Surf Sci* **2008**, *254*, 6972-6975.
55. X. F. Zhao, Y. C. Zhang, S. L. Xu, X. D. Lei and F. Z. Zhang, *J Phys Chem C* **2012**, *116*, 5288-5294.

CHAPTER 5

NANOSTRUCTURED METAL/CARBON COMPOSITES FROM HETEROBIMETALLIC BLOCK COPOLYMERS WITH CONTROLLED MAGNETIC PROPERTIES [†]

[†] J. Zhang, Y. Yan, J. H. Chen, W. M. Chance, J. Hayat, Z. Gai and C. Tang, *Chem. Mater.* **2014**, *26*, 3185-3190. Reprinted here with permission of publisher.

5.1 ABSTRACT

We reported the utilization of a series of heterobimetallic diblock copolymers to prepare different iron-cobalt/carbon and iron-cobalt phosphide/carbon magnetic materials. Through the control of compositions of ferrocene- and cobaltocenium-containing blocks, a transition of final inorganic materials from metal phosphide to metal alloy was observed. These metal elements were embedded on amorphous carbon films or encapsulated in crystallized multi-walled carbon nanotubes. Detailed magnetic characterization showed that all these inorganic materials were ferromagnetic under room temperature with great difference in their magnetic susceptibilities. The saturated magnetization was related with the weight fraction of phosphorus and cobalt, indicating the ability to control the magnetization of these inorganic materials via polymer compositions.

5.1 INTRODUCTION

Nanostructured metal-containing materials have received a lot of attention due to their potential applications in a variety of fields.[1-5] For example, metallic FeCo hybrids in nanoscale could be used in magnetic resonance imaging, magnetic data storage and high-temperature space power systems.[6-7] Transition metal phosphide materials (e.g. Fe_2P, Co_2P and Fe_xCo_yP) have been utilized as semiconductors, luminescent devices, and water-splitting catalysts.[8-10] Among these versatile metal-containing materials, metal/carbon materials have gained particular interest from chemists due to their combined properties from metal and carbon, such as excellent mechanical properties, magnetic properties and enhanced biocompatibility.[6, 11-14] As a result, core/shell metal carbon materials with high resistance toward environment degradations have been widely

utilized in many advanced applications.[15-18] Carbon materials in these core/shell metal-containing materials are usually prepared as amorphous carbon, crystallized graphite or graphene, and carbon nanotubes, according to specific preparation methods.[15, 19] Each of these carbon states has unique functions and could be used in different applications.[2, 6, 15, 18]

Scheme 5.1. Preparation of nanostructured inorganic iron/cobalt-containing materials with controlled magnetic properties from a series of cobaltocenium/ferrocene-containing heterobimetallic block copolymers with different block ratios.

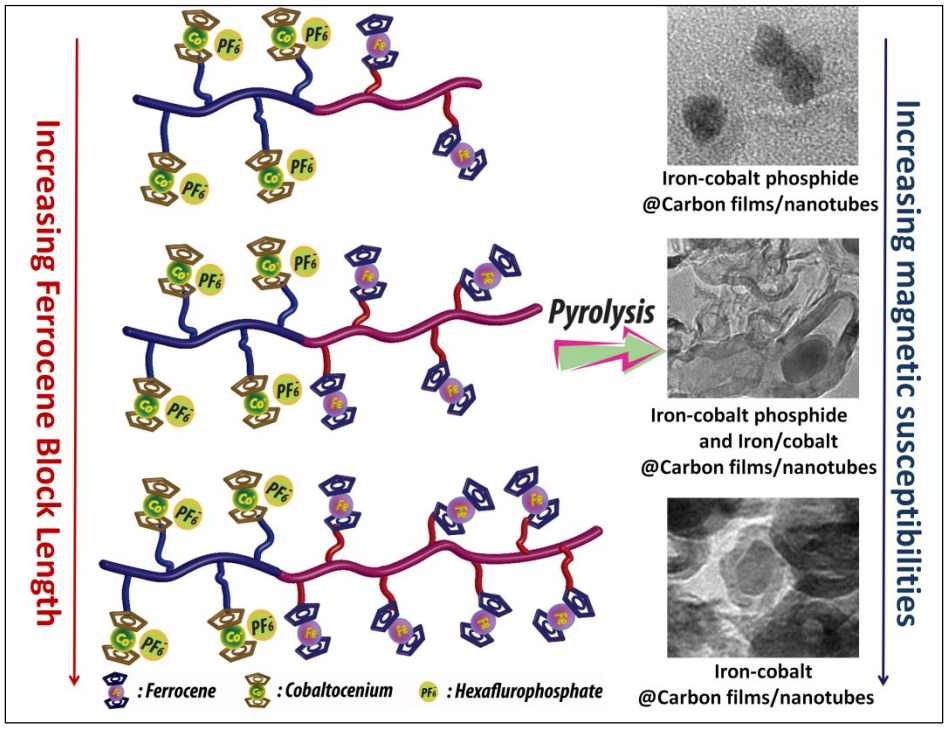

There have been various methods to prepare metal/carbon nanocomposite, including carbon arc techniques, pyrolysis of organometallics, annealing and pyrolysis of polymeric precursors blended with metals, catalytic carbonization process and chemical vapor deposition.[11, 20-25] Among these techniques, utilization of polymeric precursors to prepare metal/carbon nanocomposite is now receiving increasing attention due to the intrinsic advantages of polymers, such as controlled molecular weight, chemical

compositions and architectures as well as versatile nanoscale morphologies that are benefited from recent breakthrough on controlled/living polymerization techniques.[11-12, 26-29] Currently, most metal/carbon materials from polymeric precursors are based on polymer/metal blends, polymer/metal homopolymers and self-assembled block copolymers with installation of metal elements via post-polymerization modification.[14, 27, 30-31] Direct utilization of metallic block copolymers as precursors to prepare metal/carbon materials is far less explored, partially due to the synthetic challenge to prepare well-defined metallic block copolymers.[12, 26, 32-36] Ian Manners and his coworkers reported the utilization of ferrocene-containing main-chain homopolymers with post-polymerization modified cobalt-containing units to prepare Fe/Co nanoparticles on carbon films.[30-31] Our recent work has preliminarily demonstrated the ability of heterobimetallic diblock copolymers (containing cobaltocenium and ferrocene) to form well-defined Co/Fe nanoscale hybrids and $CoFe_2O_4$ nanoparticles with the utilization of their solution self-assembled structures.[33, 37-39] By adjusting block ratios in precursors, it is believed that metal-containing block copolymers are more feasible for unique morphologies, controlled magnetic properties and final compositions of metal/carbon materials.[38, 40-41]

Here we reported an advanced utilization of cobaltocenium/ferrocene-containing heterobimetallic block copolymers to prepare different nanostructured iron-cobalt/carbon materials with controlled magnetic properties (**Scheme 5.1**). Core/shell metal/carbon nanoparticles were produced by facile thermal pyrolysis of these metallic diblock copolymers. These metal nanoparticles were embedded on amorphous carbon films or encapsuled in well-graphitized carbon nanotubes. Metal compositional analysis indicated

a transition from iron-cobalt hybrids to iron-cobalt phosphides when the compositions of precursors changed. Besides, a gradual change of magnetic susceptibilities was also observed through the control of these metallic diblock copolymer compositions. This study provided a novel and convenient strategy to prepare versatile nanostructured iron-cobalt/carbon and iron-cobalt phosphide/carbon materials with well-controlled magnetic properties.

5.3 Results and Discussion

Preparation of Inorganic Iron-cobalt Materials from Heterobimetallic Diblock Copolymers. A cobaltocenium-containing homopolymer with hexaflurophosphate as counterion (M_n = 22,000 g/mol, M_w/M_n = 1.25) was synthesized via reversible addition-fragmentation chain-transfer polymerization (RAFT) according to our previous reports.[33, 37] Ferrocene-containing methacrylate monomers were chain-extended from the cobaltocenium-containing homopolymer to form heterobimetallic diblock copolymers (coded as cobaltocenium-*b*-ferrocene).[37] Three diblock copolymers were prepared with different lengths of the ferrocene block. According to ^{1}H NMR spectra (**Figure 5.1**), the block ratios of three diblock copolymers were determined to be 45:26, 45:98 and 45:171 (cobaltocenium : ferrocene) by comparing the integrations from the peaks of cobaltocenium (peaks at 5.90-6.20 ppm) and ferrocene (4.00-5.00 ppm) units.

Heterobimetallic diblock copolymers were further pyrolyzed at 800 ^{o}C under reductive atmosphere (H_2/N_2, 5 v/v% H_2) to obtain iron-cobalt/carbon materials. From different block copolymers, a clear transition of these inorganic materials from metal (iron-cobalt) phosphide to iron-cobalt alloy was identified by powder X-ray diffraction (PXRD) and selected area electron diffraction (SAED). Peaks in the PXRD patterns were

matched to previously reported phases and assigned as indicated in Figure 2. Peaks observed at 40.4º, 42.6º, 43.9º, 48.6º, 49.3º, 51.5º etc., matched with iron-cobalt phosphide $(Fe_{0.7}Co_{0.3})_2P$ (100% phase content).[33] In Figure 2B, peaks at 40.4º, 42.6º, 43.9º, 48.6º, 49.3º, 51.5º, 44.6º and 64.9º were matched to iron-cobalt phosphide ($(Fe_{0.7}Co_{0.3})_2P$) and an iron cobalt alloy ($Co_{11}Fe_5$).[6, 33] According to the intensity of peaks from PXRD, the percentages of $(Fe_{0.7}Co_{0.3})_2P$ and iron cobalt alloy were 71% and 29%, respectively. Peaks in **Figure 5.2C** at 44.5º and 64.8º matched with another iron cobalt alloy, $Fe_{13}Co_3$ with a percentage of 62%. Meanwhile, peaks in **Figure 5.2C** at 40.4º, 42.6º, 43.9º, 48.6º, 49.3º, 51.5º indicated the product of iron-cobalt phosphide, $(Fe_{0.7}Co_{0.3})_2P$, with a percentage of 38%. These results were consistent with SAED patterns of these inorganic materials, which were shown in **Figure 5.2G**, **5.2H** and **5.2I**. In order to explain this composition variation, Inductively Coupled Plasma Mass Spectrometry (ICP-MS) was utilized to analyze contents of iron, cobalt and phosphorus in materials prepared from different diblock copolymers. As shown in **Table 5.1**, when increasing the length of ferrocene block in diblock copolymers, the weight percentage of iron increased and phosphorus decreased. It appeared that the reduction of phosphorus from hexafluorophosphate (counterions of cobaltocenium moieties) led to insufficient binding with metal elements. For Composite **1** (materials from block copolymer **1** (Mn= 30900) with the shortest ferrocene block), only metal phosphides (iron-cobalt phosphide and trace amount of cobalt phosphide) were obtained due to the existence of large amount of phosphorus. For Composite **2** (materials from block copolymer **2 (**Mn=55500) with increasing amount of ferrocene), only partial pyrolyzed products were metal phosphide with concurrent formation of iron-cobalt alloy. While for Composite **3** (materials from

block copolymer **3** (Mn=80500) with the longest length of ferrocene block), metal phosphides became minority products and iron-cobalt alloy dominated the composites. Given that $(Fe_{0.7}Co_{0.3})_2P$ is the only cobalt-iron phosphide reported in the literature and that it shares the same space group as Co_2P,[42] it is likely that the compositions of the mixed-metal phosphides produced from thermal decomposition of the copolymers differ from this composition and are members of a solid solution series($(Fe_xCo_{1-x})_2P$, x=0~1). Using the elemental analysis data from ICP-MS, the stoichiometry of the product in Composite **1** can be estimated as $(Fe_{0.3}Co_{0.7})_2P$. With a similar method, the stoichiometry of the product in Composite **2** was estimated as $(Fe_{0.57}Co_{0.43})_2P$ and $Fe_{11}Co_5$. For Composite **3**, the stoichiometry of the product was possibly $(Fe_{0.6}Co_{0.4})_2P$ and $Fe_{13}Co_3$.

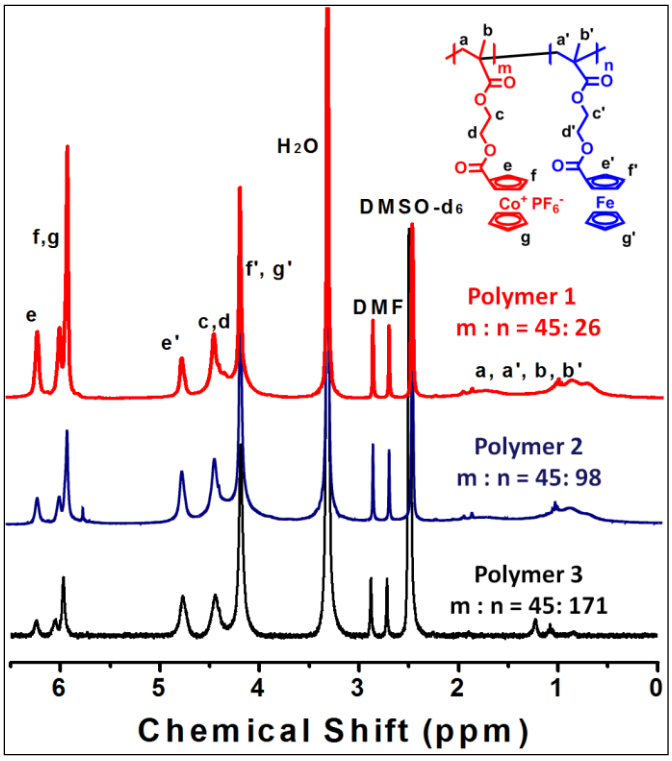

Figure 5.1. ^1H NMR spectra of heterobimetallic diblock copolymers (**1, 2, 3**) with different block ratios (cobaltocenium : ferrocene = 45: 26, 45:98 and 45:171).

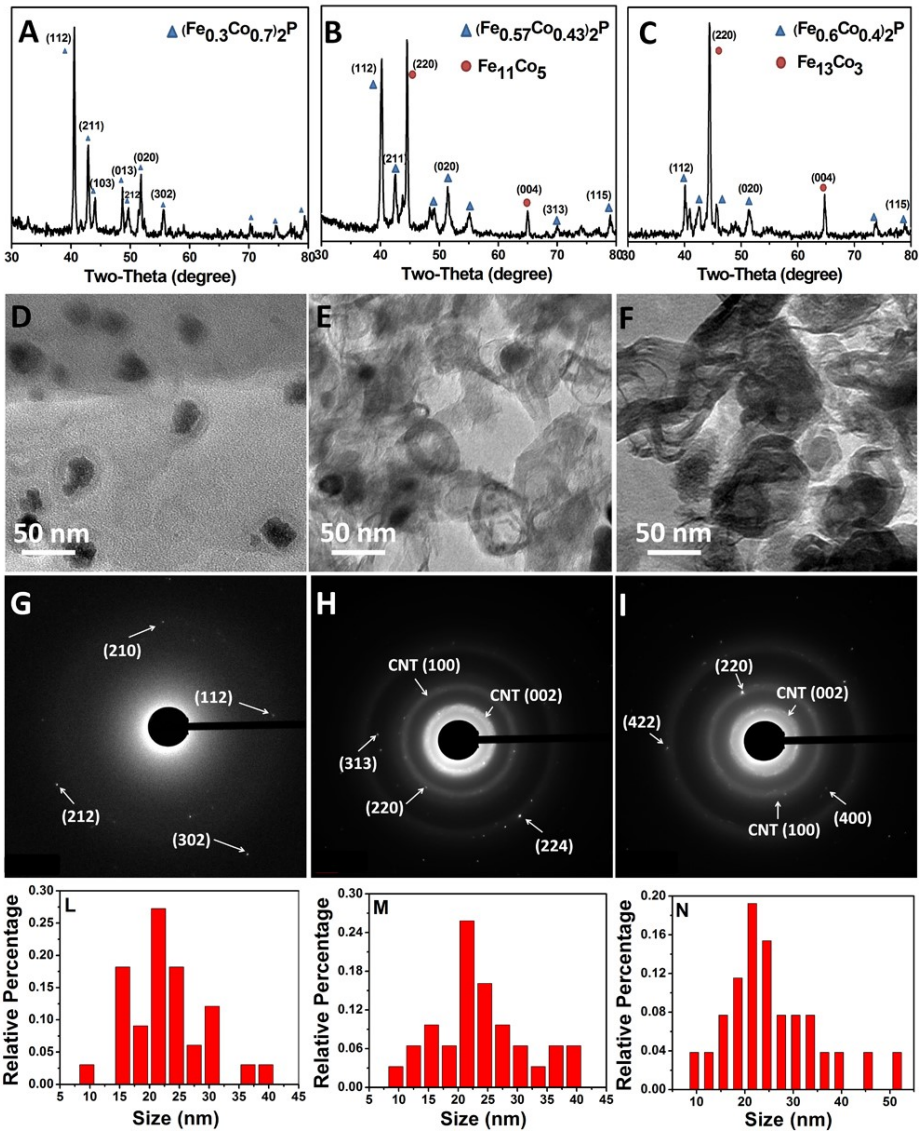

Figure 5.2. PXRD patterns and TEM images of different heterobimetallic block copolymers after thermal treatment (800 ºC) under reductive atmosphere (H_2/N_2, 5 v/v% H_2). XRD spectra: (A) Composite **1**; (B) Composite **2**; (C) Composite **3**. (D), (E) and (F) are TEM images of these pyrolyzed metallopolymers: (D) Composite **1**; (E) Composite **2**; (F) Composite **3**. (G), (H) and (I) are SAED patterns for pyrolyzed materials in Figure (D), (E) and (F). (L), (M) and (N) are size distributions for nanoparticles in Composite **1**, **2** and **3**, respectively.

Morphology of Inorganic Iron-Cobalt Materials from Different Heterobimetallic Diblock Polymers. As shown in **Table 5.1**, the weight percentage of inorganic materials in final composites was around 22-31%. The rest of the materials should be residual carbon derived from organic components of polymers, as

demonstrated in later sections of this paper. The carbon provided the matrix for these inorganic iron-cobalt species. The carbon matrixes from three heterobimetallic diblock copolymers were similar, which were amorphous carbon films and multi-walled carbon nanotubes. This result could be demonstrated by Raman spectra (**Figure 5.3**). Peaks at D and G bands at about 1300 and 1600 cm^{-1} demonstrated the co-existence of carbon nanotubes and amorphous carbon in carbon materials in three samples.[43] The obtained inorganic materials and their matrix were further characterized by TEM (**Figure 5.2D, 5.2E** and **5.2F**). After thermal treatment, all metal/carbon nanoparticles from different metallopolymers showed similar morphologies with similar size distributions (**Figure 5.2L, 5.2M** and **5.2N**). The average size for these nanoparticles in composite **1**, composite **2** and composite **3** are 22.8 nm, 23.9 nm and 25.0 nm, respectively. As shown in **Figure 5.2D**, some nanoparticles were embedded on amorphous carbon films, which were consistent with Raman spectra. These nanoparticles were also found to be encapsulated in multi-walled carbon nanotubes (**Figure 5.2E, 5.2F** and **Figure 5.4**). Diffraction rings PolyCNT (100) and CNT (002) in SAED patterns from **Figure 5.2H** and **5.2I** indicated the crystallinity from carbon nanotubes.[44] The thickness of each carbon layer was 0.33 nm, which was determined by high resolution TEM (**Figure 5.4C**). Considering the metallocene units in polymer chains, such observance of carbon nanotubes in these inorganic materials were reasonable. Early work has demonstrated that metallocenes are common catalysts to produce carbon nanotubes, due to their capability to provide both carbon sources (organic cyclopentadienyl rings) and catalyst centers (metals). [45-47]

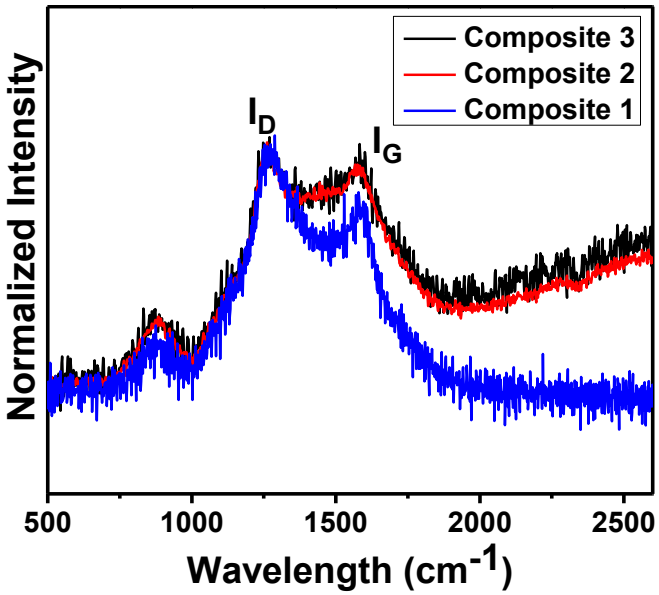

Figure 5.3. Raman spectra of pyrolyzed materials from heterobimetallic diblock copolymers with different block ratios after thermal treatment (800 °C) under reductive atmosphere (H_2/N_2, 5 v/v% H_2) (Spectra were normalized by setting I_D peak as 1).

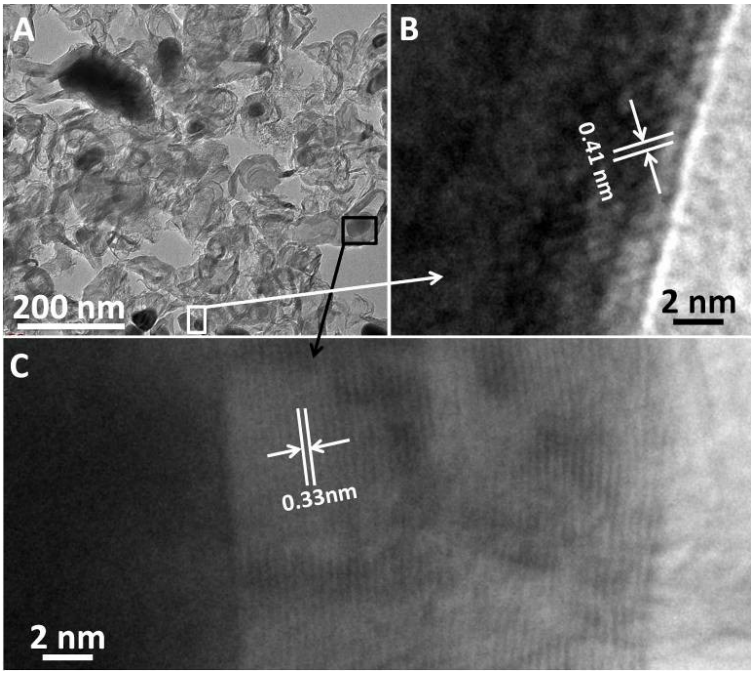

Figure 5.4. (A) TEM image of core/shell metal/carbon nanotube materials prepared from heterobimetallic diblock copolymer **2**. (B) High resolution TEM image of metal-containing nanoparticles from enlarged part of **Figure 5.4A**. (C) High resolution TEM image of multi-walled carbon nanotubes from enlarged part of **Figure 5.4A**.

Table 5.1. Element compositions of pyrolyzed heterobimetallic diblock copolymers.

Weight %	Composite 1	Composite 2	Composite 3
Cobalt %	17.1%	8.38%	4.87%
Iron %	6.77%	13.2%	14.9%
Phosphorus %	7.13%	4.44%	2.43%
Carbon % [a]	69.0%	74.0%	77.8%

a. The carbon% in Table 1 is the weight percentage of carbon in the final materials, which was calculated by deducting all inorganic materials (cobalt, iron and phosphorus).

Magnetic Transition of Inorganic Iron-Cobalt Materials from Different Heterobimetallic Diblock Polymer. The compositions of heterobimetallic block copolymers also had a significant impact on magnetic behaviors of resultant inorganic materials obtained by pyrolysis. Temperature dependence of magnetization curves under Zero-Field Cooled (ZFC) and Field Cooled (FC) (**Figure 5**) conditions indicated that inorganic materials from pyrolyzed heterobimetallic diblock copolymers behaved like typical superparamagnetic materials.[12, 48] For magnetic materials obtained from block copolymers with longer ferrocene chains (polymer **2** and polymer **3**), the blocking temperature (T_B) was above 385K. While for materials obtained from polymer **1** (shortest ferrocene chain), T_B decreased to 320K, which might be due to the transition of metal/carbon materials to metal phosphide/carbon materials. Besides, considering that blocking temperature is very sensitive to particle size,[49-50] different size distributions of these composites might also result in the change of the blocking temperature. These results also indicated that at room temperature these pyrolyzed materials are ferromagnetic, which was further confirmed by hysteresis loops at 300K. Hysteresis loops under different temperatures (5K, 100K, 200K, 300K and 385K) (**Figure 5.7A**)

were measured for Composite **1**. The relationship between coercivity (*Hc*)**,** remnant magnetization *(M_r)* and temperature were summarized and plotted in Figure 7B. The results showed there were 3% remanence magnetization and 10% coercivity left at 385K (**Figure 5.7B**), which was most probably due to the particle size distribution of these composites.[49-50] As indicated in **Figure 5.6**, all magnetic materials reached saturation under high field strength of 1.2T. Similar coercivity was observed (400 Oe) for all inorganic materials under an applied field of 3T (**Table 5.2**). While for saturated magnetization, with the longer ferrocene-containing block, the higher magnetic saturation (**Figure 5.6B**, inserted picture) can be reached at 212.0 emu/g and 107.2 emu/g respectively for pyrolyzed materials from polymer **3** and polymer **2,** normalized by the weight percentage of effective inorganic materials (cobalt, iron and phosphorus) shown in **Table 5.1**. However, inorganic materials from polymer **1** could only reach 20.8 emu/g. Considering the huge difference in saturated magnetization of iron, cobalt and iron-cobalt phosphide, such saturation change was not surprising. According to previous reports,[51-53] the saturation moment of pure iron-cobalt alloy (Fe_xCo_y, w(Co)%=20~30%) was about 230 emu/g, while the value for its phosphide ($(Fe_xCo_{1-x})_2P$, x=0~1)was only from 11.6 to 101.9 emu/g, respectively. Saturation moments of these compounds were converted from Bohr magnetons (μ_B per formula unit), which were about 2.30 μB for Fe_xCo_y (w(Co)%= 20~30%),[52] 0.31~2.65 μB for $(Fe_xCo_{1-x})_2P$ (x=0~1) [51, 53], ($1\mu B/mol = 9.274\times10^{-21}$ $emu\cdot g^{-1}\cdot M_w^{-1}$, M_w is the molecular weight of the compound). Considering phosphorus content (**Table 5.1**) in the final materials from polymer **1**, most of metal elements were reacted with phosphorus to form $(Fe_{0.3}Co_{0.7})_2P$, which could give saturated magnetization at around 29.9 emu/g. While for Composite **2**, a higher saturated magnetization could be

estimated due to the less content of phosphorus, which led the formation of 71% $(Fe_xCo_{1-x})_2P$ (x=~0.57) and 29% Fe_xCo_y (w(Co)%=20~30%) with saturated magnetizations from 69.0 -140.0 emu/g. For Composite **3**, an even higher saturated magnetization could be anticipated at around 161.0 emu/g, which was due to the high content (62%) of Fe_xCo_y (w(Co)%=20~30%). Magnetization values of these inorganic materials were highly related with phosphorus content, indicating that we can control the magnetization of these functional materials by manipulating the block copolymer compositions.

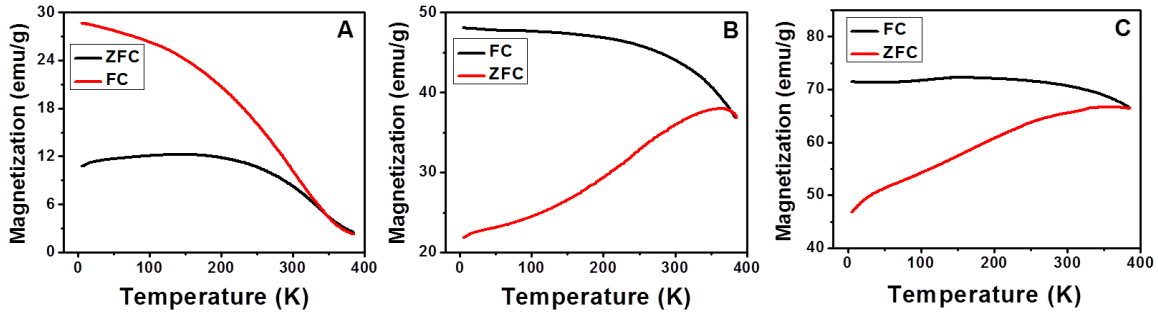

Figure 5.5. Zero-Field Cooled (ZFC) and Field Cooled (FC) curves for iron-cobalt/carbon and iron-cobalt phosphide/carbon materials from heterobimetallic block copolymers: (A) Composite 1, (B) Composite 2 and (C) Composite 3. Magnetization values were normalized by the weight percentage of effective inorganic materials (cobalt, iron and phosphorus) shown in **Table 5.1**.

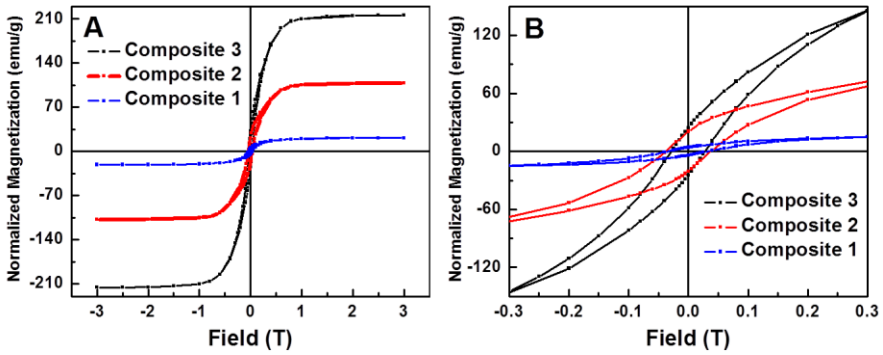

Figure 5.6. (A) Hysteresis loop for pyrolyzed block copolymers; (B) Enlarged part of Figure 6A at low field magnetization.

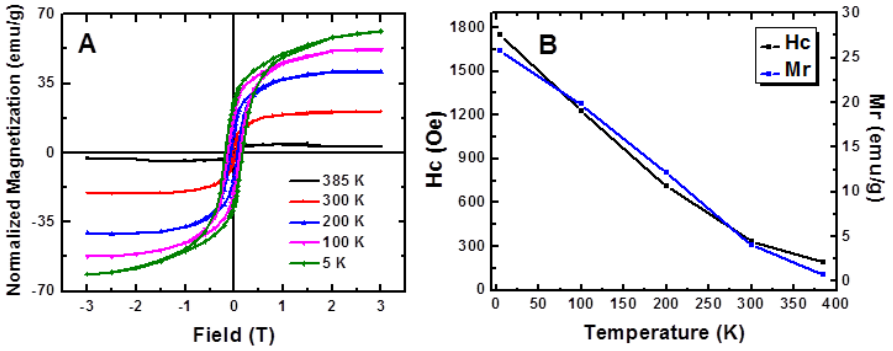

Figure 5.7. (A) Hysteresis loops of Composite **1** under different temperatures (5K, 100K, 200K, 300K and 385K). (B) The plot of *Hc*, *Mr* with temperature for Composite **1** based on **Figure 5.7A**.

Table 5.2. Values of saturation magnetization (M_s), remnant magnetization (M_r) and coercivity (H_c) for Composite 1, Composite 2 and Composite 3.

	Ms **(emu/g)**	***Mr*** **(emu/g)**	***Hc*** **(Oe)**
Composite 1	20.8	4.1	328.2
Composite 2	107.2	20.0	389.0
Composite 3	212.0	23.6	271.0

5.4 EXPERIMENTAL

Materials. Chain transfer agent cumyl dithiobenzoate (97%, CDB) was purchased from Aldrich, and used directly. Cobaltocenium-containing methacrylate polymer with hexafluorophosphate anion (poly(2-(methacrylolyoxy)ethyl cobaltoceniumcarboxylate hexafluorophosphate)) was synthesized according to our earlier reports [33, 37] (M_n = 22,000 g/mol, determined by ^{1}H NMR conversion; M_w/M_n = 1.25, polydispersity was measured for polymers after cleaving all cobaltocenium groups). Side-chain ferrocene-containing monomer (2-(methacrylolyoxy) ethyl

ferrocenecarboxylate) (MAEFc) was synthesized according to our previous report.[33, 37] All other chemicals were from commercial sources and used as received.

Characterization. ^{1}H NMR (400 MHz) spectra were recorded on a Varian Mercury 400 spectrometer with tetramethylsilane (TMS) as an internal reference. Transmission electron microscopy (TEM) samples were conducted using a Zeiss Libra 120. TEM experiments were performed at 120kV with an emission current of 6μA in order to minimize electron-beam-induced nanoparticle change or damage. Lindberg bluem furnace was used to pyrolyze polymers under H2/N2 (H2, 5% volume) flow or under air flow at 800 oC. X-ray diffraction (XRD) measurements were conducted on a Rigaku D/Max 2100 Powder X-Ray Diffractometer (Cu Kα radiation) instrument and scanned from 10o to 85o with a step size of 0.005o and a step rate of 6 s. The data were collected at the second scan. Magnetic measurements were performed at Oak Ridge National Laboratory using a SQUID magnetometer. Bulk elemental chemical microanalyses were performed by inductively coupled plasma Mass Spectrometry (ICP-MS).

Synthesis of heterobimetallic diblock copolymers (cobaltocenium-b-ferrocene) with different block ratios. Heterobimetallic diblock copolymers were synthesized according to previous reports.[33, 37] MAEFc monomers were chain-extended from side-chain cobaltocenium-containing homopolymer (*Mn* = 22,000 g/mol, *Mw*/*M*n = 1.25). Specifically, the side-chain cobaltocenium-containing methacrylate homopolymer (250 mg, 1.1×10-2 mmol), azobisisobutyronitrile (AIBN, 0.38 mg, 2.2×10-3 mmol), and MAEFc (1.40 g, 4.1 mmol) were dissolved into 1.2 mL dry DMF. The mixture was degassed and reacted for 2 hours under 90 oC. The conversion of MAEFc was controlled

at ~50% to obtain the block ratio at 45:171 (cobaltocenium : ferrocene). Other diblock copolymers were prepared in a similar way with different feed ratios of ferrocene-containing monomers. The final diblock copolymers were collected, dried and stored under the protection of nitrogen. ^{1}H NMR spectrum for heterobimetallic diblock copolymers (400 MHz, DMSO-d6, δ): 6.3, 6.2, 5.9 (broad, Cp from Cp2Co), 4.0-4.8 (broad, C*H2*C*H2*, Cp from Cp2Fe), 2.1(s, C*H3*), 0.6-1.0 (broad, C*H2*C).

General preparation and characterization of inorganic materials from heterobimetallic diblock copolymers with different block ratios. Inorganic materials were obtained by pyrolysis of metallic diblock copolymers under 800 oC in reductive atmosphere (H2/N2, 5 v/v% H2) for 8 hours. For each pyrolysis, 50 mg of each polymer was used. After pyrolysis, black powders were immediately collected and protected in a glove box. XRD samples of these products were prepared by sealing in X-ray sample holder with grease in a glove box. These black powders were also sealed in a vial by parafilm and stored in a glove box. And then TEM samples were prepared by dispersing these powders in 1 mL ethanol for further characterization.

Magnetic characterization of pyrolyzed materials from heterobimetallic diblock copolymers. The black powders were sealed under the protection of nitrogen before the magnetic characterization. Hysteresis loops for all inorganic materials were characterized by a SQUID magnetometer under 300 K and the applied field was swept from -3T to 3T. For the zero-field-cooling (ZFC) M(T) measurement, the sample was cooled down to 3 K without any applied field and then the data were collected during warming up from 3 K to 385 K. For the field-cooling (FC) measurement, the data were collected when cooling down from 385 K to 3 K.

Sample preparation for Inductively Coupled Plasma Mass Spectrometry (ICP-MS) measurement. ICP-MS samples were prepared by digesting the samples in 2 mL of aqua regia. The samples were analyzed immediately after the initial calibration, and the target element results were within the calibration range. The samples were analyzed for Fe, Co and P using the Finnigan ELEMENT2 double focusing magnetic sector field inductively coupled plasma-mass spectrometer (ICP-MS). Iridium (1 ppb) was used as the internal standard. The following is the summary of the quality control information associated with the analysis: (1) the instrument was calibrated for element Fe, Co and P. The calibration range was from 10 to 600 ppb. The R squared value for the initial calibration curve was greater than 0.99; (2) the Fe and P results were corrected from the method blank; (3) the ending continuing calibration verification recoveries were 105% for Fe, 108% for P, and 101% for Co.

5.5 CONCLUSION

In conclusion, we reported the preparation of various iron-cobalt/carbon and iron-cobalt phosphide/carbon magnetic materials using a series of heterobimetallic diblock copolymers as precursors. Through the control of block ratios of ferrocene-containing block to cobaltocenium-containing block in the precursors, a transition of pyrolyzed materials from metal phosphide to metal alloy was observed, although it was not fully converted. Besides, these metal elements were embedded or encapsulated in carbon films or multi-walled carbon nanotubes. Magnetic characterization demonstrated that all these pyrolyzed materials are ferromagnetic under room temperature. However, their magnetization was drastically different, depending on their compositions. These results showed that the saturated magnetization was closely related with weight percentage of

phosphorus and cobalt, indicating a tunable magnetization of these inorganic materials via adjusting heterobimetallic diblock copolymer compositions. Considering our early controlled self-assembly study on these diblock copolymers,[33, 37, 39] this work laid a foundation for the pursing of more advanced nanostructured core/shell iron-cobalt materials with desirable magnetic properties through directly utilization of metallopolymers. Such carbon nanotubes protected and controlled magnetic materials with high tolerance towards harsh conditions could be possibly applied in various applications, such as novel oxygen reduction catalysts[13] and magnetic bioimaging devices[7].

5.6 ACKNOWLEDGEMENT

We would like to acknowledge National Science Foundation (CHE-1151479). A portion of this research was conducted at the Center for Nanophase Materials Sciences, which is sponsored at Oak Ridge National Laboratory by the Division of Scientific User Facilities, Office of Basic Energy Sciences, U.S. Department of Energy.

5.7 REFERENCES

1. U. Schubert, N. Husing and A. Lorenz, *Chem. Mater.* **1995**, *7*, 2010-2027.
2. P. Poizot, S. Laruelle, S. Grugeon, L. Dupont and J. M. Tarascon, *Nature* **2000**, *407*, 496-499.
3. F. Jakle, *Chem. Rev.* **2010**, *110*, 3985-4022.
4. Y. C. Yang, G. F. Wang and X. D. Li, *Nano Lett.* **2011**, *11*, 2845-2848.
5. X. L. Wu, Y. T. Zhu, Y. G. Wei and Q. Wei, *Phys. Rev. Lett.* **2009**, *103*.
6. S. P. Sherlock, S. M. Tabakman, L. M. Xie and H. J. Dai, *Acs. Nano* **2011**, *5*, 1505-1512.
7. W. S. Seo, J. H. Lee, X. M. Sun, Y. Suzuki, D. Mann, Z. Liu, M. Terashima, P. C. Yang, M. V. McConnell, D. G. Nishimura and H. J. Dai, *Nat. Mater.* **2006**, *5*, 971-976.
8. J. Park, B. Koo, K. Y. Yoon, Y. Hwang, M. Kang, J. G. Park and T. Hyeon, *J. Am. Chem. Soc.* **2005**, *127*, 8433-8440.
9. Y. Li, M. A. Malik and P. O'Brien, *J. Am. Chem. Soc.* **2005**, *127*, 16020-16021.
10. A. E. Henkes, Y. Vasquez and R. E. Schaak, *J. Am. Chem. Soc.* **2007**, *129*, 1896-1897.

11. M. Zhong, E. K. Kim, J. P. McGann, S. E. Chun, J. F. Whitacre, M. Jaroniec, K. Matyjaszewski and T. Kowalewski, *J. Am. Chem. Soc.* **2012**, *134*, 14846-14857.
12. Z. M. Al-Badri, R. R. Maddikeri, Y. P. Zha, H. D. Thaker, P. Dobriyal, R. Shunmugam, T. P. Russell and G. N. Tew, *Nat. Commun.* **2011**, *2*.
13. D. H. Deng, L. Yu, X. Q. Chen, G. X. Wang, L. Jin, X. L. Pan, J. Deng, G. Q. Sun and X. H. Bao, *Angew. Chem. Int. Ed.* **2013**, *52*, 371-375.
14. J. W. Lee, H. J. Jeon, H. J. Shin and J. K. Kang, *Chem. Commun.* **2012**, *48*, 422-424.
15. G. G. Wildgoose, C. E. Banks and R. G. Compton, *Small* **2006**, *2*, 182-193.
16. C. X. Lu, Y. Fan, H. Li, Y. Yang, B. K. Tay, E. Teo and Q. Zhang, *Carbon* **2013**, *63*, 54-60.
17. M. D. Gimenez-Lopez, F. Moro, A. La Torre, C. J. Gomez-Garcia, P. D. Brown, J. van Slageren and A. N. Khlobystov, *Nat. Commun.* **2011**, *2*.
18. F. Rossella, C. Soldano, V. Bellani and M. Tommasini, *Adv. Mater.* **2012**, *24*, 2453-2458.
19. S. Subramoney, *Adv. Mater.* **1998**, *10*, 1157-1171.
20. Y. Lu, Z. P. Zhu and Z. Y. Liu, *Carbon* **2005**, *43*, 369-374.
21. Y. L. Hsin, C. F. Lin, Y. C. Liang, K. C. Hwang, J. C. Horng, J. A. A. Ho, C. C. Lin and J. R. Hwu, *Adv. Funct. Mater.* **2008**, *18*, 2048-2056.
22. W. H. Chiang, M. Sakr, X. P. A. Gao and R. M. Sankaran, *Acs. Nano* **2009**, *3*, 4023-4032.
23. D. Barreca, C. Massignan, S. Daolio, M. Fabrizio, C. Piccirillo, L. Armelao and E. Tondello, *Chem. Mater.* **2001**, *13*, 588-593.
24. J. H. Fendler, *Chem. Mater.* **1996**, *8*, 1616-1624.
25. C. G. Hardy, J. Zhang, Y. Yan, L. Ren and C. Tang, *Prog. Polym. Sci.* **2014**, *DOI: 10.1016/j.progpolymsci.2014.03.002*.
26. S. E. Bowles, W. Wu, T. Kowalewski, M. C. Schalnat, R. J. Davis, J. E. Pemberton, I. Shim, B. D. Korth and J. Pyun, *J. Am. Chem. Soc.* **2007**, *129*, 8694-8670.
27. M. Mullner, T. Lunkenbein, J. Breu, F. Caruso and A. H. E. Muller, *Chem. Mater.* **2012**, *24*, 1802-1810.
28. K. Matyjaszewski and N. V. Tsarevsky, *Nat. Chem.* **2009**, *1*, 276-288.
29. X. S. Wang and R. McHale, *Macromol. Rapid Comm.* **2010**, *31*, 331-350.
30. A. Berenbaum, M. Ginzburg-Margau, N. Coombs, A. J. Lough, A. Safa-Sefat, J. E. Greedan, G. A. Ozin and I. Manners, *Adv. Mater.* **2003**, *15*, 51-55.
31. K. Liu, S. B. Clendenning, L. Friebe, W. Y. Chan, X. B. Zhu, M. R. Freeman, G. C. Yang, C. M. Yip, D. Grozea, Z. H. Lu and I. Manners, *Chem. Mater.* **2006**, *18*, 2591-2601.
32. L. Ren, C. G. Hardy and C. Tang, *J. Am. Chem. Soc.* **2010**, *132*, 8874-8875.
33. J. Zhang, Y. Yan, M. W. Chance, J. H. Chen, J. Hayat, S. G. Ma and C. Tang, *Angew. Chem. Int. Ed.* **2013**, 13387-13391.
34. R. B. Grubbs, *J. Polym. Sci. Pol. Chem.* **2005**, *43*, 4323-4336.
35. J. M. Stanley and B. J. Holliday, *Coord. Chem. Rev.* **2012**, *256*, 1520-1530.
36. J. B. Gilroy, S. K. Patra, J. M. Mitchels, M. A. Winnik and I. Manners, *Angew. Chem. Int. Ed.* **2011**, *50*, 5851-5855.

37. L. Ren, J. Zhang, C. G. Hardy, S. G. Ma and C. Tang, *Macromol. Rapid Comm.* **2012**, *33*, 510-516.
38. C. G. Hardy, L. X. Ren, S. G. Ma and C. Tang, *Chem. Commun.* **2013**, *49*, 4373-4375.
39. J. Zhang, L. Ren, C. G. Hardy and C. Tang, *Macromolecules* **2012**, dx.doi.org/10.1021/ma3012784.
40. C. Tang, K. Qi, K. L. Wooley, K. Matyjaszewski and T. Kowalewski, *Angew. Chem. Int. Ed.* **2004**, *43*, 2783-2787.
41. Q. Dong, G. J. Li, C. L. Ho, M. Faisal, C. W. Leung, P. W. T. Pong, K. Liu, B. Z. Tang, I. Manners and W. Y. Wong, *Adv. Mater.* **2012**, *24*, 1034-1040.
42. W. Maneeprakorn, M. A. Malik and P. O'Brien, *J. Mater. Chem.* **2010**, *20*, 2329-2335.
43. A. A. Koos, R. J. Nicholls, F. Dillon, K. Kertesz, L. P. Biro, A. Crossley and N. Grobert, *Carbon* **2012**, *50*, 2816-2823.
44. B. Wen, J. J. Zhao, T. J. Li, C. Dong and J. Z. Jin, *J. Phys-Condens. Mat.* **2005**, *17*, L513-L519.
45. A. L. Elias, J. A. Rodriguez-Manzo, M. R. McCartney, D. Golberg, A. Zamudio, S. E. Baltazar, F. Lopez-Urias, E. Munoz-Sandoval, L. Gu, C. C. Tang, D. J. Smith, Y. Bando, H. Terrones and M. Terrones, *Nano Lett.* **2005**, *5*, 467-472.
46. A. Leonhardt, A. Ritschel, R. Kozhuharova, A. Graff, T. Muhl, R. Huhle, I. Monch, D. Elefant and C. M. Schneider, *Diam. Relat. Mater.* **2003**, *12*, 790-793.
47. Q. Z. Jiao, L. Hao, Q. Y. Shao and Y. Zhao, *Carbon* **2013**, *61*, 647-649.
48. M. Castrillon, A. Mayoral, A. Urtizberea, C. Marquina, S. Irusta, J. G. Meier and J. Santamarıa, *Nanotechnology* **2013**, *24*.
49. D. Caruntu, G. Caruntu and C. J. O'Connor, *J. Phys. D Appl. Phys.* **2007**, *40*, 5801-5809.
50. A. Lak, M. Kraken, F. Ludwig, A. Kornowski, D. Eberbeck, S. Sievers, F. J. Litterst, H. Weller and M. Schilling, *Nanoscale* **2013**, *5*, 12286-12295.
51. S. K. Jain, S. Kumar, P. S. R. Krishna, A. B. Shinde, A. Krishnamurthy and B. K. Srivastava, *J. Alloy Compd.* **2007**, *439*, 13-17.
52. M. C. Nguyen, X. Zhao, M. Ji, C. Z. Wang, B. Harmon and K. M. Ho, *J. Appl. Phys.* **2012**, *111*, 07E338-307E338-333.
53. S. Kumar, A. Krishnamurthy and B. K. Srivastava, *J. Phys. D Appl. Phys.* **2008**, *41*, 055001.

CHAPTER 6

ANTIMICROBIAL METALLOPOLYMERS AND THEIR BIOCONJUGATES WITH CONVENTIONAL ANTIBIOTICS AGAINST MULTIDRUG RESISTANT BACTERIA[†]

[†] J. Zhang, Y. P. Chen, K. P. Miller, M. S. Ganewatta, M. Bam, Y. Yan, M. Nagarkatti, A. W. Decho and C. Tang, *J. Am. Chem. Soc.* **2014**, *136*, 4873-4876. Reprinted here with permission of publisher.

6.1 ABSTRACT

Bacteria are now becoming more resistant to most conventional antibiotics. Methicillin-resistant *Staphylococcus aureus* (MRSA), a complex of multidrug resistant Gram-positive bacterial strains, has proven especially problematic in both hospital and community-settings by deactivating conventional β-lactam antibiotics, including penicillins, cephalosporins, and carbapenems through various mechanisms, resulting in increased mortality rates and hospitalization costs. Here we introduce a class of charged metallopolymers that exhibits synergistic effects against MRSA by effectively lysing bacterial cells and efficiently inhibiting activity of β-lactamase. Various conventional β-lactam antibiotics, including penicillin-G, amoxicillin, ampicillin and cefazolin, are protected from β-lactamase hydrolysis via the formation of unique ion-pairs between their carboxylate anions and cationic cobaltocenium moieties. These discoveries could provide a new pathway to designing macromolecular scaffolds to regenerate vitality of conventional antibiotics to kill multidrug resistant bacteria and superbugs.

6.1 INTRODUCTION

Bacteria are rapidly developing resistance to one or more of the most frequently used antibiotics.[1-4] The extent of this global crisis is highlighted by the fact that, for example, annually two million patients suffer from hospital-acquired infections in the United States, with 99,000 deaths. Nearly 30% of these infections are identified as methicillin-resistant *Staphylococcus aureus* (MRSA).[2, 5] Nowadays, 40~60% of *Staphylococcus aureus* strains in hospitals (hospital-associated MRSA, HA-MRSA) are resistant to penicillin, methicillin and many other β-lactam antibiotics.[6-7] There are multiple mechanisms used by MRSA to undermine the effects of conventional antibiotics.

For example, the class A β-lactamase enzyme catastrophically hydrolyzes conventional β-lactam antibiotics including penicillins, cephalosporins, and carbapenems.[8-10]

Currently, vancomycin and amoxicillin/clavulanic acid are among the most commonly used antibiotics for the treatment of MRSA infections.[1, 8] Although these antibiotics are among the strongest of their classes, the high frequency use has resulted in their decreased susceptibility against MRSA.[8-9] In an effort to circumvent antibiotic resistance, novel β-lactamase inhibitors, including boronic acid derivatives, phosphonates and phosphonamidates,[11-12] have been designed, although none of these agents have entered Phase I development.[9] Alternatively, synthetic macromolecules have been introduced as antimicrobial agents.[13-17] Rather than targeting penicillin-binding proteins (PBP) as the most β-lactam antibiotics do, novel cationic polymers or peptides[18-19] can disrupt thick cell walls or membranes, and have shown efficacy against MRSA.[20-21] Some conventional antibiotics have exhibited activity against MRSA by modification with polymers via covalent bonds or encapsulation in a polymeric matrix.[22-24] However, most of these strategies have been restricted by their inherent limitations, such as the high toxicity of cationic polymers and peptides, poor release of antibiotics, and relatively low targeting efficiency toward bacteria.[20, 23] In contrast, as the development of organometallic compounds and macromolecules,[25] novel metallopolymers have been previously used as anticancer drugs, targeting agents, and enzyme inhibitors.[26-29] However, their use as antimicrobial materials still remains in the early stages, and most have not yet achieved an optimal balance between toxicity and bioactivity.[27, 30]

Here we introduce a class of charged metallopolymers, which can not only effectively lyse bacterial cells, but also show efficiency to reduce β-lactamase activity

(**Scheme 6.1**). Our results reveal that these metallopolymers attack both β-lactamase enzymes and cell walls, and protect conjugated antibiotics via ion-pairing between polymers and antibiotics (**Scheme 6.1**). Specifically, these charged metallopolymers are based on cationic cobaltocenium-containing polymers. Due to the unique ability of cationic cobaltocenium moieties to complex with carboxylate anions, various commercial β-lactam antibiotics, including penicillin-G, amoxicillin, ampicillin and cefazolin, can be protected from β-lactamase via the formation of stable ion-pairs with cationic cobaltocenium-containing polymers. Considering these synergistic attributes, these metallopolymers show high efficiency against multidrug-resistant MRSA, while exhibiting non-hemolytic activity and minimal *in vitro* and *in vivo* toxicity.

Scheme 6.1. Illustration of several key interactions involving β-lactamase and β-lactam antibiotics. a. MRSA cells; b. typical β-lactamase hydrolysis of β-lactam antibiotics; c. proposed interactions between β-lactam antibiotics-metallopolymers bioconjugates, β-lactamase and cell wall.

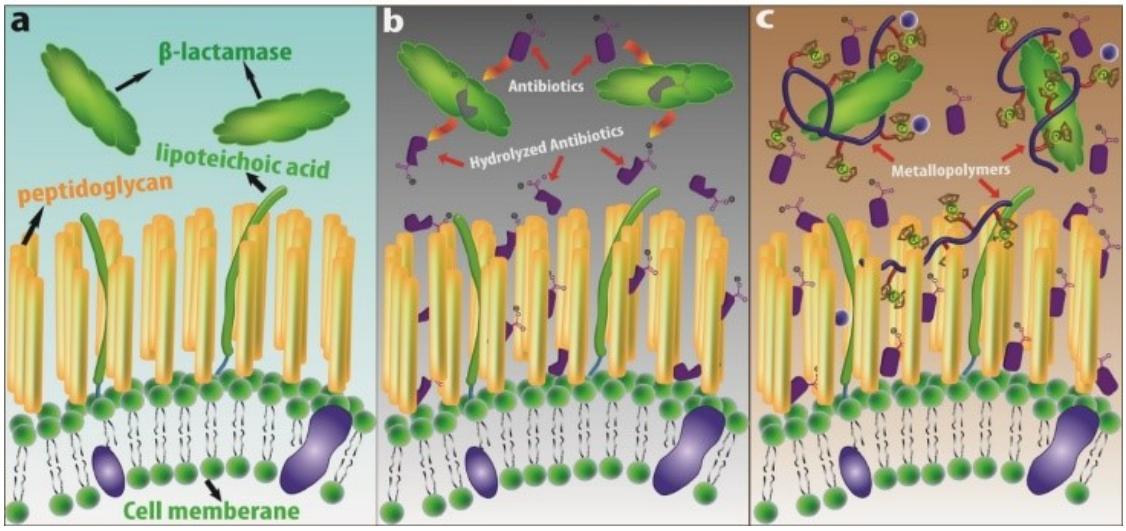

6.3 RESULTS AND DISCUSSION

We recently discovered a class of cationic metallopolymers containing cobaltocenium moieties that exhibited unique ion-pairing ability.[31-35] Hexafluorophosphate (PF_6^-)–paired cobaltocenium-containing polymers, poly(2-(methacrylolyoxy)ethyl cobaltoceniumcarboxylate hexafluorophosphate) (M_n = 15,600 g/mol, M_w/M_n = 1.25), was prepared and used for this study.[31, 33] Halide anion- (Cl^-, Br^- and I^-) paired cationic cobaltocenium polymers were subsequently prepared.[33-34] All halide-paired polymers are hydrophilic and highly soluble in water (solubility > 800 mg/mL).

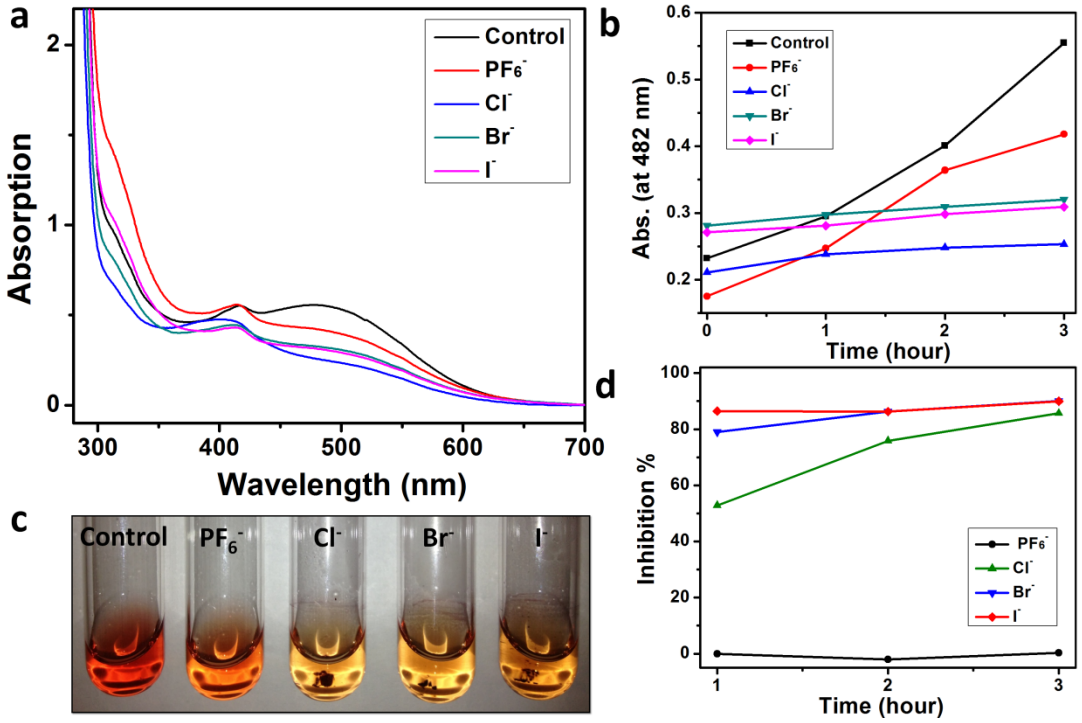

Figure 6.1. a. UV-vis absorption of nitrocefin solution with 5 μM anion-paired metallopolymers and β-lactamase incubated for 3 hours; **b.** incubation time-dependent absorption (at 482 nm) of nitrocefin solution with different anion-paired metallopolymers at 5 μM and β-lactamase; **c.** optical view of nitrocefin solution with different anion-paired metallopolymers at 5 μM and β-lactamase incubated for 3 hours; **d.** the level of β-lactamase activity inhibition by different anion-paired cationic cobaltocenium-containing polymers at 5 μM.

β-Lactamase production and excretion is a major defense mechanism employed by several drug-resistant bacterial pathogens, such as various strains of MRSA.[8-9] Effects of cationic cobaltocenium-containing polymers on β-lactamase activity were conducted by incubation of β-lactamase (obtained from HA-MRSA (ATCC 29213) extracellular solution) with nitrocefin and halide-paired cobaltocenium-containing polymers together. Nitrocefin is a chromogenic cephalosporin that is classified as a β-lactam antibiotic and is typically used to indicate the existence of β-lactamase.[36] A solution of nitrocefin with a pristine β-lactam ring typically appears yellow with an absorption peak near 380 nm. However, after hydrolysis of the β-lactam ring by β-lactamase, the solution typically turns red with an absorption peak near 480 nm.[36] As shown in **Figure 6.1a** and **6.1c**, incubation of β-lactamase with halide–paired polymers and nitrocefin resulted in little hydrolysis (solutions remained yellow with low absorption at 482 nm), although those with PF_6^-–paired polymers resulted in significant hydrolysis of nitrocefin (the solution turned red with high absorption at 482 nm). A time-dependent study was conducted by measuring absorption at 482 nm at different time intervals (**Figure 6.1b**). The inhibition of β-lactamase was shown in **Figure 6.1d**. More than 80% inhibition of β-lactamase activity was achieved by metallopolymers at 5 μM. The use of metallopolymers at 10 μM shut down the β-lactamase hydrolysis completely (**Figure 6.14**). However, negligible inhibition of β-lactamase was observed for PF_6^-–paired metallopolymer, due to its poor solubility in water.

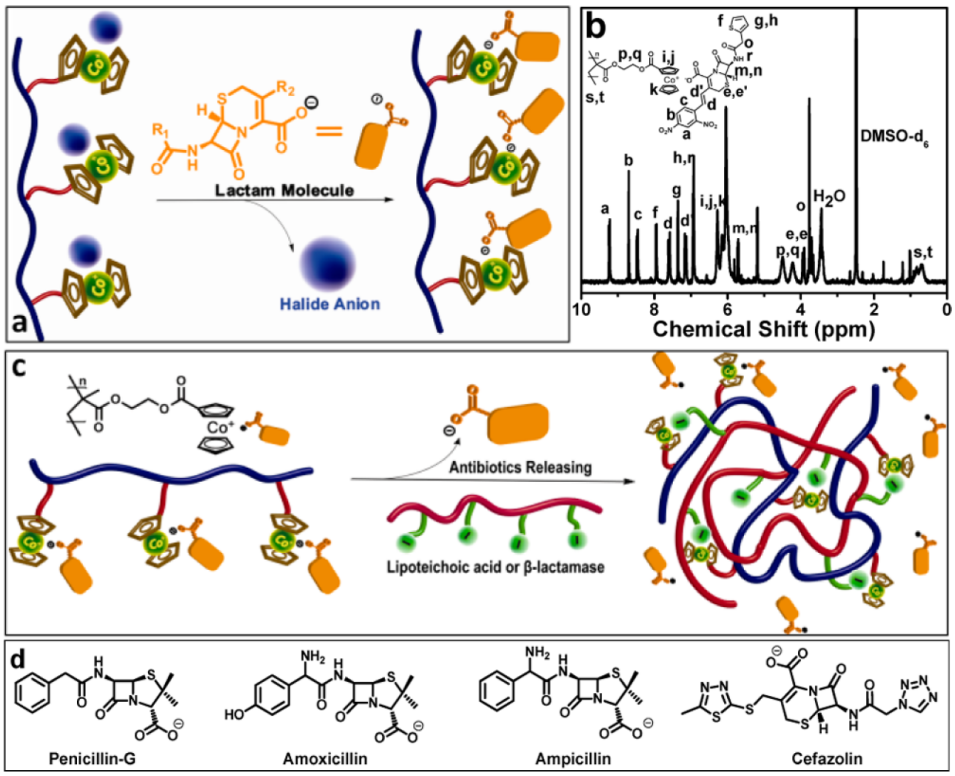

Figure 6.2. a. Formation of ion-pairs between β-lactam antibiotics and cationic cobaltocenium-containing polymers; **b.** ^{1}H NMR spectrum for ion-pairs of nitrocefin and cationic cobaltocenium-containing polymers. **c.** Antibiotic release from antibiotic-metallopolymers ion-pairs via Lipoteichoic acid or β-lactamases. **d.** Four β-lactam antibiotics used in this study.

The protection of nitrocefin by metallopolymers may be due to the unique ability of cationic cobaltocenium moieties to form ion-pairs with the carboxylate anion in nitrocefin. Carboxylate anions in nitrocefin could readily perform counter-ion exchange with halide counter-ions in these cobaltocenium-containing polymers, leading to the formation of nitrocefin-metallopolymer conjugates with 1:1 pairing between nitrocefin and cobaltocenium moieties (**Figure 6.2a**, **6.2b** and **Figure 6.25**). As illustrated in **Figure 6.11**, preliminary study indicated that such ion-pairing interaction may block the electrostatic anchoring by amino acid residue (Lys_{234})[37-38] and could also prevent the key acylation and deacylation steps from Glu_{166} in β-lactamases produced by MRSA.[8-9] However, detailed mechanisms are still under study.

Considering the similarity in structure between nitrocefin and other β-lactam antibiotics, cationic cobaltocenium-containing polymers could be extended to protect other conventional β-lactam antibiotics using a similar approach (**Figure 6.2a** and **2d**). As indicated by ^{1}H NMR analysis (**Figure 6.6-6.9**), penicillin-G, cefazolin, amoxicillin and ampicillin can form conjugates with cationic metallopolymers. Furthermore, we found that antibiotics were released, when antibiotic-metallopolymer bioconjugates performed ion-exchange with negatively-charged cell walls or with carboxylate anions in extracellular solution (**Figure 6.2c**). We carried out model studies to mimic interactions between cationic cobaltocenium-containing polymers and cell walls, as well as β-lactamase. Lipoteichoic acid was chosen as it critically contributes to the negative charge of cell wall (**Scheme 6.1**).[39] We also selected poly(acrylic acid), as its pK_a (≈ 4.2) is very similar to that of Glu_{166} in β-lactamase scaffold. These interactions are included in Figures S8 and S9. Interestingly, the results showed that the ion-pair interactions can enable lipoteichoic acid or β-lactamase to bind with these metallopolymers and subsequently release previously-complexed β-lactam antibiotics (**Figure 6.2c**).

Disk-diffusion assays were used to evaluate the antimicrobial activities of penicillin-G, cefazolin, amoxicillin, ampicillin and their bioconjugates with cobaltocenium-containing polymers against drug-resistant MRSA cells (**Figure 6.3a** and **Figure 6.15**). Three different strains of MRSA, including community-associated MRSA (CA-MRSA) (ATCC 1717), HA-MRSA (ATCC 29213) and MRSA-252 (ATCC 1720), were incubated for 24 hours with antibiotics only, Cl^{-}-paired metallopolymers only, and a mixture of the two components (compositions are summarized in **Table 6.2**). For mixtures of two components, the molar ratio of cobaltocenium moieties to antibiotics was

controlled at > 1:1, recognizing that in extracellular solution, species with carboxylate groups would complex with cobaltocenium moieties. Cl^--metallopolymers and antibiotics were mixed to form stable antibiotic-metallopolymer ion-pairs before being added to the disks. As shown in **Figure 6.3a** and **Figure 6.15**, at a concentration of 1~2.2 μM, metallopolymers alone showed very little inhibition against MRSA cells, while most antibiotics alone also exhibited low toxicity. However, their corresponding bioconjugates showed significantly enhanced effects in activities against different strains of MRSA, especially for HA-MRSA. The growth of CA-MRSA and MRSA-252 was also inhibited, but to a lesser extent than HA-MRSA, which may be due to other resistant mechanisms in CA-MRSA and MRSA-252.[3] The inhibition of HA-MRSA growth was also observed by confocal scanning laser microscopy (CSLM) and scanning electron microscopy (SEM) imaging, as shown in **Figure 6.3b**.

We further discovered that these cationic metallopolymers themselves also showed efficient inhibition against different MRSA cells when their concentrations were increased to about 5 μM (3~5 times of their concentrations in the above antibiotic-metallopolymer bioconjugate study). This is different from other types of β-lactamase inhibitors, as they are mostly not antimicrobial. The inhibitory concentration (IC_{90}) of each halide-paired cobalt-containing polymer was determined for methicillin-sensitive *Staphylococcus aureus* (MSSA, ATCC-1718), HA-MRSA, CA-MRSA, and MRSA-252. As shown in **Figure 6.4a**, both Br^- and Cl^-–paired metallopolymers have IC_{90} values at 3~5 μM against HA-MRSA, CA-MRSA, and MRSA-252, while only 1.00 μM against MSSA cells. I^-–paired metallopolymers are slightly less effective, while PF_6^-–paired cobaltocenium-containing polymers showed much weaker antimicrobial effects, mostly

due to their limited solubility in aqueous media.[34] Compared with other cationic antimicrobial polymers, these metallopolymers showed comparable or even lower minimum inhibitory concentrations (30-100 μg/mL) against bacteria.[20-21, 24] SEM was utilized to illustrate the influence of halide-paired cationic cobaltocenium-containing polymers on MRSA cell membranes. **Figure 6.4c** shows representative images of HA-MRSA cells treated with halide–paired cationic metallopolymers. Compared to control cells, all MRSA cells exhibited partial or complete membrane lysis. Through electrostatic interactions, cationic cobaltocenium-containing polymers could adsorb to the negatively-charged MRSA cell walls, damage the cell wells, and thus lead to cell death, similar to other cationic antimicrobial polymers.[14, 20-21]

Although these cationic metallopolymers exhibited excellent ability to lyse microbial cells, they showed negligible hemolytic effects on red blood cells. As shown in **Figure 6.4b**, halide-paired metallopolymers showed extremely low levels of hemolysis (less than 1%) at concentrations up to 500 μg/mL for metallopolymers (~40 μM for Cl^--paired cobaltocenium-containing polymers). This result is important because it indicates our metallopolymers exhibit an extremely low cytotoxicity to red blood cells, and highly-selective against bacterial cells.[20, 24] Furthermore, cytotoxicity of these metallopolymers was also investigated in *in vitro and in vivo* tests, which indicated little toxicity[20-21] (See discussion in **Figures 6.16, 6.17** and **6.18**).

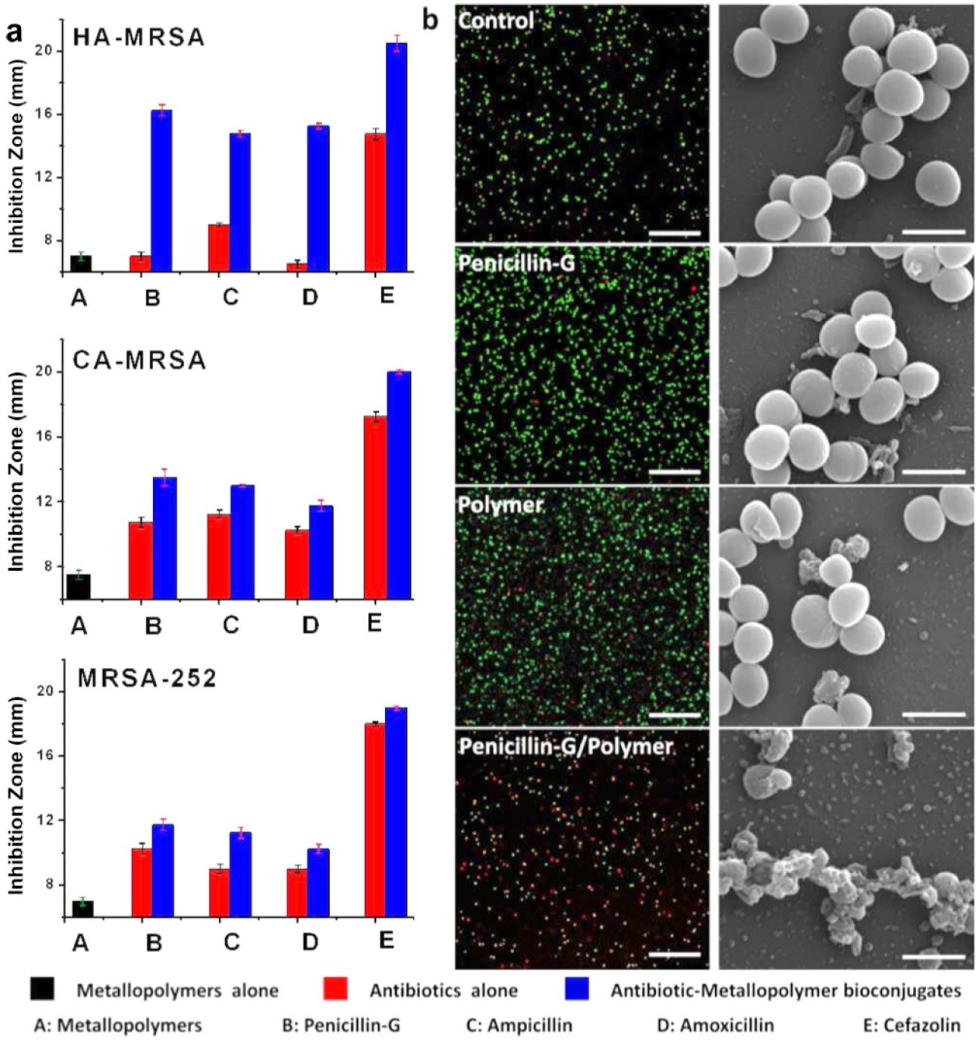

Figure 6.3. a. Results of disk-diffusion assays to test antimicrobial effects of conventional antibiotics (red bar), Cl^--paired metallopolymers (black bar), and their conjugates (blue bar) against HA-MRSA, CA-MRSA, and MRSA-252 (concentrations of metallopolymer were 1~2.2 μM, exact concentrations are summarized in **Table 6.2**); **b.** CSLM images (left column) and corresponding SEM images (right column) of HA-MRSA cells incubated respectively in the presence of control solution, 5.6 μM penicillin-G (2 μg/mL), 1 μM Cl^--paired cationic cobaltocenium-containing polymers (12.5 μg/mL) , and penicillin-G-metallopolymer bioconjugate (5.6 μM penicillin-G and 1 μM metallopolymers). CSLM imaging employed BacLight live/dead stain (green cells indicate live cells, red indicates dead cells. Scale bar in confocal images: 50 μm; Scale bar in SEM images: 1 μm.

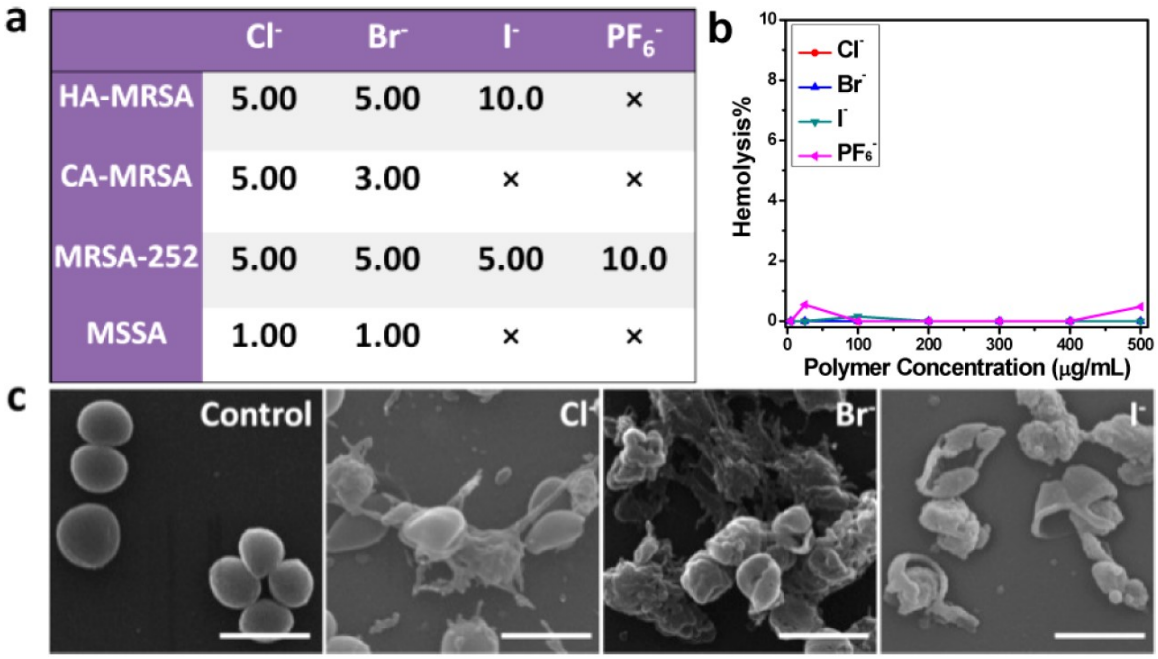

Figure 6.4. a. IC_{90} values (μM) of Cl^-, Br^-, I^- and PF_6^--paired cobaltocenium-containing polymers against MSSA, HA-MRSA, CA-MRSA, and MRSA-252 from standard solution micro-broth measurement. × indicate less than 90% inhibition at 10 μM (**Table 6.1**). For halide and PF_6^--paired cobaltocenium-containing polymers, 1 μM is equal to 12.5 ~ 15.6 μg/mL, respectively; **b.** Hemolytic activities of halide-paired cationic cobaltocenium-containing polymers against mouse red blood cells; **c.** SEM images of HA-MRSA cells before (control) and after incubation with halide-paired cobaltocenium-containing polymers at 5 μM for 9 hours. Scale bars represent 1 μm.

6.3 EXPERIMENTAL

Materials. Cobaltocenium-containing methacrylate polymers with hexafluorophosphate anion (poly(2-(methacrylolyoxy)ethyl cobaltoceniumcarboxylate hexafluorophosphate)) and its halide-paired cobaltocenium-containing polymers were synthesized according to our earlier reports[33, 40] (M_n = 15,600 g/mol, M_w/M_n = 1.25). Nitrocefin was purchased from TOKU-E and used as received. Sodium salts of antibiotic, including amoxicillin, ampicillin, penicillin-G, and cefazolin were purchased from VWR and used as received. Polyacrylic acid was purchased from Sigma-Aldrich (St. Louis, MO.) with a molecular weight at 1,800 g/mol. Lipoteichoic acid from *Staphylococcus*

aureus was purchased from Sigma-Aldrich. All other chemicals were from commercial sources and used as received.

Characterization. ^{1}H NMR (300 MHz) and ^{13}C NMR (100 MHz) spectra were recorded on a Varian Mercury 300 spectrometer with tetramethylsilane (TMS) as an internal reference. Gel permeation chromatography (GPC) was performed at 50ºC on a Varian system equipped with a Varian 356-LC refractive index detector and a Prostar 210 pump. The columns were STYRAGEL HR1, HR2 (300 × 7.5 mm) from Waters. HPLC grade DMF with 0.01 wt% LiBr was used as eluent at a flow rate of 1.0 mL/min. Polystyrene standards were used for calibration. Mass spectrometry was carried out on a Waters Micromass Q-Tof mass spectrometer, with a positive ion electrospray as the ionization source. UV-vis spectroscopy was carried out on a Shimadzu UV-2450 spectrophotometer, scanning monochromatic light in the range of 190-900 nm. A quartz cuvette with a path length of 10.00 mm was used, and the solvent was dimethylformamide (DMF). FTIR spectra were recorded on a PerkinElmer Spectrum 100 FTIR spectrometer equipped with a Universal ATR sampling accessory. Thermal transitions of the polymers were measured by differential scanning calorimetry (DSC) using a TA Instruments Q2000 in a temperature range from -70 to 150 ºC at heating and cooling rates of 5 ºC/min under constant nitrogen flow at a rate of 50 mL/min. Samples (between 3-8 mg) were placed in aluminum hermetic pans and sealed. The data were collected on the second heating run.

Synthesis of metallopolymers-based bioconjugates (Nitrocefin, Glutamic acid, Penicillin-G, amoxicillin, ampicillin and cefazolin). Cobaltocenium-containing polymers with different anions were synthesized by reversible addition−fragmentation

chain-transfer polymerization (RAFT) and phase transfer anion exchange methods according to previous reports.[33, 40] Syntheses of antibiotic-metallopolymers followed a similar approach. For example, penicillin sodium salts (6.2 mg, 1.85×10^{-2} mmol) and chloride-paired cobaltocenium-containing polymers (7.0 mg, 5.60×10^{-4} mmol, M_n = 12,500 g/mol) were first dissolved in deionized water (1 mL) to molar ratios (penicillin salt to cobaltocenium moieties) between of 1.1 to 1. The solution was stirred for 20 minutes and then dialyzed against 3L (1L×3 times) deionized water for 9 hours. The solution in dialysis bag was collected and freeze-dried. A yellow powder was obtained with a yield = 9.6mg, 86%,with the resulting ^{1}H NMR spectrum (D_2O, δ, ppm) (**Figure 6.6**): 7.15 (m, Ph, 5H), 5.60-6.00 (Cp, 9H), 5.33 (m, NHC*H*$_2$C*H*$_2$S, 4H), 4.15-4.40 (broad, OC*H*$_2$C*H*$_2$O, 4H), 4.00 (m, NC*H*COO, 1H), 3.47 (m, PhC*H*$_2$, 2H), 1.31-1.41 (m, C(C*H*$_3$)$_2$, 6H). ^{1}H NMR spectrum for nitrocefin-metallopolymer ion-pairs (DMSO-d_6, δ, ppm) (**Figure 6.3a**): 8.50-9.21 (m, NO_2Ph, 3H), 7.60 (m, C*H*CHC, 1H), 7.16 (m, CHC*H*C, 1H), 7.90, 7.37 and 6.96 (T, 3H), 6.95 (m, CON*H*, 1H), 5.90-6.10 (Cp, 9H), 5.72 (m, NHC*H*CHS, 1H), 5.20 (m, NHCHC*H*S, 1H), 4.31-4.52 (broad, OC*H*$_2$C*H*$_2$O, 4H), 3.68-3.90 (SCC*H*$_2$, 2H; SCC*H*$_2$CO, 2H),0.80-1.00 (broad, CC*H*$_2$, 2H). ^{1}H NMR spectrum for Glu-metallopolymer ion-pairs (D_2O, δ, ppm) (**Figure 6.10**): 5.75-6.17 (Cp, 9H), 4.21-4.50 (broad, OC*H*$_2$C*H*$_2$O, 4H), 3.62 (m, C*H*NH_2, 0.6H), 2.21 (m, C*H*$_2$COO, 1.2H), 1.93 (m, C*H*$_2$CH, 0.6H), 0.80-2.00 (broad, C*H*CC*H*$_3$, 4H). ^{1}H NMR spectrum for amoxicillin-metallopolymer ion-pairs (D_2O, δ, ppm) (**Figure 6.7**): 7.32 (m, Ph, 4H), 5.74-6.11 (Cp, 9H), 5.35 (m, NHC*H*$_2$C*H*$_2$S, 4H), 4.69 (m, NH_2C*H*CONH, 1H), 4.20-4.50 (broad, OC*H*$_2$C*H*$_2$O, 4H), 4.03 (m, NC*H*COO, 1H), 1.32 (m, C(C*H*$_3$)$_2$, 6H). ^{1}H NMR spectrum for cefazolin-metallopolymer ion-pairs (D_2O, δ, ppm) (**Figure 6.9**): 9.13 (m, triazole, 1H),

5.70-6.10 (Cp, 9H), 5.40 (m, NCH_2CONH, 2H), 5.50 (m, NHC*H*CO, 1H), 4.92 (NHCHC*H*S, 1H), 4.16-4.33 (broad, OCH_2CH_2O, 4H), 4.35 and 3.78 (m, SCH_2C, 2H), 3.23-3.62 (m, CCH_2S, 2H), 2.52 (m, NCCH_3, 3H). ^{1}H NMR spectrum for ampicillin-metallopolymer ion-pairs (D_2O, δ, ppm) (**Figure 6.8**): 6.76-7.18 (m, Ph, 4H), 5.70-6.10 (Cp, 9H), 5.32-5.50 (m, NHCH_2CH_2S, 4H), 4.78 (m, NH_2C*H*CONH, 1H), 4.18-4.46 (broad, OCH_2CH_2O, 4H), 4.00 (m, NC*H*COO, 1H), 1.28 (m, C(CH_3)$_2$, 6H).

Antibiotic-release experiments. The release of penicillin-G from penicillin-metallopolymer conjugates was studied by mixing penicillin-G-metallopolymer bioconjugates with polyacrylic acid (M_w =1,800 g/mol) in deionized water for 20 minutes. The mixture was then dialyzed to remove released antibiotics, and the dialyzed mixture was then characterized by ^{1}H NMR. By comparing the integrations of peaks from penicillin-G and cobaltocenium moieties in the mixture, the amount of the released antibiotics could be determined. Different concentrations of polyacrylic acid were added into antibiotic-metallopolymer ion-pairs. A release profile of antibiotic was then obtained (Figure 6.12). Another releasing study from lipoteichoic acid was also studied. Lipoteichoic acid is a critical moiety in contributing to the negative charge of MRSA cell walls.[39, 41] A 10 wt% (relatively to antibiotics-metallopolymer ion-pairs) solution of lipoteichoic acid was added into an antibiotic-metallopolymer ion-pair solution and the mixture was stirred for 5 minutes. Metallopolymers were precipitated, and the solution was characterized by ^{1}H NMR, which demonstrated an approx. 85% release for penicillin-G (**Figure 6.13**).

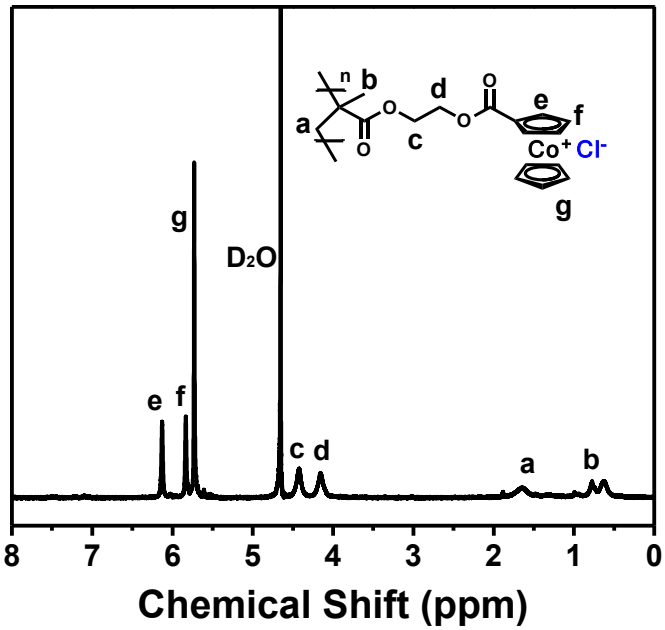

Figure 6.5. ^{1}H NMR spectrum for metallopolymers before complexion with antibiotics.

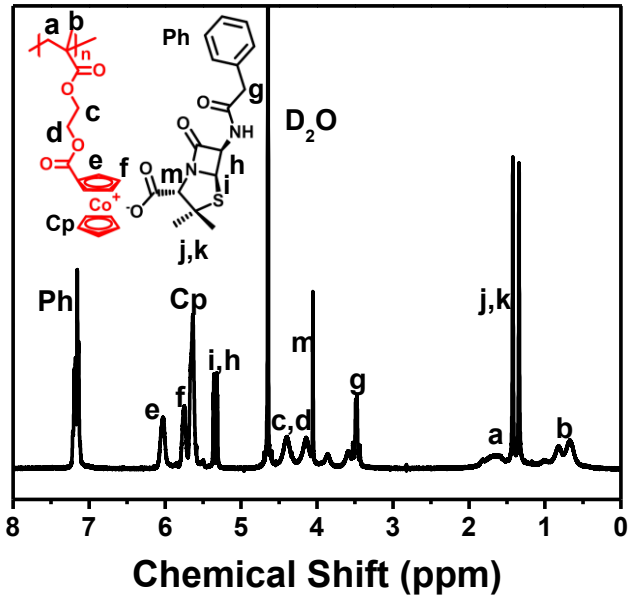

Figure 6.6. ^{1}H NMR spectrum for penicillin G-metallopolymer bioconjugates. The ratio of integration of peaks at 7.10 ppm and 5.60-6.00 ppm was 5:9, indicative of quantitative pairing effects.

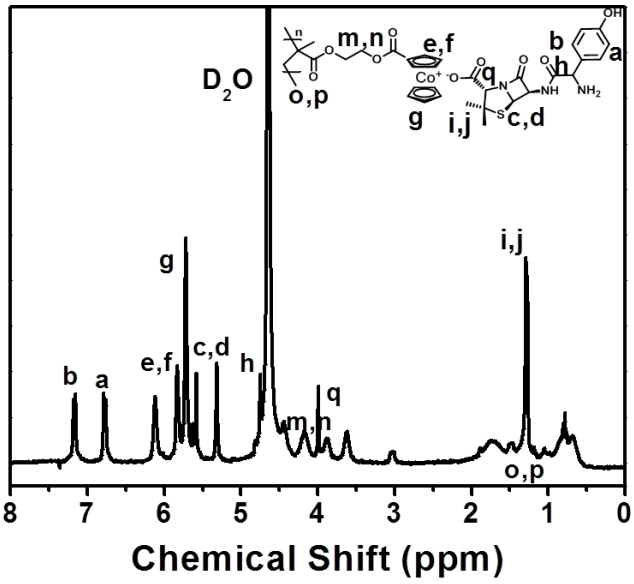

Figure 6.7. [1]H NMR spectrum for amoxicillin-metallopolymer bioconjugates.

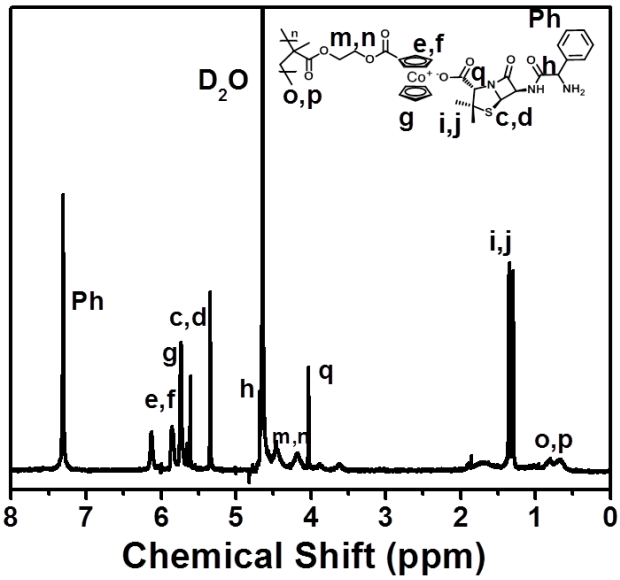

Figure 6.8. [1]H NMR spectrum for ampicillin-metallopolymer bioconjugates.

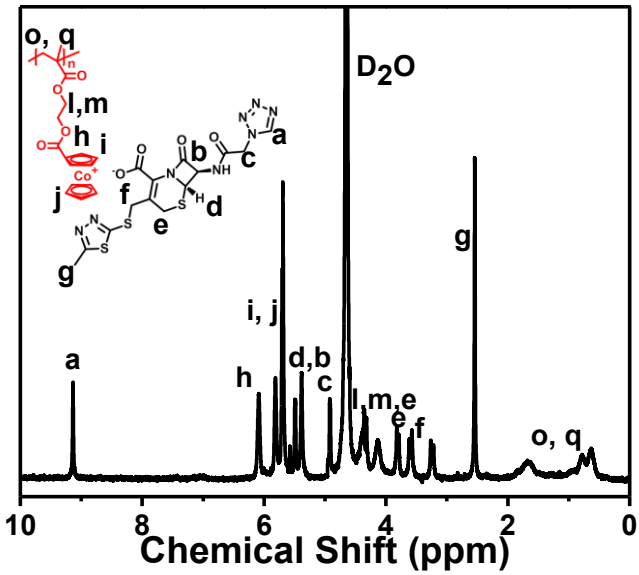

Figure 6.9. [1]H NMR spectrum for cefazolin-metallopolymer bioconjugates.

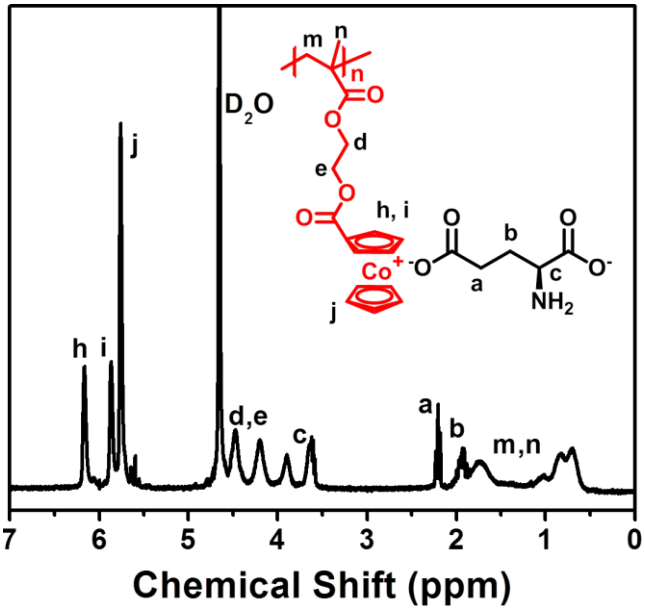

Figure 6.10. [1]H NMR spectrum for glutamic acid-metallopolymer bioconjugates.

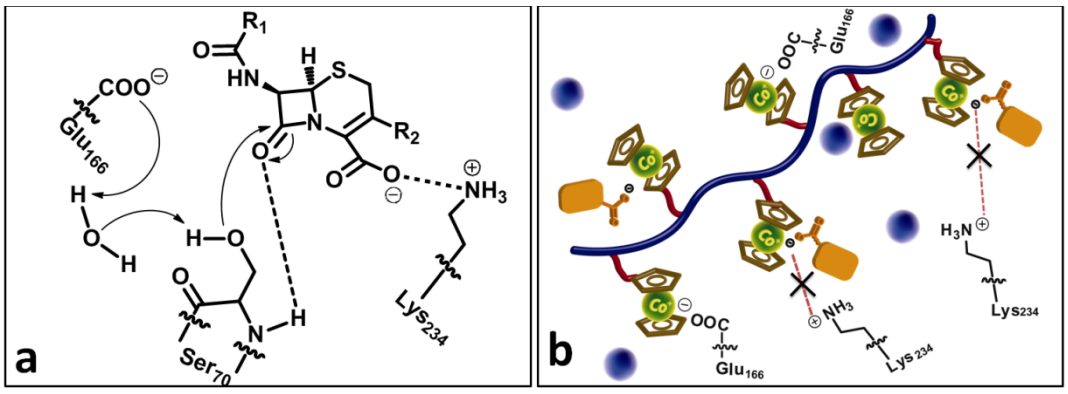

Figure 6.11. a. General mechanism for the hydrolysis of β-lactam ring via class A β-lactamase; Several mechanisms have been proposed for hydrolysis of β-lactam antibiotics by β-lactamases produced by MRSA.[8-9] Most of these mechanisms involve key roles played by three amino acid residues in β-lactamase: Glu_{166}, lysine (Lys_{73} and Lys_{234}) and serine (Ser_{70} and Ser_{130}).[8-9] As illustrated in **Figure 6.11a**, it is generally accepted that Glu_{166} activates a water molecule to deprotonate the hydroxyl group in Ser_{70} (acylation step), and also facilitates Lys_{73} to deprotonate Ser_{130} (deacylation step, not shown in **Figure 6.11b**). Residue Lys_{234} would act as an electrostatic anchor for β-lactam antibiotics via the anionic carboxylate,[37-38] and simultaneously deprotonated Ser_{70} and Ser_{130} attack the carbonyl group in the β-lactam ring and eventually hydrolyze the four-member β-lactam ring. **b.** Proposed mechanism of interactions between Glu_{166} and Lys_{234} residues, and cationic cobaltocenium-containing polymers. When there are excess cationic cobaltocenium polymers in solution, carboxylate anions in Glu_{166} residues could form ion-pairs with cobaltocenium moieties instead of activating water molecules. If the former occurs, this complexation is possible to stop key acylation and deacylation steps. The pairing effects could be observed by model complexation between glutamic acid and metallopolymers. Glutamic acid-metallopolymer ion-pairs were immediately formed when both were mixed together (**Figure 6.10**). Meanwhile, the ion-pairs between antibiotics and metallopolymers effectively could block the electrostatic anchoring from Lys_{234} residue in β-lactamase (**Figure 6.11a**), which further protects the β-lactam antibiotics.

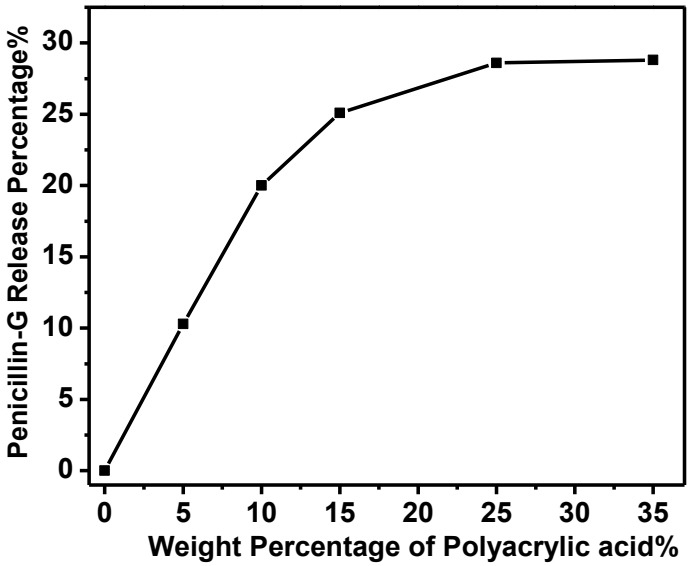

Figure 6.12. Antibiotic-release profiles for penicillin G-metallopolymer bioconjugates. The release of penicillin-G from penicillin-G-metallopolymer conjugates was studied by mixing 10 mg penicillin-G-metallopolymer bioconjugates with different amount of polyacrylic acid (0.5 mg, 1 mg, 1.5 mg, 2.5 mg and 3.5 mg) in 1 mL water for 20 minutes. The mixtures were then dialyzed to remove released antibiotics, and the dialyzed mixtures were then characterized by ^1H NMR. By comparing the integrations of peaks from penicillin-G and cobaltocenium moieties in the mixture, the percentages of the released antibiotics were determined. Due to the different amounts of polyacrylic acid added into antibiotic-metallopolymer bioconjugates, a release profile of antibiotics was

obtained. **Figure 6.12** shows that the released penicillin-G increased monotonically with the weight percentage of polyacrylic acid when it was under 15%. Higher than 15% made the solution turbid, due to significant reduction of solubility of the complexed structure. Thus it is no longer to obtain accurate release based on ^{1}H NMR analysis. Higher percentage (>35%) of polyacrylic acid led obvious precipitation of polymers in solution.

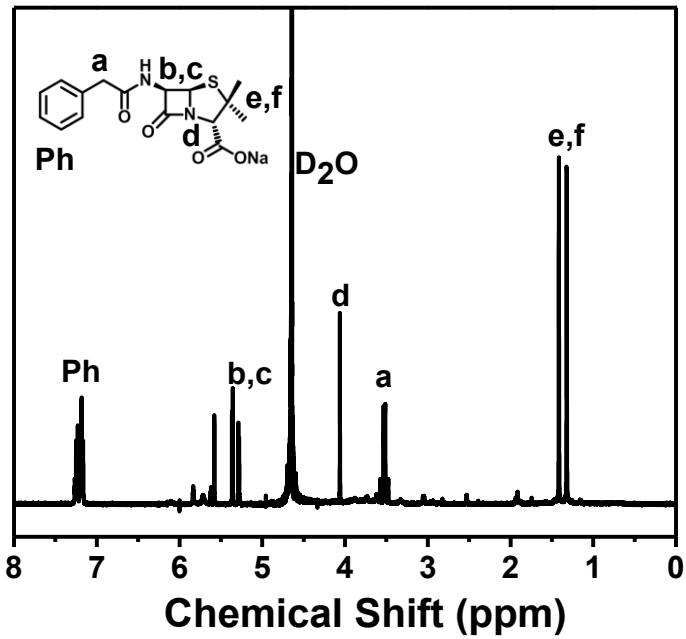

Figure 6.13. ^{1}H NMR spectrum for the collected products of penicillin-G-metallopolymer bioconjugates after addition of lipoteichoic acid. Lipoteichoic (1 mg) acid was added into 10 mg antibiotic-metallopolymer bioconjugate (contained 4.8 mg penicillin). The mixture was stirred for 5 min. Precipitation (complexes between lipoteichoic acid and metallopolymers) was observed. The resulting solution was then centrifuged and freeze-dried. The resulting light yellow powder (4.1 mg, release level = 85%) was characterized using ^{1}H NMR, which showed only the presence of penicillin-G (**Figure 6.13**). Lipoteichoic acid is critically contributed to the negative charge of the MRSA cell walls.[39, 41]

Growth of bacteria. The following *Staphylococcus aureus* strains were purchased from ATCC: MRSA-252 (ATCCBAA-1720), CA-MRSA (ATCCBAA-1717), HA-MRSA (ATCCBAA-29213), and MSSA (ATCCBAA-1718). For these bacteria, a single colony was inoculated in 30 mL Tryptic Soy broth (TSB) at 37 °C for 24 hours, shaking at 190 rpm/min. All bacteria were grown to an optical density of about 1.00 (OD_{600} = ~1.00) for further use.

Effects of metallopolymers on β-lactamase activity. HA-MRSA cells were inoculated in 30 mL Tryptic Soy broth at 37 °C for 24 hours, with shaking at 190 rpm/min. All bacteria were grown to a similar optical density (OD_{600} = ~1.00). The cultured cell solution was then centrifuged (1000 rpm for 10 minutes) at 5 °C. Supernatant was collected and re-suspended in 15 mL PBS buffer (50 mM, pH=7.0). The solution was then cooled (0 °C) and centrifuged (10 minutes; 1000 rpm) to remove cell debris. The homogenous solution contained β-lactamase. The amount of protein in solution was 0.8 μg/mL (determined by Bio-rad Protein Assay). 50 μg nitrocefin was added into 100 μL of the obtained β-lactamase solution and diluted to 1 mL using PBS buffer (50 mM, pH=7.0). Then, Cl^-, Br^-, I^- and PF_6^--paired cobaltocenium-containing polymers, respectively, were added to the solution. The final concentration of each polymer was set at 5 μM or 10 μM. A solution without polymers were prepared as a control. β-lactamase activity was measured by absorbance (480 nm) at different time intervals. Inhibition on β-lactamase activity was calculated by **Equation 6.1** and summarized in **Figure 6.1d** (5 μM) and **Figure 6.14** (10 μM).

$$\text{Inhibition}\% = \frac{Abs_s\,(t) - Abs_s\,(t=0)}{Abs_c\,(t) - Abs_c\,(t=0)} \times 100\% \qquad \textbf{(Equation 6.1)}$$

Here, $Abs_s\,(t=0)$ was the initial sample absorbance (with metallopolymers) at 480 nm; $Abs_s\,(t)$ was sample absorbance at 480 nm (with metallopolymers) after t hours. $Abs_c\,(t=0)$ indicates initial absorbance of the control sample (without metallopolymers) at 480 nm; $Abs_c\,(0)$ indicates initial control sample absorbance (without metallopolymers) at 480 nm after t hours.

Improvement of conventional antibiotics by cationic cobaltocenium-containing polymers. The enhancement of conventional antibiotics activity by metallopolymers was evaluated using the standard disk-diffusion assay (ASTM: the Kirby Bauer diffusion test). In general, 20 mL of sterile melted agar medium was solidified on agar plates (24 °C), and then then 100 μL MRSA cell solution (OD = ~1.0)

was applied on TSB agar plate. Then six mm filter discs were added to the each plate surface and different amount of antimicrobial agent in 30 μL water or DMSO was added to a disc (amount were summarized in **Table 6.2**). All plates were incubated at 37 ºC for 24 h. The development of a clear zone around the disk was indicative of the ability of the antimicrobial compounds to kill bacteria (**Figure 6.15**) and was summaried in **Figure 6. 3a** (Error bars were standard deviation from independent samples. Statistical analyses by one-way ANOVA with a Turkey post-hoc comparison of the means using OriginPro8.0 were considered (statistically significant at $p<0.05$).

Inhibitory concentration determination (IC_{90}). A series of aqueous solutions of Cl^-, Br^-, and I^--paired cobaltocenium-containing polymers were prepared (DMSO was used for PF_6^--paired polymers). The concentrations were 200 μM, 140 μM, 100 μM, 60 μM, 40 μM and 20 μM. The solution, without polymers, was used as the control. The prepared polymer stock solutions (10 μL), or control solution (10 μL), were then added to the wells with 190 μL of MRSA cells (OD=~0.1) or MSSA cells (190 μL) (OD=~0.1). The final concentrations of polymers in each well for each microbe were summarized in Table S1. The assay plate was incubated at 37 ºC for 12 hours. Bacterial growth was detected at OD_{600} and was compared to controls of TSB without polymers. The inhibitory concentration (IC_{90}), the concentration at which 90% inhibition of cell growth occurs, was determined. Inhibitory percentages were calculated according to **Equation 6.2** and summarized in **Table 6.1**. All assays were carried out in duplicate in the same assay plate.

$$\text{Inhibition}\% = \frac{OD_{600}\,(t) - OD_{600}\,(t=0)}{OD_{600}\,(t)_c - OD_{600}\,(t=0)_c} \times 100\% \qquad \textbf{(Equation 6.2)}$$

Here, OD_{600} (t=0) indicates the initial OD_{600} value, and OD_{600} (t) is the OD_{600} value for cells after incubation with metallopolymers for t hours. OD_{600} $(t=0)_c$ is the initial OD_{600} value and OD_{600} $(t)_c$ is the OD_{600} value for control samples after incubation for t hours.

LIVE/DEAD bacterial viability assays. HA-MRSA cells were inoculated and prepared by a similar procedure as inhibitory concentration determination study. One mL of active bacterial stock of HA-MRSA was introduced to 2 μg penicillin-G, 12.5 μg of chloride-paired metallopolymer, and 14.5 μg penicillin-G-metallopolymer bioconjugates (penicillin-G weight: 2 μg), respectively. An untreated cell suspension was used as the control. Following 24-hour incubation at 37 ^{o}C, 1 μL LIVE/DEAD BacLight (Bacterial Viability Kit; Invitrogen Inc.) was added to the incubation solution. After incubation for 15 minutes, cells were imaged using a Leica TCS SP5 Laser Scanning Confocal Microscope with 63X oil immersion lense. When excited at 488 nm with Argon and Helium/Neon lasers, bacteria with intact membranes display green fluorescence (Emission = 500 nm) and bacteria with disrupted membranes fluoresce red (Emission = 635 nm).

Bacterial morphology by FE-SEM. The morphology of HA-MRSA after incubation with penicillin, metallopolymers and their bioconjugates were examined by field-emission scanning electron microcopy (FE-SEM) with the same procedure. In general, 20 μL of HA-MRSA cell solution was grown on one glass slide in six-well plate containing 2 mL TSB medium at 37 ^{o}C overnight. Cell suspensions were diluted to OD_{600} = 1.0. 2 μg penicillin G, 12.5 μg of chloride-paired metallopolymer, and 14.5 μg penicillin G-metallopolymer bioconjugates (Penicillin G weight: 2 μg), was added to the 1 mL cell stock solution, respectively and incubated at 37 ^{o}C overnight. A cell suspension without any chemicals was used as the control. The samples were then fixed in cacodylate buffered with 2.5% glutaraldehyde solution (pH = 7.2) for 2–3 h at 4 ^{o}C and post-fixed with 1% osmium tetraoxide at 4 ^{o}C for 1 h. Samples were dehydrated in an

ethanol series (50%, 70%, 80%, 95%) for 10 min each. After dehydration with 100% ethanol for 10 min twice, the samples were dried under critical point, then coated with gold using Denton Dest II Sputter Coater for 45 s and observed by FE-SEM. Samples incubated with Cl^-, Br^-, and I^--paired cobaltocenium-containing polymers (60.5 µg, 66.5 µg, and 75.0 µg, respectively) were also imaged by FE-SEM following a similar procedure.

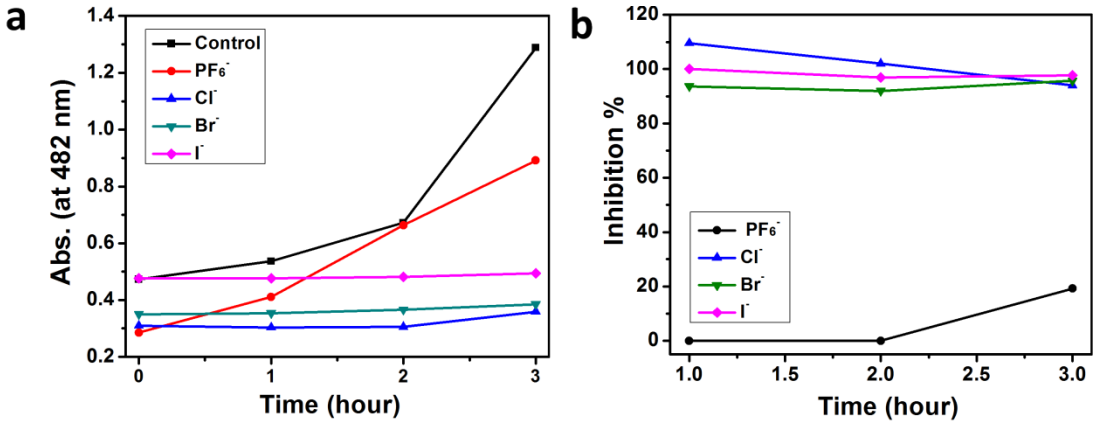

Figure 6.14. a. Incubation time-dependent UV-vis absorbance (at 482 nm) of nitrocefin solution with 10 µM different anion-paired metallopolymers and β-lactamase; **b.** the level of β-lactamase activity inhibition by 10 µM different anion-paired cationic cobaltocenium-containing polymers.

Table 6.1. Inhibition of Cl^-, Br^-, I^- and PF_6^--paired cobaltocenium-containing polymers against MSSA, HA-MRSA, CA-MRSA, and MRSA-252 under different concentrations (at µM) by standard solution micro-broth measurement. Inhibition% was calculated according to **Equation 6.2**.

Concentration (µM)	**Inhibition% of HA-MRSA**			
	Cl^-	**Br^-**	**I^-**	**PF_6^-**
10	>99.9%	>99.9%	95.8%	52.5%
5	96.0%	95.2%	86.1%	47.2%
2	74.5%	78.1%	62.2%	42.0%
Concentration (µM)	**Inhibition% of CA-MRSA**			
	Cl^-	**Br^-**	**I^-**	**PF_6^-**
10	>99.9%	>99.9%	83.5%	30.7%
5	97.0%	>99.9%	87.8%	25.9%
3	84.6%	>99.9%	0.00%	44.9%
Concentration (µM)	**Inhibition% of MRSA-252**			
	Cl^-	**Br^-**	**I^-**	**PF_6^-**
10	>99.9%	>99.9%	>99.9%	>99.9%
7	>99.9%	>99.9%	>99.9%	31.5%

5	>99.9%	>99.9%	>99.9%	35.7%
Concentration (μM)	**Inhibition% of MSSA**			
	Cl^-	**Br^-**	**I^-**	**PF_6^-**
5	>99.9%	96.2%	81.5%	22.2%
3	>99.9%	95.6%	23.7%	12.1%
1	>99.9%	>99.9%	78.2%	0.00%

Table 6.2. Concentrations of antibiotics, metallopolymers and their conjugates used for disk diffusion test against different MRSA strains.

HA-MRSA	**Control [a]**		**Antibiotic-polymer conjugates [a]**	
	Antibiotics (μg)	**Polymer (μg)**	**Antibiotics (μg)**	**Polymer (μg)**
Penicillin-G	2	12.5	2	12.5
Ampicillin	2	12.5	2	12.5
Amoxicillin	2	12.5	2	12.5
Cefazolin	2	12.5	2	12.5
CA-MRSA	**Control**		**Antibiotic-polymer conjugates**	
	Antibiotics (μg)	**Polymer (μg)**	**Antibiotics (μg)**	**Polymer (μg)**
Penicillin-G	8	30	8	30
Ampicillin	7	30	7	30
Amoxicillin	6	30	6	30
Cefazolin	2	30	2	30
MRSA-252	**Control**		**Antibiotic-polymer conjugates**	
	Antibiotics (μg)	**Polymer (μg)**	**Antibiotics (μg)**	**Polymer (μg)**
Penicillin-G	12	30	12	30
Ampicillin	10	30	10	30
Amoxicillin	10	30	10	30
Cefazolin	4	30	4	30

a. Two controls are used in the experiments. Controls for antibiotics refer to only antibiotics loaded on disks. Controls for polymer refer to only chloride-paired cobaltocenium-containing polymers loaded on disks. Antibiotic-polymer conjugates are disks loaded with antibiotic-metallopolymer bioconjugates. The concentration of antibiotics and metallopolymers controls were the same as those used in their bioconjugates.

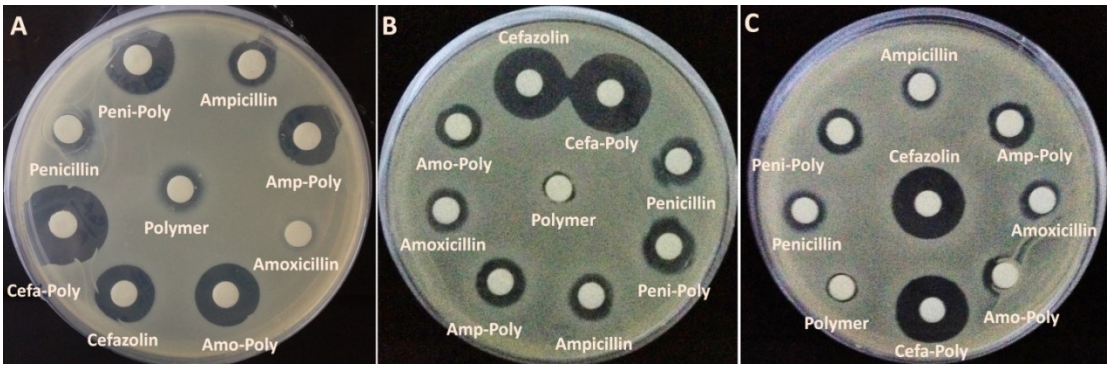

Figure 6.15. Agar diffusion method used to test antimicrobial activities of antibiotics, chloride anion-paired cobaltocenium-containing polymers and their conjugates against different strains of MRSA: (A) HA-MRSA, (B) CA-MRSA, and (C) MRSA-252. Penicillin-G, amoxicillin, ampicillin and cefazolin indicate only antibiotics; Polymer indicates only chloride-paired cobaltocenium-containing polymers; while cefa-poly, peni-poly, amo-poly and amp-poly refers to cefazolin-metallopolymer, penicillin-G-metallopolymer, amoxicillin-polymer and ampicillin-polymer bioconjugates, respectively. The development of a clear zone around the disk was indicative of the ability of the antimicrobial compounds to kill bacteria.

Cytotoxicity Evaluation Discussion. As shown in Figure 6.16, halide-paired metallopolymers were not toxic as they did not induce increased apoptosis in *in vitro* test at a concentration of 50 μg/mL. For *in vivo* test, it showed that all mice tested lived beyond 48 hours after injection with the cationic cobaltocenium-containing polymers (10 mg/kg; estimated concentration in blood: ~19.0 μM, assuming that the blood volume of the mouse is about 1 mL). As shown in Figure 6.17, no significant effects were seen on the induction of apoptosis in splenocytes of the mice. Besides, as indicated in Figure 6.18, we did not observe any difference in the percentages of the CD3+CD4+ T helper/regulatory cells and CD3+CD8+ cytotoxic cells as well as the percentages of B cells when metallopolymer-treated groups were compared with the control group. According to these results, cationic cobaltocenium-containing polymers showed minimal toxicity to the mice during the testing period.

Hemolysis test. Fresh mouse red blood cells (RBC) were washed with *Phosphate Buffered Saline (*PBS) for three times. Then 10×10^6 red blood cell suspension in 50 μL

PBS (4% in volume) was placed in each well of 96-well round bottom plates. Cl^-, Br^- and I^- paired polymers were dissolved in PBS added in individual wells at concentrations of 0, 25, 100, 200, 300, 400, 500 μg/mL. PF_6^--paired polymer was dissolved in DMSO and added in individual wells in another plate at concentrations of 0, 25, 100, 200, 300, 400, 500 μg/mL where the final concentration of DMSO in each well was 1%. For halide-paired metallopolymers, control solutions were PBS (negative control) and PBS with 0.5% Triton (positive control). While for PF_6^--paired metallopolymers, PBS with 1% DMSO solution was used as negative control and PBS with 0.5% Triton solution was used as positive control. All wells were adjusted with PBS to make the final volumes to be 200 μL. A humidified 5% CO_2 incubator was used to incubate the plates at 37 ^oC for 1 h. After incubation the plates were centrifuged at 1000g for 10 min. Then 100 μL of supernatants from each well were transferred to wells in a 96-well flat bottom plate. The absorbance at 576 nm for hemoglobin release from RBC was measured using a Wallac 1420 VICTOR^{2TM} Multilabel Counter (PerkinElmer, Shelton, CT). Absorbance of supernatants from RBC lysed with 5% Triton was taken as 100% hemolysis.

Percentage hemolysis was calculated using the following formula: Polymers in PBS, Hemolysis (%) = [($OD_{576\ nm}$ in the polymer solution – $OD_{576\ nm}$ in PBS)/ ($OD_{576\ nm}$ in 0.5% Triton – $OD_{576\ nm}$ in PBS)] × 100

Polymer in DMSO, Hemolysis (%) = [($OD_{576\ nm}$ in the polymer solution – $OD_{576\ nm}$ in PBS – $OD_{576\ nm}$ in DMSO)/ ($OD_{576\ nm}$ in 0.5% Triton – $OD_{576\ nm}$ in PBS)] × 100

Preparation of splenocytes. Spleens from mice were harvested and placed in complete RPMI 1640 medium. Single-cell suspensions of spleens were prepared and RBC lysed as described previously.[42] Cell viability was determined on a hemocytometer

(Hausser Scientific, Horsham, PA) by staining the cells with trypan blue dye and using an inverted phase-contrast microscope (Nikon, Inc., Melville, NY).

***In vivo* exposure of mice to the polymers.** To determine the effect of the polymers on the splenocytes in normal mice, a single dose of 10mg/kg body weight was administered (intravenously) into groups of mice. Mice treated with vehicle were used as control.

Detection of apoptosis in splenocytes. Splenocytes from mice exposed to polymer or vehicle were analyzed for apoptosis by using the Terminal deoxynucleotidyl transferase dUTP nick end labeling (TUNEL) assay kit (In Situ Cell Death Detection Kit, Fluorescein, Roche Diagnostics, Indianapolis, IN) as described previously, which is a very sensitive technique to detect cell death.[43] In brief, splenocytes (1×10^6) from various groups of mice were cultured for 24 h in complete RPMI 1640 medium, after which, the cells were washed twice with PBS, fixed with 4% paraformaldehyde for 30 minutes at room temperature, permeabilized with 0.1% Triton® X-100 in 0.1% sodium citrate on ice for 2 min and incubated with FITC-dUTP for 1 h at 37°C. Fluorescence of the cells was measured by flow cytometry and apoptotic cells were quantified as the average number of TUNEL-positive cells.

Assessment of immune cell subpopulations. Splenocytes (1×10^6) from vehicle- and polymer-treated groups of mice were washed with PBS (Invitrogen) and incubated for 30 min on ice with 0.5 µg of the following primary antibodies: fluorescein isothiocyanate (FITC)-conjugated anti-CD3, phycoerythrin (PE)–anti-CD8 and allophycocyanin (APC)–anti-CD4 or FITC-anti-CD19 (BD Pharmingen, San Diego, CA, USA). For triple-staining studies, directly-conjugated monoclonal antibodies (mAb) were

simultaneously added to the sample. Negative controls consisted of cells that were not stained with mAbs and represented autofluorescence. Flow cytometric analysis was performed by a Cytomics FC500 flow cytometer (Beckman Coulter, Inc.) using the operating software. Thirty thousand cells were collected per sample. Dead cells, clumps and debris were excluded electronically by gating on forward (FSC) versus side scatter (SSC).

T and B cell proliferation to mitogens by MTT Assay. Splenocytes (1×10^5) were cultured for 48h at 37°C with 5% CO_2 with either the T cell mitogen, ConA (Concanavalin A, 1.5µg/ml) or the B cell mitogen, LPS (Lipopolysaccharide, 1µg/ml) in the presence of vehicle, 10 or 50µg/ml of the polymers. After 48h, MTT solution (20µl/well of 5mg/ml MTT solution) was added followed by incubation for 3h in dark at 37°C. This was followed by addition of MTT solvent (200µl of acidic Isopropanol) and incubated further for 1h. The absorbance of the resulting colored solution was read at 570nm in an ELISA plate reader immediately. The reactions were performed in triplicate and the average of the absorbance values were used for analysis.

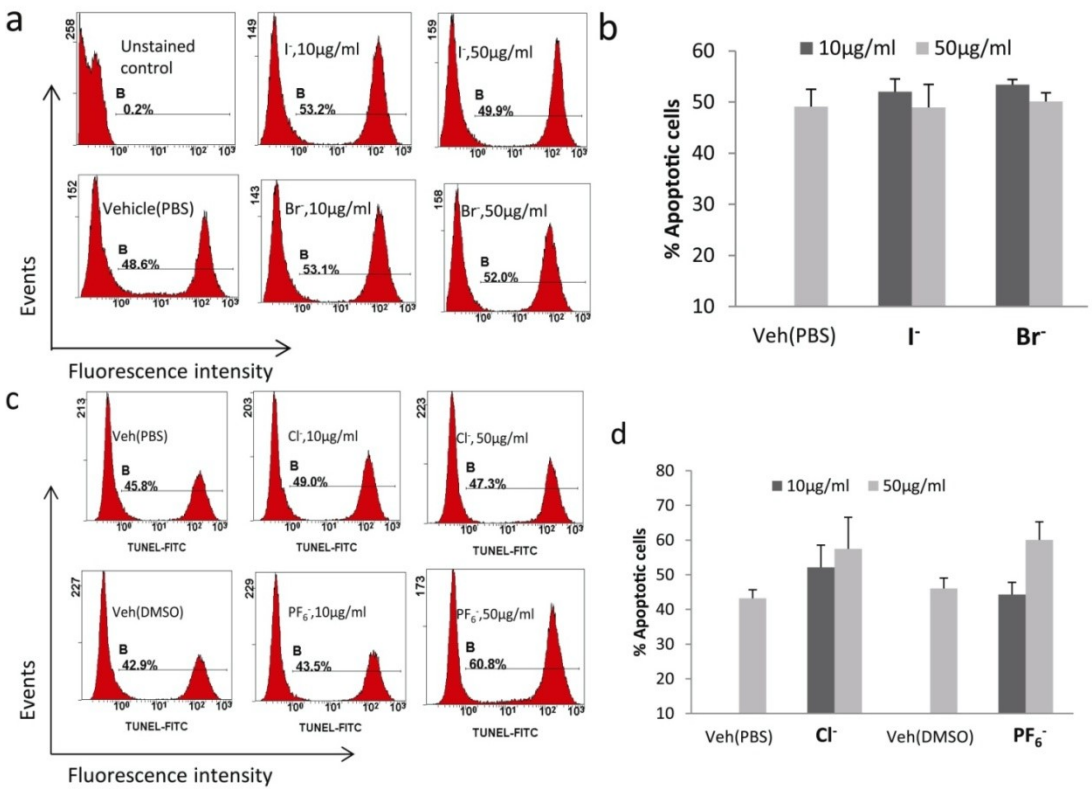

Figure 6.16. *Splenocytes are resistant to induction of apoptosis following in vitro treatment with the polymers.* Splenocytes from mice were cultured for 24 h with vehicle or the polymers, at 10 and 50µg/mL and apoptosis was detected following TUNEL staining using flow cytometry. **Figure 6.16a** and **6.16c**: Representative figures after flow cytometry analysis of apoptotic cells detected following treatment with vehicle, I^-, Br^-, Cl^- and PF_6^--paired metallopolymers following TUNEL staining. Upper left panel represents negative control of unstained cells. **Figure 6.16b** and **6.16d** represent mean ± S.E. of the apoptotic cell percentages of triplicates. In order to determine the toxicity of the polymers, we first examined their ability to mediate programmed cell death known as apoptosis. For this purpose, we cultured the cells with vehicle, 10 or 50µg/mL of I^- or Br^- metallopolymers (**Figure 6.16a** and **6.16c**), Cl^- or PF_6^- metallopolymers (**Figure 6.16b** and **6.16d**) for 24 h and then performed the TUNEL assay to determine apoptotic cells. There was no significant change in the percentages of the apoptotic cells when the cells were treated with 10µg/mL of the polymers. The percentages of apoptotic cells after treatment with 50µg/mL of polymers were very similar to that of the vehicle-treated groups except for PF_6^- wherein we observed a slight increase in the percentage of apoptotic cells at only the higher concentration of 50µg/mL.

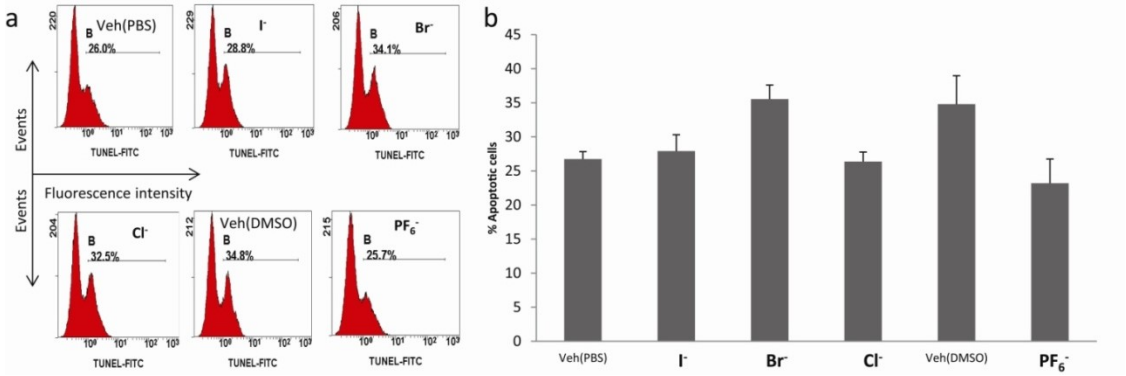

Figure 6.17. *In vivo treatment of mice with polymers does not affect the induction of apoptosis in splenocytes when compared to vehicle-treated group.* Splenocytes from mice injected with the polymers at 10mg/kg body weight were harvested 48 h following treatment. The cells were cultured for 24 h and subjected to TUNEL followed by detection of apoptosis by flow cytometry. The percentages of apoptotic cells in each of the panels are depicted (**Figure 6.17**). No mice died and and no evidence of adverse effects on mice was observed after treatment with metallopolymers at 10mg/kg body weight. There was no significant change in the percentages of apoptotic cells between the vehicle and polymer treated groups. **Figure 6.17b** is a graphical representation of the mean±S.E. values of the groups. To study the in vivo effect of the polymers on the immune cells, we administered mice with the polymers through intravenous injection of a single dose of 10mg/kg body weight and 48hr later harvested the spleens. Freshly isolated splenocytes from the vehicle or polymer-injected mice were cultured for an additional 24 h and analyzed for apoptosis by TUNEL assay followed by flow cytometry. As seen from the results (**Figure 6.17a** and **6.17b**), there was no significant difference in the percentages of apoptotic splenocytes in I^-, Br^- and Cl^--paired metallopolymers-treated mice when compared with the PBS vehicle-treated group. Similarly, there was no difference between apoptotic cells in the PF_6^--paired metallopolymers-treated group when compared with the DMSO-treated vehicle controls.

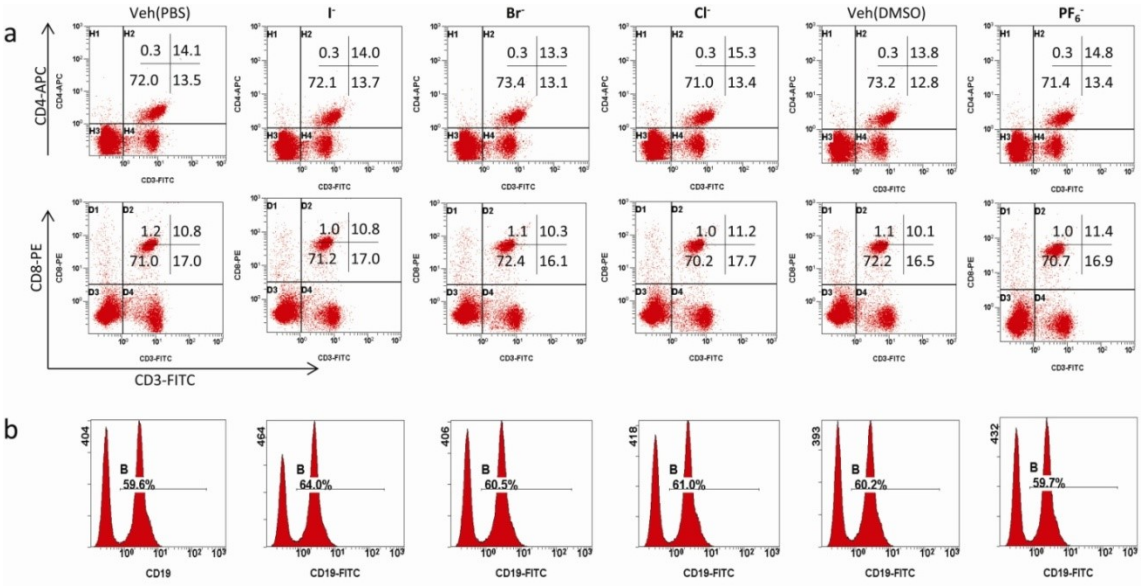

Figure 6.18. *In vivo treatment with polymers did not alter the ratios of T and B cells in the spleen.* Mice were injected with vehicle or the polymers at 10mg/kg body weight and 48 h later, the spleen cell CD3+CD4+ and CD3+CD8+ T cell subpopulations as well as B cells (CD19+) were determined by flow cytometry. **Figure 6.18**: Top panels represent dot plots of CD3+CD4+T helper/regulatory cells in the upper right quadrant. Lower panel represents CD3+CD8+ cytotoxic T cells in the upper right quadrant. **Figure 6.18b** represents histograms of B cells stained with FITC-anti-CD19 Abs. We enumerated the T cell subpopulations (CD3+ CD8+ and CD3+ CD4+) and B (CD19+) cells in splenocytes following staining with FITC-conjugated anti-CD3, APC-labelled anti-CD4 and PE-labelled anti-CD8 antibodies (Abs) by flow cytometry (**Figure 6.18a** and **6.18b**), 48 h following in vivo treatment of mice with the vehicle or metallopolymers. We did not observe any difference in the percentages of the CD3+CD4+ T helper/regulatory cells and CD3+CD8+ cytotoxic cells as well as the percentages of B cells when metallopolymer-treated groups were compared with the vehicle-treated group.

6.5 CONCLUSIONS

In conclusion, a class of metallopolymers, cobaltocenium-containing polymers, was discovered to form bioconjugates with various β-lactam antibiotics, including penicillin, ampicillin, amoxicillin and cefazolin, via ionic complexation. These antibiotic-metallopolymer bioconjugates showed high resistance towards β-lactamase-assisted hydrolysis of β-lactam antibiotics and significantly improved efficacy against various strains of MRSA cells over conventional antibiotics. In addition, these metallopolymers themselves, at higher concentrations, also showed excellent antimicrobial activities against different strains of MRSA by selectively disrupting their cell membranes, while maintaining extremely low cytotoxicity against red blood cells and low *in vivo* toxicity. These discoveries could pave a new platform to design antibiotics and antimicrobial agents to battle multidrug resistant bacteria and superbugs.

6.6 ACKNOWLEDGMENT

The supports from the National Science Foundation (CHE-1151479 and DMR-1206072) are acknowledged.

6.7 REFERENCES

1. C. Walsh, *Nature* **2000**, *406*, 775-781.
2. C. A. Arias and B. E. Murray, *New Engl. J. Med.* **2009**, *360*, 439-443.
3. K. M. G. O'Connell, J. T. Hodgkinson, H. F. Sore, M. Welch, G. P. C. Salmond and D. R. Spring, *Angew. Chem. Int. Ed.* **2013**, *52*, 10706-10733.
4. H. S. Gold and R. C. Moellering, *New Engl. J. Med.* **1996**, *335*, 1445-1453.
5. P. Nordmann, T. Naas, N. Fortineau and L. Poirel, *Curr. Opin. Microbiol.* **2007**, *10*, 436-440.
6. R. R. Watkins, M. Z. David and R. A. Salata, *J. Med. Microbiol.* **2012**, *61*, 1179-1193.
7. S. B. Levy and B. Marshall, *Nat. Med.* **2004**, *10*, S122-S129.
8. S. M. Drawz and R. A. Bonomo, *Clin. Microbiol. Rev.* **2010**, *23*, 160-201.
9. F. J. Perez-Llarena and G. Bou, *Curr. Med. Chem.* **2009**, *16*, 3740-3765.
10. D. L. Paterson and R. A. Bonomo, *Clin. Microbiol. Rev.* **2005**, *18*, 657-686.
11. F. Morandi, E. Caselli, S. Morandi, P. J. Focia, J. Blazquez, B. K. Shoichet and F. Prati, *J. Am. Chem. Soc.* **2003**, *125*, 685-695.
12. K. Kaur, M. J. K. Lan and R. F. Pratt, *J. Am. Chem. Soc.* **2001**, *123*, 10436-10443.
13. K. A. Brogden, *Nat. Rev. Microbiol.* **2005**, *3*, 238-250.
14. E. R. Kenawy, S. D. Worley and R. Broughton, *Biomacromolecules* **2007**, *8*, 1359-1384.
15. K. Lienkamp, A. E. Madkour, A. Musante, C. F. Nelson, K. Nusslein and G. N. Tew, *J. Am. Chem. Soc.* **2008**, *130*, 9836-9843.
16. J. F. Wang, Y. P. Chen, K. J. Yao, P. A. Wilbon, W. J. Zhang, L. X. Ren, J. H. Zhou, M. Nagarkatti, C. P. Wang, F. X. Chu, X. M. He, A. W. Decho and C. B. Tang, *Chem. Commun.* **2012**, *48*, 916-918.
17. Y. Chen, P. A. Wilbon, Y. P. Chen, J. H. Zhou, M. Nagarkatti, C. P. Wang, F. X. Chu, A. W. Decho and C. B. Tang, *Rsc Adv.* **2012**, *2*, 10275-10282.
18. J. Ramos, J. Forcada and R. Hidalgo-Alvarez, *Chem. Rev.* **2014**, *114*, 367-428.
19. S. K. Samal, M. Dash, S. Van Vlierberghe, D. L. Kaplan, E. Chiellini, C. van Blitterswijk, L. Moroni and P. Dubruel, *Chem. Soc. Rev.* **2012**, *41*, 7147-7194.
20. F. Nederberg, Y. Zhang, J. P. K. Tan, K. J. Xu, H. Y. Wang, C. Yang, S. J. Gao, X. D. Guo, K. Fukushima, L. J. Li, J. L. Hedrick and Y. Y. Yang, *Nat. Chem.* **2011**, *3*, 409-414.
21. P. Li, Y. F. Poon, W. F. Li, H. Y. Zhu, S. H. Yeap, Y. Cao, X. B. Qi, C. C. Zhou, M. Lamrani, R. W. Beuerman, E. T. Kang, Y. G. Mu, C. M. Li, M. W. Chang, S. S. J. Leong and M. B. Chan-Park, *Nat. Mater.* **2011**, *10*, 149-156.
22. E. Turos, G. S. K. Reddy, K. Greenhalgh, P. Ramaraju, S. C. Abeylath, S. Jang, S. Dickey and D. V. Lim, *Bioorg. Med. Chem. Lett.* **2007**, *17*, 3468-3472.
23. M. S. Yavuz, Y. Y. Cheng, J. Y. Chen, C. M. Cobley, Q. Zhang, M. Rycenga, J. W. Xie, C. Kim, K. H. Song, A. G. Schwartz, L. H. V. Wang and Y. N. Xia, *Nat. Mater.* **2009**, *8*, 935-939.
24. V. W. L. Ng, X. Ke, A. L. Z. Lee, J. L. Hedrick and Y. Yang, *Adv. Mater.* **2013**, *25*, 6730-6736.
25. G. R. Whittell, M. D. Hager, U. S. Schubert and I. Manners, *Nat. Mater.* **2011**, *10*, 176-188.
26. G. R. Whittell and I. Manners, *Adv. Mater.* **2007**, *19*, 3439-3468.
27. G. Gasser, I. Ott and N. Metzler-Nolte, *J. Med. Chem.* **2011**, *54*, 3-25.

28. B. Happ, A. Winter, M. D. Hager and U. S. Schubert, *Chem. Soc. Rev.* **2012**, *41*, 2222-2255.
29. F. Noor, A. Wustholz, R. Kinscherf and N. Metzler-Nolte, *Angew. Chem. Int. Ed.* **2005**, *44*, 2429-2432.
30. C. G. Hartinger, N. Metzler-Nolte and P. J. Dyson, *Organometallics* **2012**, *31*, 5677-5685.
31. L. Ren, C. Hardy and C. Tang, *J. Am. Chem. Soc.* **2010**, *132*, 8874-8875.
32. J. Zhang, P. Pellechia, J. Hayat, C. Hardy and C. Tang, *Macromolecules* **2013**, *46*, 1618-1624.
33. J. Zhang, L. Ren, C. Hardy and C. Tang, *Macromolecules* **2012**, *45*, 6857-6863.
34. J. Zhang, Y. Yan, C. W., C. J., H. J., M. S. and C. Tang, *Angew. Chem. Int. Ed.* **2013**, *52*, 13387-13391.
35. L. X. Ren, J. Y. Zhang, X. L. Bai, C. G. Hardy, K. D. Shimizu and C. B. Tang, *Chem. Sci.* **2012**, *3*, 580-583.
36. Ocallagh.Ch, A. H. Shingler, S. M. Kirby and A. Morris, *Antimicrob. Agents. Ch.* **1972**, *1*, 283-288.
37. L. M. Ellerby, W. A. Escobar, A. L. Fink, C. Mitchinson and J. A. Wells, *Biochemistry* **1990**, *29*, 5797-5806.
38. O. Herzberg and J. Moult, *Science* **1987**, *236*, 694-701.
39. M. Gross, S. E. Cramton, F. Gotz and A. Peschel, *Infect. Immun.* **2001**, *69*, 3423-3426.
40. J. Zhang, Y. Yan, C. W., C. J., H. J., M. S. and C. Tang, *Angew. Chem. Int. Ed.* **2013**, DOI: 10.1002/anie.201306432.
41. S. Morath, S. von Aulock and T. Hartung, *J Endotoxin Res* **2005**, *11*, 348-356.
42. I. A. Camacho, M. Nagarkatti and P. S. Nagarkatti, *Arch. Toxicol.* **2004**, *78*, 290-300.
43. N. P. Singh, M. Nagarkatti and P. Nagarkatti, *Mol. Pharmacol.* **2008**, *73*, 1722-1735.

CHAPTER 7

CONCLUSIONS[†]

[†]C. G. Hardy,[*] J. Zhang,[*] Y. Yan, L. Ren and C. Tang, *Prog. Polym. Sci.* **2014**, *39*, 1742-1796. ([*]Co-first Author)

7.1 DISSERTATION SUMMARY

The incorporation of metallocene/metallocenium with polymers is creating exciting science for many areas, including medicinal chemistry, energy-related science, and advanced catalytic chemistry. RAFT polymerization of cobaltocenium-containing monomers lays the foundation to prepare novel cobaltocenium-containing polymers with diverse architectures. Cobaltocenium-containing homopolymers and different diblock copolymers were prepared and characterized in details. The following work majorly focuses on anion-exchange impact on ion-responsive cobaltocenium-containing polymers. In this work, 2D-diffusion NMR was applied to comprehensively investigate the ion-exchange and the diffusion of ions in metal-containing polymers. We also firstly reported the synthesis of polymer brushes with anion responsive properties. We also investigated a universal phase-transfer anion-exchange technique for cationic metallopolymers and utilized metallopolymers to prepare inorganic nanomaterials. With this facile ion-exchange strategy, ions were easily switched, which offered opportunities for the further application of cationic metallocene-containing polymers. Furthermore, in the last two years of my PhD, I majorly studied the utilization of heterobimetallic diblock copolymers to prepare inorganic materials with controlled magnetic properties. Superparamagnetic materials with controlled saturated magnetic response were conveniently prepared via these heterobimetallic polymers. The final part of my work offers a novel platform to build antimicrobial polymeric materials based on cationic cobaltocenium-containing polymers. Drug resistant bacteria were greatly inhibited by our metallopolymers. Commercially available β-lactam antibiotics were also re-activated by metallopolymers against these resistant pathogens.

7.2 FUTURE DIRECTION

Metallopolymers has combined different features from both inorganic and organic materials. A lot of issues should be addressed and investigated for them, including their potential synthetic techniques and incorporation of their advantages in different applications. The most important parts are listed as follows:

Catalysts for Engineering Polymers/Plastics: metallocenes are important catalysts for production of olefin polymers for diverse applications.[1-2] While research in this direction is still ongoing, the level of active efforts is apparently waning down. Due to the maturation of polyolefin production, the requirement of the breakthrough in designing new organometallic catalysts is necessary for other classes of engineering polymers. Typically, the following characters should be achieved to design new catalysts for these engineering polymers:[3-4] (I) Metal catalysts are usually electron-deficient; (II) The active metal center should have at least one coordination site; (III) Steric protection for the metal center is generally required for the control of the molecular weight of resultant polymers. New efforts could start from synthetic organometallic and coordination molecules, which are targets for synthesis of metal-containing polymers. Considering the combined characters from metal centers and polymeric materials, these metallopolymers can provide improved catalytic efficiency, enhanced environmental tolerance and will also directly bring suitable substrates for their catalytic applications in industrial utilization.

Advanced Materials: while the outlook of metallopolymers for large scale production still remains difficult, their use for niche applications has obtained a lot of attention. For example, the redox chemistry can be used as the center property to

constructing functional materials such as stimuli-responsive materials. Another fiel is the use of heavy metals for etching such as lithographic resists. The third primary application is the use as precursors to synthesize advanced inorganic (or magnetic) materials. A lot of potential applications could be explored for development of other advanced materials. For example, considering the unique properties of metal-containing moieties with distinguished absorption in the visible region and luminescence, some biosensoring and bioimaging polymeric materials have been designed and prepared.[5] However, synthesis of diverse metallopolymers is still challenging, thus hindering the variability of these novel optical materials. Other opportunities, such as incorporation of magnetic metal moieties into polymers and surface coating with metal-containing polymers, could offer novel and functional materials, including magnetic responsive materials, novel surface-coated electrodes.

Biomaterials: A lot of research has been carried out to take advantage of redox properties of metallopolymers in the biomedical applications. Biosensing and drug/gene delivery are two promising areas. One almost missing piece is the use of metallopolymers for medicinal chemistry.[6] Lots of research efforts have been addressed on the use of organometallic compounds as anticancer drugs.[7] Several major challenges currently limit the design and application of these polymeric biomaterials, including high toxicity, instability and poor solubility in aqueous solution. The level of cytotoxicity for most organometallic compounds is usually very high, which could be difficult for further utilization as biomaterials. The stability of these organometallic molecules under physiological conditions is also a concern for bio-applications. Direct release of metal elements into human tissues is harmful for many kinds of cells. Finally, after

incorporation of organometallic molecules into polymers, these polymers are usually not water compatible, which limits their applications in biosensors and drug delivery. These problems should be well addressed before the broad utilization of metallopolymers.

7.3 REFERENCES

1. W. Kaminsky, *J. Chem. Soc., Dalton Trans.* **1998**, 1413-1418.
2. H. H. Brintzinger, D. Fischer, R. Mülhaupt, B. Rieger and R. M. Waymouth, *Angew. Chem. Int. Ed. Engl.* **1995**, *34*, 1143-1170.
3. B. Heurtefeu, C. Bouilhac, E. Cloutet, D. Taton, A. Deffieux and H. Cramail, *Prog. Polym. Sci.* **2011**, *36*, 89-126.
4. G. J. P. Britovsek, V. C. Gibson and D. F. Wass, *Angew. Chem. Int. Ed.* **1999**, *38*, 428-447.
5. J. M. Stanley and B. J. Holliday, *Coord. Chem. Rev.* **2012**, *256*, 1520-1530.
6. E. Neuse, *J Inorg Organomet Polym* **2005**, *15*, 3-31.
7. G. Gasser, I. Ott and N. Metzler-Nolte, *J. Med. Chem.* **2010**, *54*, 3-25.

APPENDIX A
COPYRIGHT RELEASES

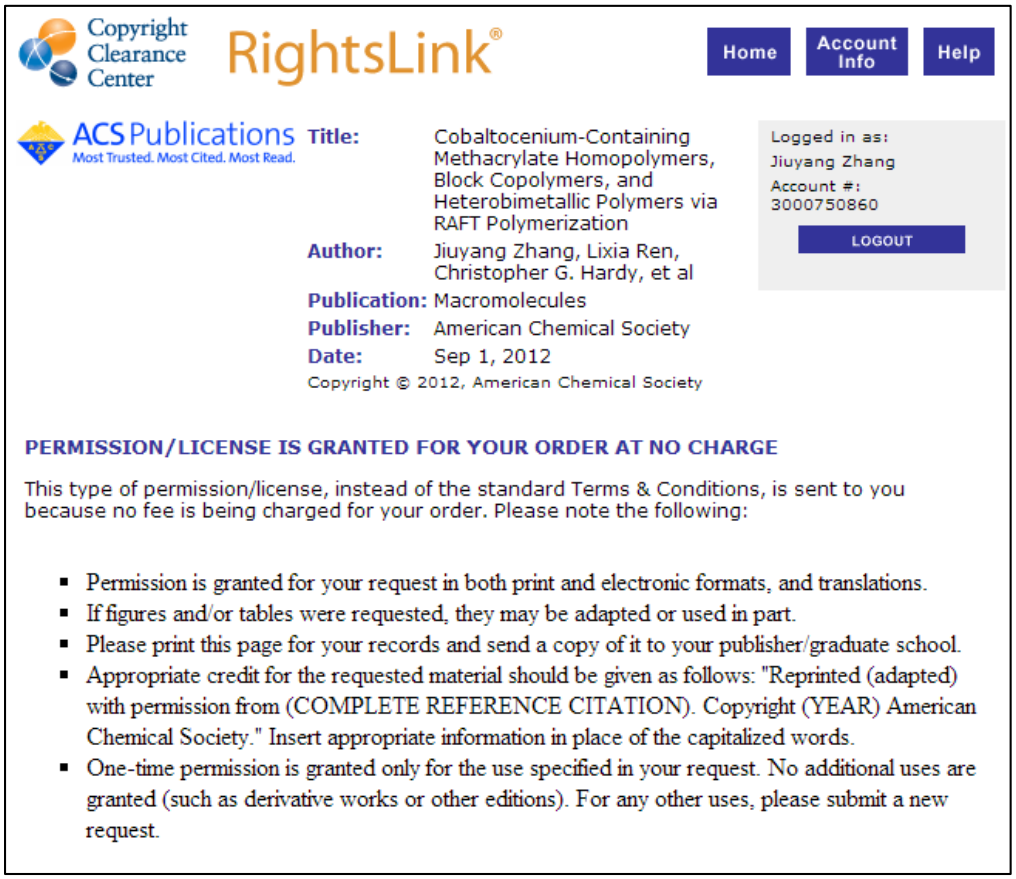

Figure A.1. Copyright release for Chapter 2.

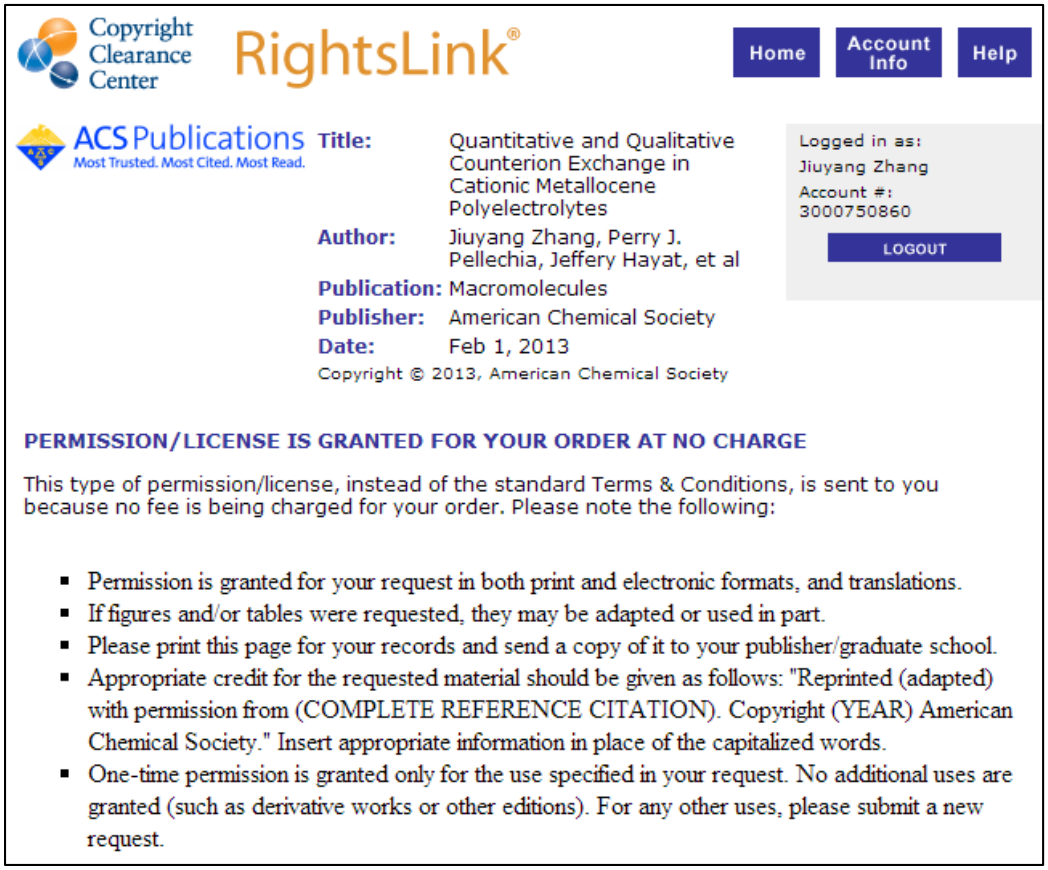

Figure A.2. Copyright release for Chapter 3.

Copyright Clearance Center RightsLink®

Home | Account Info | Help

Title: Charged Metallopolymers as Universal Precursors for Versatile Cobalt Materials
Author: Jiuyang Zhang,Yi Yan,Michael W. Chance,Jihua Chen,Jeffery Hayat,Shuguo Ma,Chuanbing Tang
Publication: Angewandte Chemie International Edition
Publisher: John Wiley and Sons
Date: Oct 16, 2013
Copyright © 2013 WILEY-VCH Verlag GmbH & Co. KGaA, Weinheim

Logged in as:
Jiuyang Zhang
Account #:
3000750860
LOGOUT

Order Completed

Thank you very much for your order.

This is a License Agreement between Jiuyang Zhang ("You") and John Wiley and Sons ("John Wiley and Sons"). The license consists of your order details, the terms and conditions provided by John Wiley and Sons, and the payment terms and conditions.

Get the printable license.

License Number	3475540859800
License date	Sep 24, 2014
Licensed content publisher	John Wiley and Sons
Licensed content publication	Angewandte Chemie International Edition
Licensed content title	Charged Metallopolymers as Universal Precursors for Versatile Cobalt Materials
Licensed copyright line	Copyright © 2013 WILEY-VCH Verlag GmbH & Co. KGaA, Weinheim
Licensed content author	Jiuyang Zhang,Yi Yan,Michael W. Chance,Jihua Chen,Jeffery Hayat,Shuguo Ma,Chuanbing Tang
Licensed content date	Oct 16, 2013
Start page	13387
End page	13391
Type of use	Dissertation/Thesis
Requestor type	Author of this Wiley article
Format	Print and electronic
Portion	Full article
Will you be translating?	No
Title of your thesis / dissertation	METALLOCENE-CONTAINING POLYMERS: FROM SYNTHESIS TO APPLICATIONS
Expected completion date	Nov 2014
Expected size (number of pages)	6
Total	0.00 USD

Figure A.3. Copyright release for Chapter 4.

Copyright Clearance Center RightsLink®

Home | Account Info | Help

ACS Publications
Most Trusted. Most Cited. Most Read.

Title: Nanostructured Metal/Carbon Composites from Heterobimetallic Block Copolymers with Controlled Magnetic Properties
Author: Jiuyang Zhang, Yi Yan, Jihua Chen, et al
Publication: Chemistry of Materials
Publisher: American Chemical Society
Date: May 1, 2014
Copyright © 2014, American Chemical Society

Logged in as:
Jiuyang Zhang
Account #:
3000750860
LOGOUT

PERMISSION/LICENSE IS GRANTED FOR YOUR ORDER AT NO CHARGE

This type of permission/license, instead of the standard Terms & Conditions, is sent to you because no fee is being charged for your order. Please note the following:

- Permission is granted for your request in both print and electronic formats, and translations.
- If figures and/or tables were requested, they may be adapted or used in part.
- Please print this page for your records and send a copy of it to your publisher/graduate school.
- Appropriate credit for the requested material should be given as follows: "Reprinted (adapted) with permission from (COMPLETE REFERENCE CITATION). Copyright (YEAR) American Chemical Society." Insert appropriate information in place of the capitalized words.
- One-time permission is granted only for the use specified in your request. No additional uses are granted (such as derivative works or other editions). For any other uses, please submit a new request.

Figure A.4. Copyright release for Chapter 5.

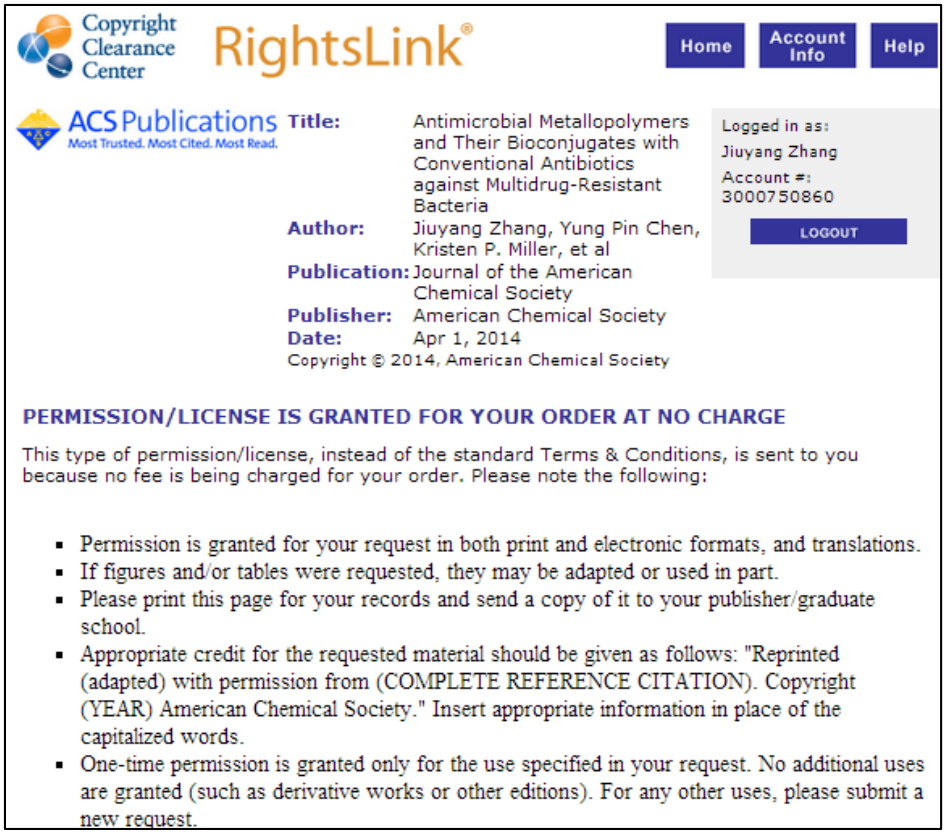

Figure A.5. Copyright release for Chapter 6.

Figure A.6. Copyright release for Chapter 1 and Chapter 7.